AD-A156 981 A COMPOSITE CLIMATOLOGICAL STUDY OF THE FREQUENCY AND 1/1
DISTRIBUTION OF SEV.. (U) AIR FORCE INST OF TECH
WRIGHT-PATTERSON AFB OH J H PETERS 1985
UNCLASSIFIED AFIT/CI/NR-85-52T F/G 4/2 NL

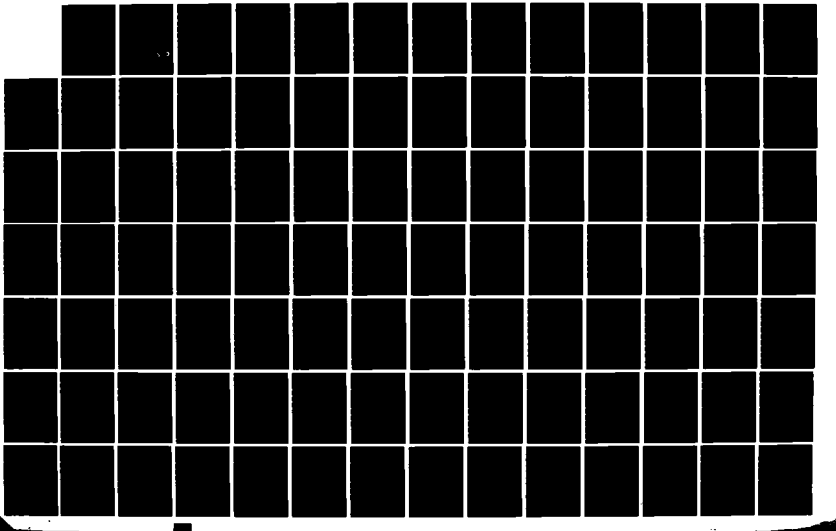

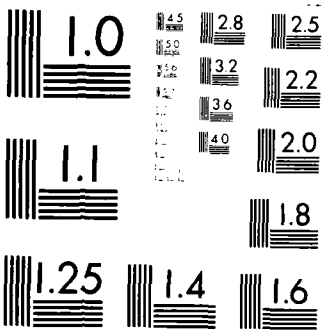

A COMPOSITE CLIMATOLOGICAL STUDY OF THE FREQUENCY AND DISTRIBUTION OF SEVERE WEATHER ASSOCIATED WITH SPRING SEASON COLORADO CYCLOGENESIS

by

JEFFREY H. PETERS

A thesis submitted in partial fulfillment of the
requirements for the degree of

MASTER OF SCIENCE
(Meteorology)

at the

UNIVERSITY OF WISCONSIN-MADISON

1985

UNCLASS

SECURITY CLASSIFICATION OF THIS PAGE (When Data Entered)

REPORT DOCUMENTATION PAGE	READ INSTRUCTIONS BEFORE COMPLETING FORM
1. REPORT NUMBER: AFIT/CI/NR 85-52T AD-A156 981	2. GOVT ACCESSION NO. / 3. RECIPIENT'S CATALOG NUMBER
4. TITLE (and Subtitle): A Composite Climatological Study of the Frequency and Distribution of Severe Weather Associated with Spring Season Colorado Cyclogenesis	5. TYPE OF REPORT & PERIOD COVERED: THESIS/DISSERTATION
	6. PERFORMING ORG. REPORT NUMBER
7. AUTHOR(s): Jeffrey H. Peters	8. CONTRACT OR GRANT NUMBER(s)
9. PERFORMING ORGANIZATION NAME AND ADDRESS: AFIT STUDENT AT: University of Wisconsin-Madison	10. PROGRAM ELEMENT, PROJECT, TASK AREA & WORK UNIT NUMBERS
11. CONTROLLING OFFICE NAME AND ADDRESS: AFIT/NR WPAFB OH 45433	12. REPORT DATE: 1985
	13. NUMBER OF PAGES: 84
14. MONITORING AGENCY NAME & ADDRESS(if different from Controlling Office)	15. SECURITY CLASS. (of this report): UNCLASS
	15a. DECLASSIFICATION/DOWNGRADING SCHEDULE

16. DISTRIBUTION STATEMENT (of this Report)

APPROVED FOR PUBLIC RELEASE; DISTRIBUTION UNLIMITED

17. DISTRIBUTION STATEMENT (of the abstract entered in Block 20, if different from Report)

18. SUPPLEMENTARY NOTES

APPROVED FOR PUBLIC RELEASE: IAW AFR 190-1

LYNN E. WOLAVER
Dean for Research and
Professional Development
AFIT, Wright-Patterson AFB OH

19. KEY WORDS (Continue on reverse side if necessary and identify by block number)

20. ABSTRACT (Continue on reverse side if necessary and identify by block number)

ATTACHED

DD FORM 1 JAN 73 1473 EDITION OF 1 NOV 65 IS OBSOLETE

UNCLASS

SECURITY CLASSIFICATION OF THIS PAGE (When Data Entered)

ABSTRACT

A composite approach is used to investigate the evolution and distribution of severe weather events for 39 cases of spring season Colorado cyclogenesis. The study also examined the incidence of severe weather during a "jet streak" subsample of 15 cases, based on the presence of a 300 mb wind maximum over the New Mexico-Texas area on the day of cyclogenesis, and a complement subsample of the cyclogenetic cases not included in the jet streak subsample. Composites were constructed of the normalized frequency of (1) tornadoes, (2) high winds, (3) large hail, (4) funnel clouds and (5) total severe weather events for the total sample of 39 cases and the two subsamples for three 24 hour intervals with the first interval coinciding with the day of cyclogenesis.

The distribution and frequency of severe weather for the three days was consistent with the mean synoptic features as the composite cyclone developed and moved away from its lee side development site in the southern Rockies. The area where severe weather occurred significantly broadened and moved northeastward on the two days following cyclogenesis. For each of the three samples, the maximum frequency of total severe storm events was highest on the day after cyclogenesis.

The relationship between the upper-tropospheric wind maximum and the frequency of total severe storm events was examined for the jet streak subsample. The greatest incidence of severe weather

occurred ahead of and to the right of the exit region of the propagating 300 mb jet streak. The presence of the composite 300 mb wind maximum in the jet streak subsample clearly enhanced the frequency of severe weather compared to the composites of the total sample of 39 cases and the complement subsample.

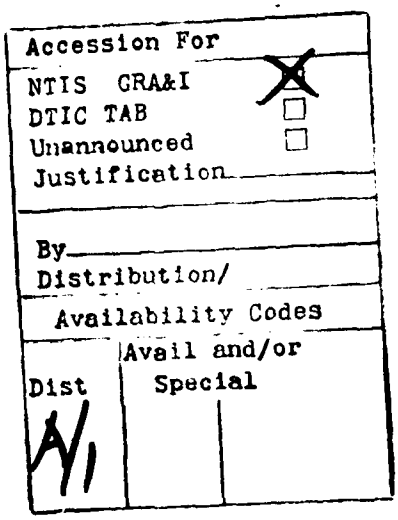

APPROVED .....

Lyle H. Horn

Professor of Meterorology

DATE ..... April 29, 1985 .....

At this also my heart trembles, And leaps from
its place.
Listen closely to the thunder of His voice,
And the rumbling that goes out from His mouth.
Under the whole heaven He lets it loose,
And His lightning to the ends of the earth.
After it, a voice roars; He thunders with His
majestic voice;
And He does not restrain the lightnings when
His voice is heard.
God thunders with His voice wondrously,
Doing great things which we cannot comprehend.
For to the snow He says, 'Fall on the earth,'
And to the shower of rain and the rain,
'Be strong.'
He seals the hand of every man, That all men may
know His work.
Then the beast goes into its lair, And remains
in its den.
Out of the chamber comes the storm, And out of
the scattering winds the cold.
From the breath of God ice is made, And the
expanse of the waters is frozen.
Also with moisture He loads the thick cloud;
He disperses the cloud of His lightning.
And it changes direction, turning around by His
guidance,
That it may do whatever He commands it on the
face of the inhabited earth.
Whether for correction, or for His world,
Or for lovingkindness, He causes it to happen.

Job 37:1-13 (NASV)

TABLE OF CONTENTS

ACKNOWLEDGEMENTS

Prior to attending this university, I had a dream of going to graduate school to obtain a Master of Science degree in Meteorology. The United States Air Force gave me the educational opportunity to do this through the Civilian Institutions Program of the Air Force Institute of Technology. I would like to express my appreciation to the many people who helped make my dream become a reality.

None of this research would have occurred without the assistance of Professor Lyle H. Horn. His previous work in the area of Colorado cyclogenesis was instrumental in laying the ground work for this research. His support and guidance during the various facets of this project were invaluable.

Throughout the course of this study, Dr. Thomas L. Koehler provided numerous helpful suggestions and comments. My best wishes to him as he prepares to leave the university to pursue new academic challenges.

I extend my thanks to Professor Frank S. Sechrist for his input as the second reader and to Russell Hovanec, Tom Achtor and Robin Marshment for their previous work with the data set.

Special thanks are due to Professor Roland B. Stull and Tim Crum for their programming assistance. Since I had no computer funds, their knowledge of the capabilities and idiosyncracies of the APPLE II microcomputer was tremendously helpful.

My office mate Gin-Rong (Hank) Liu also deserves recognition. He was always a constant source of encouragement throughout the difficult times of my studies.

Thanks are also due to those who wrote letters of recommendation for me to attend this highly respected university: Professor John J. Cahir of the Pennsylvania State University and Lt. Col. Robert E. Introne, Jr. and Maj. Robert W. Haschalk of the United States Air Force. I greatly appreciate their confidence and faith in my abilities.

Words alone cannot describe my gratitude for my wife, Carol. During the past 21 months while I was often absent from our home, she managed our household and nurtured the growth of our two active young children, Jason and Heidi. She has been a never ending source of encouragement and strength.

ABSTRACT

A composite approach is used to investigate the evolution and distribution of severe weather events for 39 cases of spring season Colorado cyclogenesis. The study also examined the incidence of severe weather during a "jet streak" subsample of 15 cases, based on the presence of a 300 mb wind maximum over the New Mexico-Texas area on the day of cyclogenesis, and a complement subsample of the cyclogenetic cases not included in the jet streak subsample. Composites were constructed of the normalized frequency of (1) tornadoes, (2) high winds, (3) large hail, (4) funnel clouds and (5) total severe weather events for the total sample of 39 cases and the two subsamples for three 24 hour intervals with the first interval coinciding with the day of cyclogenesis.

The distribution and frequency of severe weather for the three days was consistent with the mean synoptic features as the composite cyclone developed and moved away from its lee side development site in the southern Rockies. The area where severe weather occurred significantly broadened and moved northeastward on the two days following cyclogenesis. For each of the three samples, the maximum frequency of total severe storm events was highest on the day after cyclogenesis.

The relationship between the upper-tropospheric wind maximum and the frequency of total severe storm events was examined for the jet streak subsample. The greatest incidence of severe weather

occurred ahead of and to the right of the exit region of the propagating 300 mb jet streak. The presence of the composite 300 mb wind maximum in the jet streak subsample clearly enhanced the frequency of severe weather compared to the composites of the total sample of 29 cases and the complement subsample.

1. Introduction

Severe local weather annually threatens the lives and property of millions of people in the United States. Statistics compiled by NOAA's National Climatic Data Center (1983) show that between 1953 and 1983 severe weather caused an average annual loss of more than 5 billion dollars in property damage and more than 100 storm-related fatalities. The majority of property loss and fatalities occur during the spring months when severe storms are both more frequent and more violent. Annually 56% of the tornadoes occur during the spring season (April-June); however because of the greater violence, 72% of the annual tornado-related deaths occur during these months. The vast majority of thunderstorms that produce severe weather in the United States occurs over the central portion of the country between the Rocky and Appalacian Mountains. In particular, Court (1974) found tornadoes and large hail (> 19 mm in diameter) occur most frequently in central Oklahoma and Kansas (Figs. 1 and 2). Although improved radar and satellite data provide useful meteorological tools to monitor the development of severe storms and aid in their prediction, the meteorologist must continue to learn more about the mechanisms which lead to the occurrence of severe weather. This increase in knowledge should lead to the development of more accurate and timely predictions of these destructive storms.

The great majority of spring season thunderstorms that produce severe weather in the central United States develop in regions where

elongated over northwestern Iowa. This more diffuse pattern is a result of the compositing of the various tracks and speed of movement of the 39 cyclones as they moved from their lee side development sites in the southern Rockies.

The 300 and 850 mb composite wind fields at 1200 GMT for the three days of interest are shown in Figs. 4, 5 and 6. On day C a 300 mb composite jet streak is located over central Arizona ahead of a trough in the composite streamline pattern. At 850 mb a wind maximum over north central Texas is embedded in a southwesterly flow of air over the Southern Great Plains. By day C the 300 mb wind maximum has propagated eastward and intensified to 40 m/s. The 850 mb wind maximum has also strengthened and moved into central Oklahoma. The 300 mb composite jet streak continues to move eastward with little change in intensity and is centered over northern Texas on day C+2. Meanwhile at 850 mb, the wind maximum now over southeast Kansas has weakened and become broader. Compared to day C+1 at 1200 GMT, the 850 mb flow has veered allowing for a sharp decrease in the 850-500 mb directional wind shear in the exit region of the propagating 300 mb jet streak.

4. The observed severe weather frequency and distribution for day C

The normalized frequency of tornadoes, high winds, large hail and funnel clouds for sample C and the JF subsample are shown in Figs. 7a-d and 8a-d. In most instances the maximum frequencies

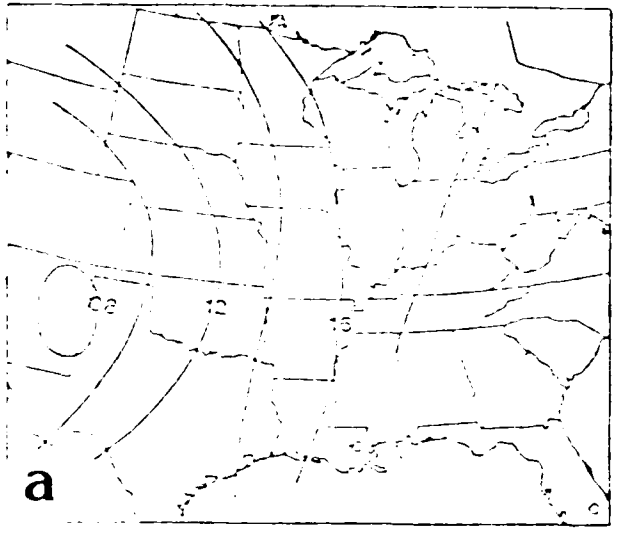

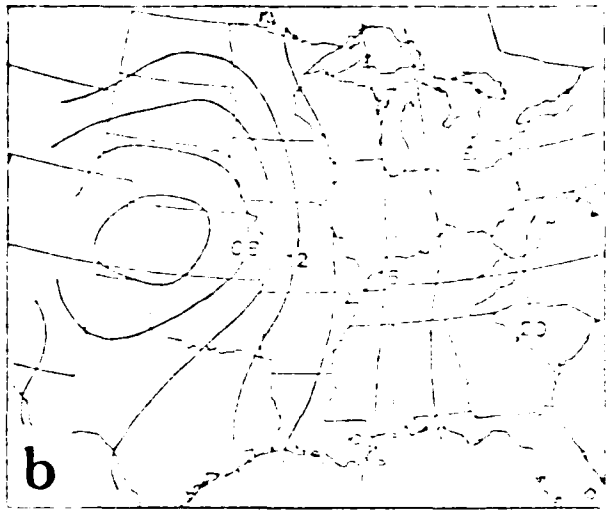

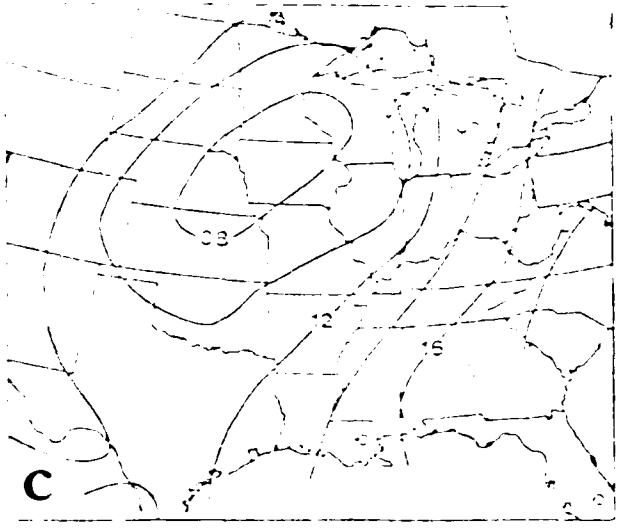

Fig. 1. Mean sea level pressure (mb) at 1200 GMT for the 39 day developing (D) sample for (a) day C, (b) day C+1 and (c) day C+2 (from Achtor and Horn, 1985).

4. Results

4.1 Mean Synoptic Features

Before examining the normalized frequency and distribution of severe weather events for the D sample and the JS and JS' subsamples for day C, day C+1 and day C+2, the mean synoptic features for the D sample as determined by Achtor and Horn will be briefly examined.[2] The composite gradients and magnitudes of the mean features are weaker than those of an individual cyclone. Achtor and Horn previously compared the mean features of the D sample and the JS subsample and found that the composite synoptic features of both samples were quite similar; however, in the JS subsample the gradients and magnitudes of these features are generally sharper and stronger.

Figs. 5 a, b and c show the mean sea level pressure distribution at 1200 GMT for days C, C+1 and C+2, respectively. As a result of compositing, a relatively weak low pressure center is located over eastern New Mexico on day C prior to the detection of initial cyclogenesis. During the next 24 hours, cyclogenesis occurs and the composite low deepens as it moves into western Kansas. On day C+2 the mean sea level low pressure center has weakened and become more

---

[2] For the purpose of comparison, the valid times of the results of the Achtor/Horn and Marshment/Horn studies were converted to the nomenclature of this study (i.e., day C of this study corresponds to the period from 1200 GMT of day C-1 to 1159 GMT of day C used in the earlier studies).

calculated totals were normalized and averaged to construct maps of the frequency of severe weather events for day C, C+1 and C+2 for the three samples. Since the area contained within the 1° latitude-longitude box varies with latitude, the totals were normalized to the area of a grid box (9775 km^2) at the midpoint latitude (37.5° N) of the data set. These totals were further normalized by dividing by the number of cyclogenetic cases in each of the three samples. To assist in data analysis, the normalized totals were then smoothed using a 2° latitude-longitude overlapping boxes averaging technique (Kelly et al., 1976), which produces values at each 1° latitude-longitude intersection. Maps were then constructed for day C, C+1 and C+2 for the developing sample (D) of 39 cases, the jet streak subsample (JS) of 15 cases and the complement subsample (JS') of 24 cases. As a result of the extremes in the magnitudes of the normalized frequency of severe weather events for each sample, the maps were analyzed using a geometric sequence technique ($3^n \times 10^{-3}$ events per case of the sample per 9775 km^2 ,where n is ≥ 0).

to determine with the available synoptic data which cyclone was responsible for the development of each severe weather event, the events occurring on the overlapping days were considered to be associated with both cyclones (e.g. an event occurring on day C+2 for one cyclone and day C for another was considered as occurring on the appropriate days for both cyclones). The overlapping occurred on only 12% of the possible days for the sample of 39 developing cases and, thus, should not significantly affect the results of this study. No overlapping occurred in the jet streak subsample, but overlapping did occur on 19% of the possible days in the complement subsample of 24 cases. Geographic distributions of severe weather events were constructed for day C, C+1 and C+2 for the sample of 39 developing cases and the subsample of 15 jet streak cases. This was done by tabulating the total number of the following severe weather events in 1° latitude-longitude boxes: (1) tornado genesis events, (2) tornado events (includes genesis events plus tornadoes that moved into the grid box), (3) high wind events, (4) large hail events, (5) funnel cloud genesis events, (6) funnel cloud events (includes genesis events plus funnel clouds that moved into the grid box) and (7) total severe storm events (summation of items (2), (3), (4) and (6)). These tables are contained in the Appendices.

2.3 Data Normalizing and Averaging

In order to observe and compare the geographic distribution of severe weather events during Colorado cyclogenesis, the previously

were extracted from the appropriate Storm Data publications for the period beginning at 1200 GMT day C and ending at 1159 GMT day C+2. The study included any severe weather event over the continental United States east of 107° W longitude. These items were catalogued by: (1) date and time (converted from local to GMT) of initial occurrence, (2) type of event(s) (e.g., thunderstorm with gusts to 30 m/s and 25 mm hail) and (3) area or path, initial to final location, of coverage (e.g., tornado moved from 8 miles southwest of Leavenworth, Kansas to Weston, Missouri). Since not all reports of severe local winds contained a measured wind gust, a Beaufort wind scale was subjectively applied to the reported damage (e.g., broken tree limbs or large uprooted trees) to determine if the maximum wind gust was greater than or equal to 26 m/s. No attempt was made to determine the hail size for hail damage to crop reports which gave no information on the time of occurrence or the size of hail. The geographic coverage or path of the events was assigned to appropriate 1° latitude-longitude grid boxes with special attention given to the genesis and final location of tornadoes and funnel clouds. The entire severe weather data sample was encoded into an APPLE II microcomputer, which was used to sort and partition the data set into the day of occurrence (C, C+1 and C+2). The short elapsed time between the development of some of the cyclones contained in the data set resulted in a few cases where the 72 hour period of interest overlapped between two cyclones (e.g. day C+2 for one cyclone corresponded with day C for another). Since it was not always possible

Table 1. Listing of the dates of initial detection of cyclogenesis of the D sample and the JS and JS'subsamples used in this study.

No.	DATE	D	JS	JS'
1	01 April 1964	X	X	
2	12 April 1964	X		X
3	19 April 1964	X		X
4	24 April 1964	X		X
5	25 April 1964	X		X
6	07 May 1964	X	X	
7	05 April 1965	X	X	
8	07 April 1965	X		X
9	09 April 1965	X		X
10	04 May 1965	X		X
11	07 May 1965	X		X
12	14 May 1965	X		X
13	11 May 1966	X	X	
14	04 April 1967	X		X
15	07 April 1967	X		X
16	13 April 1967	X	X	
17	16 April 1967	X	X	
18	21 April 1967	X	X	
19	23 April 1967	X		X
20	25 April 1967	X		X
21	30 April 1967	X	X	
22	05 May 1967	X		X
23	10 May 1967	X	X	
24	03 April 1968	X	X	
25	07 April 1968	X		X
26	13 April 1968	X		X
27	20 April 1968	X		X
28	23 April 1968	X		X
29	06 May 1968	X		X
30	14 May 1968	X		X
31	17 April 1969	X	X	
32	07 May 1969	X	X	
33	12 April 1970	X		X
34	18 April 1970	X	X	
35	28 April 1970	X	X	
36	29 April 1970	X		X
37	04 May 1971	X		X
38	18 May 1971	X		X
39	23 May 1971	X	X	

3. Procedures

3.1 General

The severe local weather events used in this research were extracted from the monthly Storm Data publication to construct maps of the frequency of these events for day C, C+1 and C+2 of the 39 developing cyclone cases described earlier. The gathering of the data proved to be a monumental task since over 3600 severe weather events were identified. As previously mentioned, a severe weather event was defined as the occurrence of a tornado, funnel cloud or severe thunderstorm accompanied by large hail (> 19 mm in diameter) and/or damaging wind gusts (≥ 26 m/s). The data were divided according to the day of occurrence (C, C+1 and C+2), and then a tabulation was made of the number of events occurring in a 1° latitude-longitude box for the sample of 39 developing cases and a subsample of 15 jet streak cases. The totals were first normalized by area and by the number of days per sample and then numerically smoothed. Maps of these normalized frequencies were then constructed and analyzed for each of the samples being studied.

3.2 Data Gathering

Using the dates of initial detection of cyclogenesis (Table 1) and the definition of a severe weather event, the severe weather data

distinct wind maxima on the occurrence of severe weather events. Taking into consideration Hovanec and Horn's definition of cyclogenesis and the diurnal distribution of severe weather occurrences, the severe weather data used in this research was partitioned into three 24 hour intervals beginning at 1200 GMT the day of initial cyclogenesis and ending at 1159 GMT three days later. These 24 hour intervals will henceforth be referred to as day C, C+1 and C+2.[1] The severe weather data used for this research was extracted from the National Climatic Center's monthly Storm Data publication.

[1]This nomenclature differs from that used in the studies by Achtor/ Horn and Marshment/Horn. They examined information for 0000 and 1200 GMT on the day of cyclogenesis, referred to as day C, and on the preceding (day C-1) and following (day C+1) days. Thus in this study, day C corresponds to the period from 1200 GMT of day C-1 to 1159 GMT of day C used in the earlier studies.

developing composite contained a disorganized 300 mb wind pattern. Because Hovanec and Horn selected their sample on the basis of Colorado cyclogenesis and not on whether a jet streak was present, Achtor and Horn subjectively chose a subsample of 15 cases from the 39 developing cases when a jet streak was located over the New Mexico-Texas area on the day of cyclogenesis. This jet streak subsample enhanced the features found in the developing sample. Marshment and Horn found the distribution and evolution of moisture associated with cyclone development was consistent with: (1) the movement of the mean surface cyclone and (2) the areas of relatively low stability indices which developed in the exit region and right front quadrant of the propagating 200 mb jet streak. They also noted that the transport of moisture at low levels from the Gulf of Mexico into the developing storm was enhanced by the presence of a propagating upper-tropospheric wind maximum and a low-level southerly jet, which was related to the lower branch of the transverse circulation in the exit region of the upper-tropospheric jet streak (Uccellini, 1980).

This study examines the 39 developing cases from the original Hovanec and Horn sample to observe the distribution of severe weather events throughout the cyclogenetic process for: (1) the total sample (D) of 39 developing cases (2) a subsample (JS) using the 15 jet streak cases chosen by Achtor/Horn and (3) a subsample (JS') of 24 cyclogenetic cases not included in the jet streak subsample. The data set was subdivided to show the effect of

2. Data Sample

The data sample used in this research originated in a study by Hovanec and Horn (1975), who examined static stability and 300 mb wind fields associated with Colorado cyclogenesis. They defined cyclogenesis as the location and time of occurrence of a closed isobar (4 mb interval) on the sea level pressure chart provided it persisted for at least 24 hours and found a total of 71 cases of spring season (April-May) cyclogenesis for the years 1964-1971. The surface maps used to determine cyclogenesis were for 0600 GMT for the 1964-1968 data and 1200 GMT for the 1968-1971 data. The Daily Weather Map series used in the evaluation were available for 12 hour intervals (valid at 0600 GMT and 1200 GMT) before May 1968. Thereafter, they were only available for 24 hour intervals (valid at 1200 GMT). Hovanec and Horn classified the cyclogenetic cases as either developing, if they maintained a closed isobar for 72 hours, or non-developing, if they did not. Achtor and Horn (1985) and Marshment and Horn (1985) expanded upon Hovanec and Horn's work by using conventional radiosonde information for 0000 GMT and 1200 GMT for the day preceding to the day following detection of cyclogenesis to: (1) construct composite cyclones of the 49 developing and 22 non-developing cases and (2) to analyze the upper (300 mb) and lower (850 mb) tropospheric wind fields and static stability fields. The developing sample composite showed a nearly classical 300 mb jet streak moving into the southern plains; however, the non-

This research uses a composite approach to examine the occurrence of severe weather events during April and May for the period 1964-1971 for the days of Colorado cyclogenesis chosen by Hovanec and Horn and later studied by Achtor and Horn (1985) and Marshment and Horn (1985). The study also examines the incidence of severe weather during a "jet streak" subsample of 15 cyclogenetic cases, subjectively chosen by Achtor and Horn based on the presence of a 300 mb jet streak over the New Mexico-Texas area on the day of cyclogenesis, and a complement subsample of the 24 cases not included in the jet streak subsample. This research focuses on the evolution of severe weather events throughout the cyclogenetic process and the distribution of these events in relation to dynamic forcing mechanisms. Using as guidelines the criteria established by the National Severe Storm Forecast Center and the United States Air Force Air Weather Service (1984), a severe weather event was defined as the the occurrence of a tornado, funnel cloud or severe thunderstorm accompanied with large hail (> 19 mm or $\geq$ 3/4 inch in diameter) and/or damaging wind gusts (> 26 m/s or $\geq$ 50 knots).

convective instability exists and where there is considerable vertical wind shear between the low-level and upper-tropospheric air flow. These regions develop in response to the rapid northward flow of lower-tropospheric warm, moist air from the Gulf of Mexico and the cool, dry air flow associated with strong westerly winds in the middle troposphere (Fawbush and Miller, 1953, 1954). The source of the dry mid-tropospheric air associated with convectively unstable environments over the Great Plains may be the result of warm, dry surface air from the high Mexican plateau flowing northeastward into the central United States where it overrides relatively cooler, moist air from the Gulf of Mexico (Carlson and Ludlum, 1968). The capping inversion, characteristic of convectively unstable environments, can also result from mid-tropospheric subsidence associated with the sinking branch of the indirect transverse circulation in the exit region of a propagating 500 mb jet streak (Uccellini and Johnson, 1979). In an environment where convective instability exists, sufficient lifting to penetrate the capping inversion can result in the development of deep convection and the formation of severe thunderstorms, that are often accompanied by large hail, damaging winds and tornadoes. Two positively correlated meteorological factors, which help create convectively unstable environments and thus favor the high frequency of severe weather over the central United States, are spring season (April-May) Colorado cyclogenesis and upper-tropospheric jet streaks. Hovanec and Horn (1975) found that significant Colorado cyclogenesis commonly occurs as an upper level wind maximum propagates into the lee of the southern Rockies.

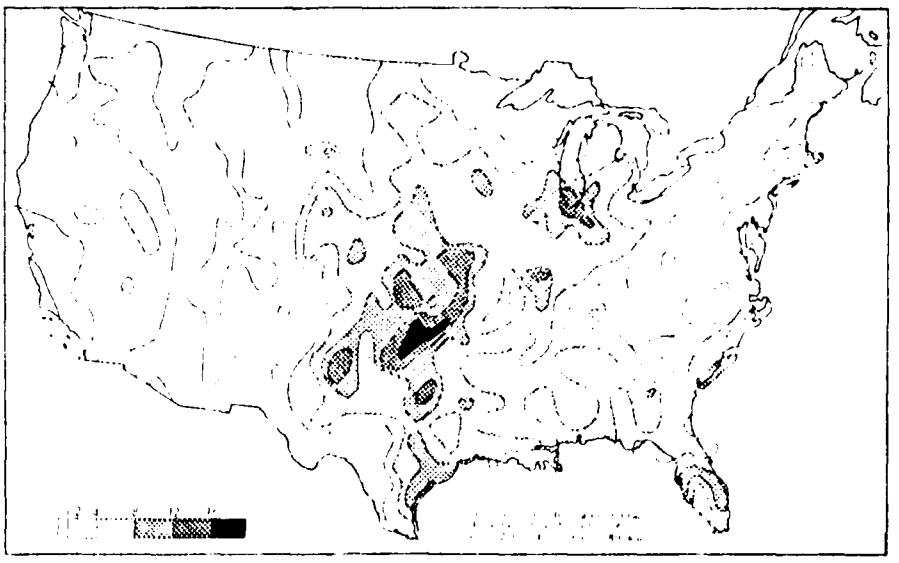

Fig. 1. Mean annual tornado incidence per 26,000 km^2, 1955-1967 (from Court, 1974).

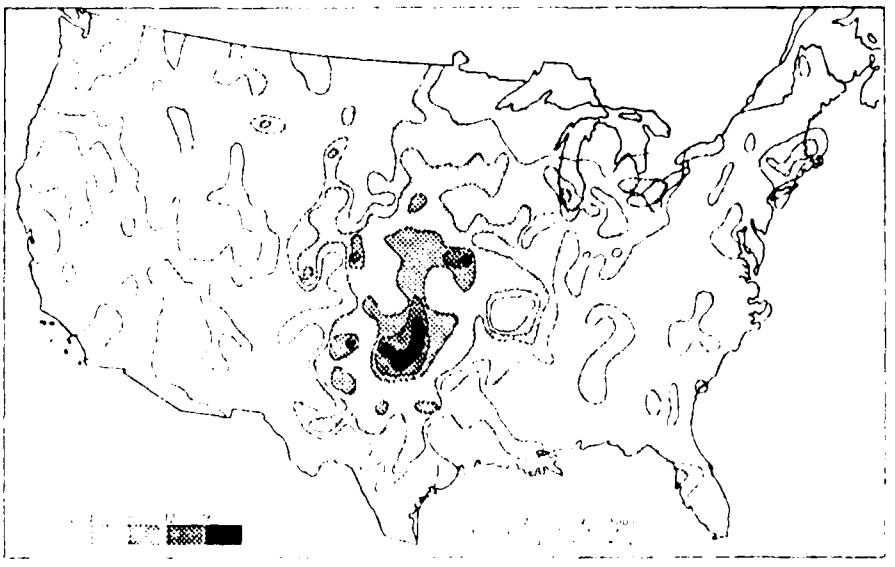

Fig. 2. Mean annual incidence of large hail (>19mm) per 26,000 km^2, 1955-1967 (from Court, 1974).

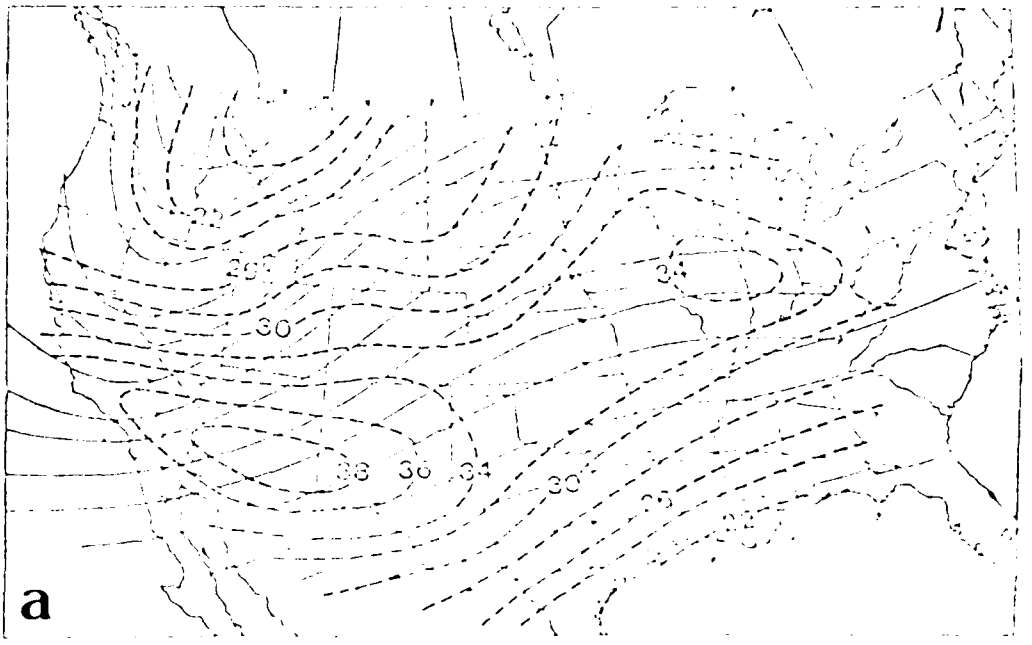
a
38
36
34
30

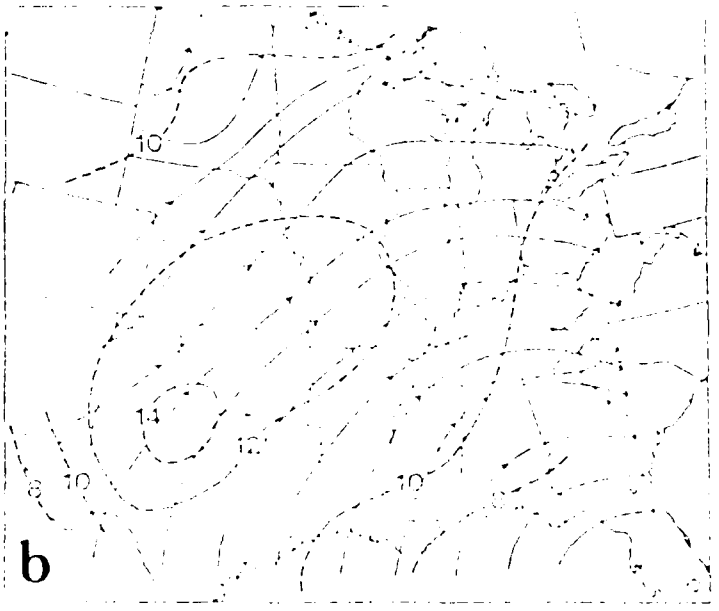
b
10
14
12
10
10

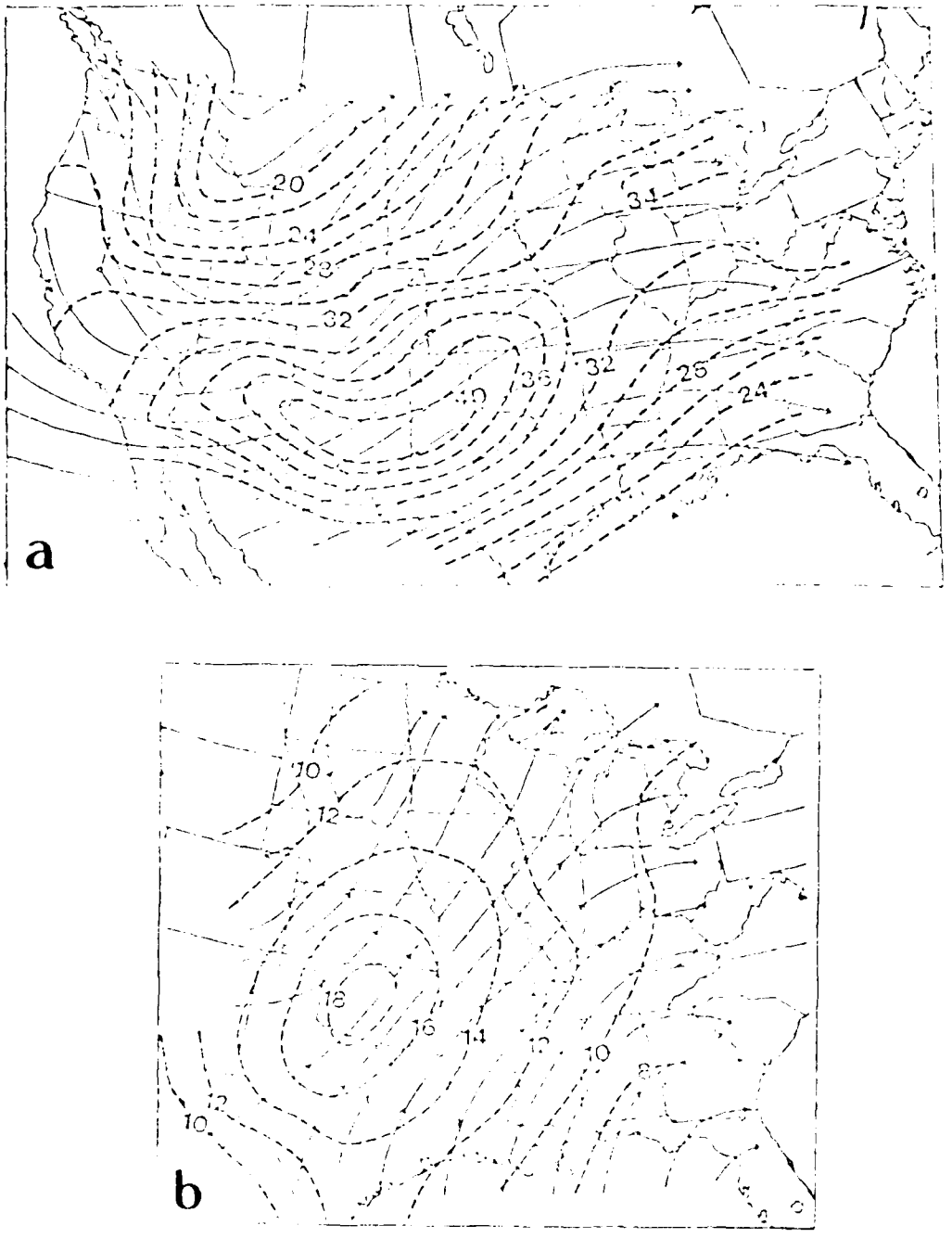

Fig. 5. Mean isotachs (m/s) and streamlines at 1200 GMT on day C+1 for the I sample at (a) 200 mb and (b) 850 mb (from Achtor and Hess, 1964).

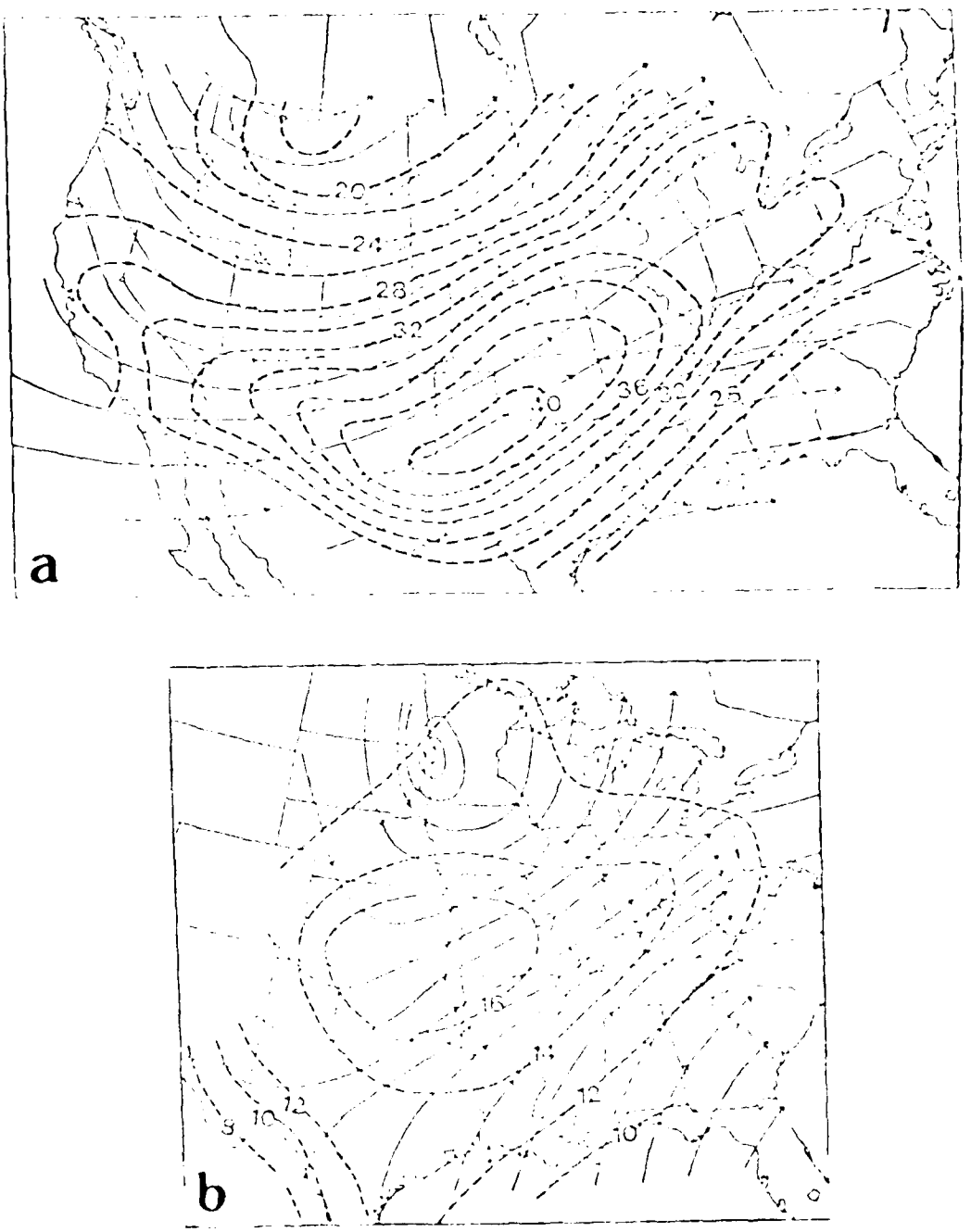

Fig. 6. Mean isotachs (m/s) and streamlines at 1200 GMT on day C+2 for the I sample at (a) 200 mb and (b) 850 mb (from Achtor and Horn, 1985).

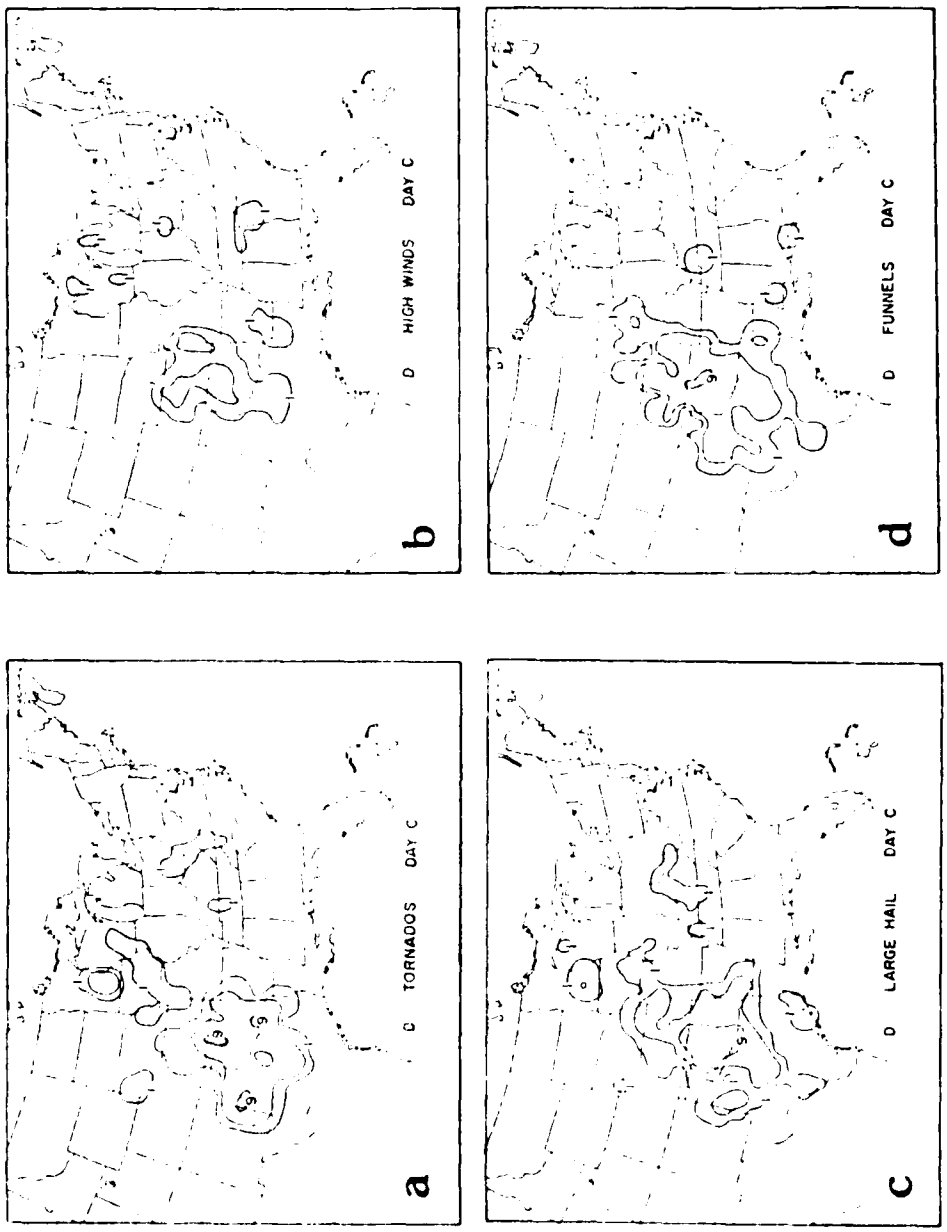

Fig. 7. Normalized and smoothed frequency (10^{-2}) of (a) tornados, (b) high winds ($\geq$ 26 m/s), (c) large hail ($>$ 19mm) and (d) funnel clouds for the D sample on day C. A geometric sequence of 3^n, where $n \geq 0$, is used for the isolines, which are labeled for 3^{2n}.

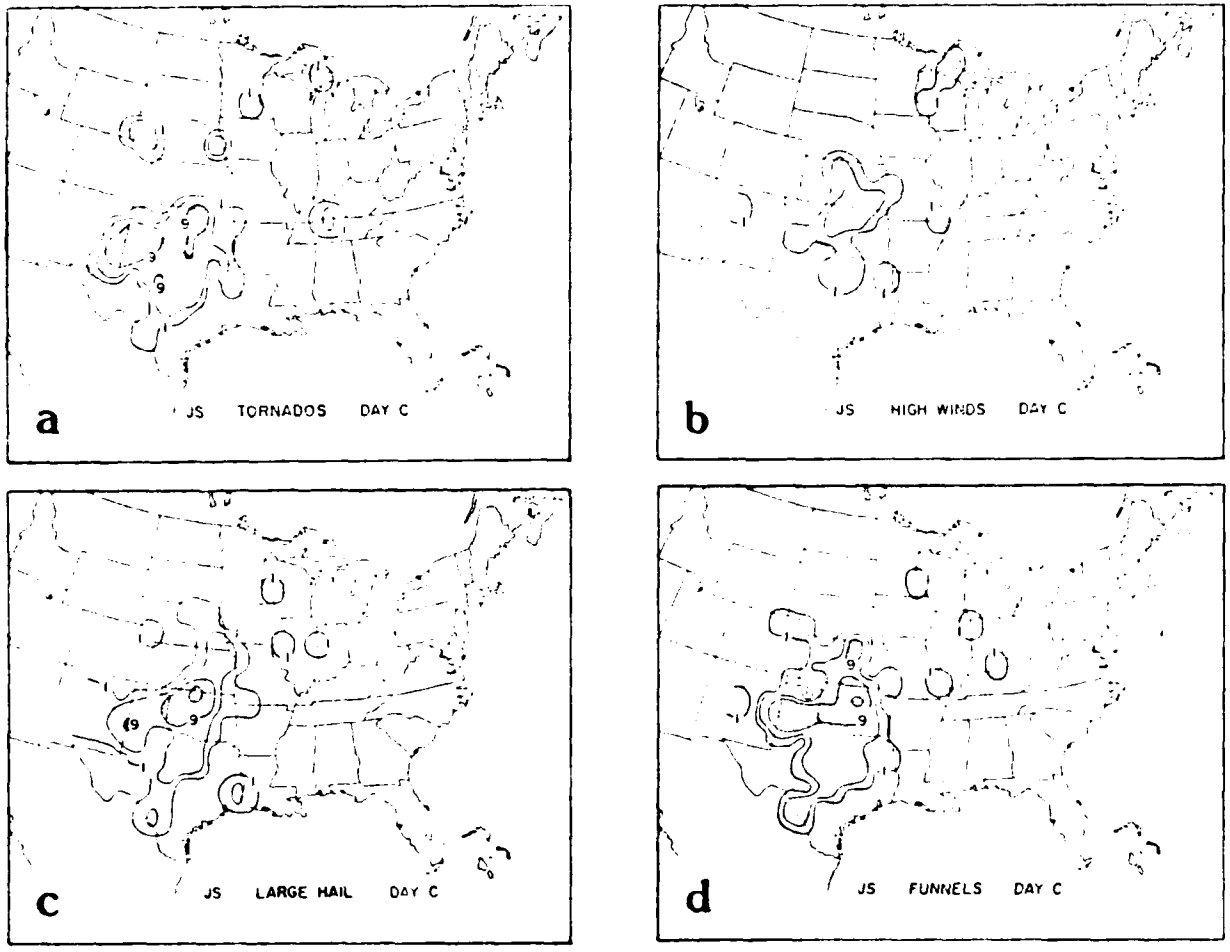

Fig. 8. Normalized and smoothed frequency (10^{-2}) of (a) tornados, (b) high winds ($\geq$ 26m/s), (c) large hail (> 19mm) and (d) funnel clouds for the JS subsample on day C.

of the various severe weather events are higher and cover a larger geographical area in the JS subsample, which was based on cyclogenetic events when a 300 mb jet streak was located in the New Mexico-Texas area on the day of cyclogenesis, than in the D sample. This feature is also evident in Figs. 9 a and b, which show the frequency of total severe storms (summation of the incidence of tornadoes, high winds, large hail and funnel clouds) for the D sample and the JS subsample. The maximum frequency of total severe storms for both samples is located over west central Oklahoma, but its magnitude is .705 for the JS subsample and only .391 for the D sample. The area enclosed by the .27 frequency isopleth is also greater in the JS subsample than in the D sample. Thus, the presence of a composite 300 mb jet streak confined to a limited geographical area in the JS subsample clearly enhances the frequency and coverage of severe weather compared with the composite of the 39 developing cyclones.

The high frequency of total severe storm events (Fig. 9a) over the southern Great Plains agrees with the findings of the moisture study by Marshment and Horn (1985). The vast majority of severe storm events for the D sample occurred in the warm, moist sector of the mean sea level low pressure center as it moved northeastward into western Kansas. Comparison with Marshment and Horn's results show that: (1) the western edge of the .09 frequency isopleth over the southern Great Plains closely coincides with the apparent composite dry line that existed on day 0 from western Texas into

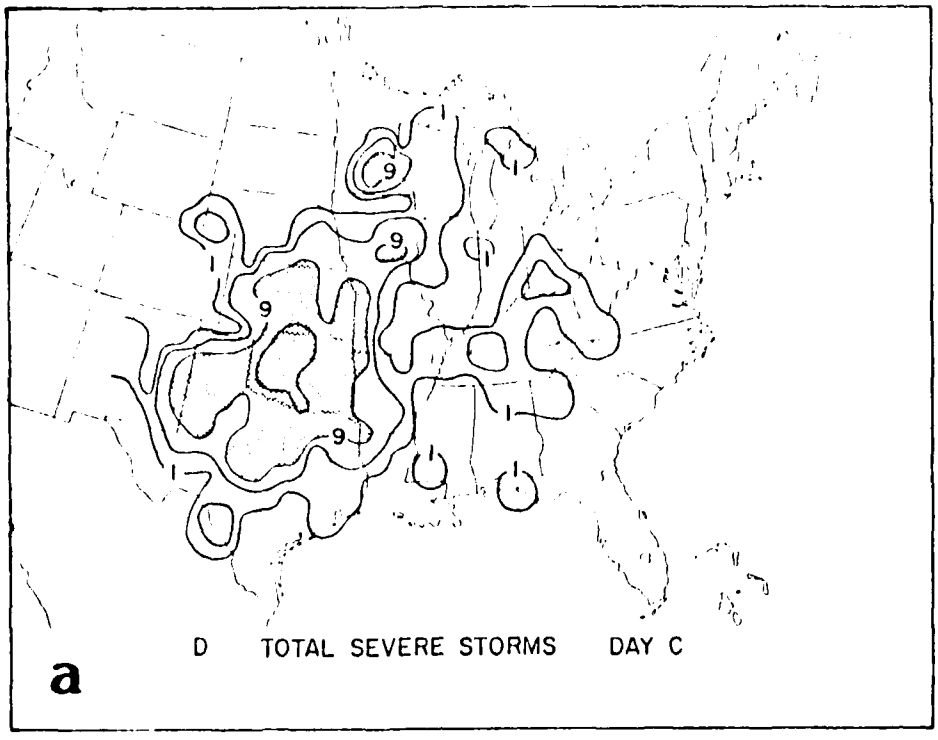

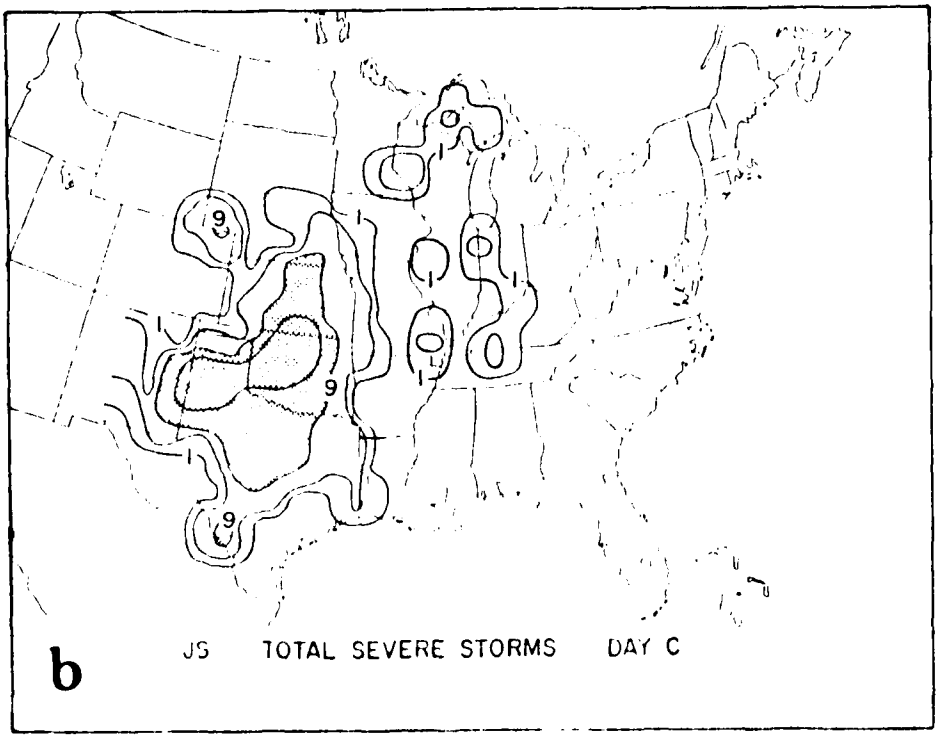

Fig. 9. Normalized and smoothed frequency (10^{-2}) of total severe storms on day C for the (a) D sample and (b) JS subsample.

western Kansas between the surface and 850 mb and (2) the moist static stability decreased during the day in the area enclosed by the .09 frequency isopleth. They suggested that the combination of moisture advection below 800 mb and the relatively dry air above this moist layer created a convectively unstable environment favorable for the occurrence of severe weather. The results obtained here support their statement.

Fig. 10 shows the 24 hour change in the lifted index, calculated by Marshment and Horn, between 1200 GMT day C and 1200 GMT day C+1 superimposed over the frequency of total severe storms greater than .09 for the D sample for day C. The incidence of severe local weather on day C is greatest along the western half of the region undergoing destabilization during the day. Note that the maximum frequency of total severe storms occurs in the vicinity of the strongest horizontal gradient of stability change over west central Oklahoma.

The relationship between the dynamic forcing mechanisms and the frequency of severe weather can be seen in Figs. 11 a and b, which show the 300 and 850 mb isotachs and streamlines at 1200 GMT and 0000 GMT superimposed over the frequency of total severe storms greater than .09 for the JS subsample. During this twelve hour period, the composite 300 mb jet streak intensified as it propagated eastward; and the 850 mb wind maximum moved to the north. Note that the 850 mb streamlines become more southerly resulting in an increase in the 850-300 mb directional wind shear over the southern Great Plains.

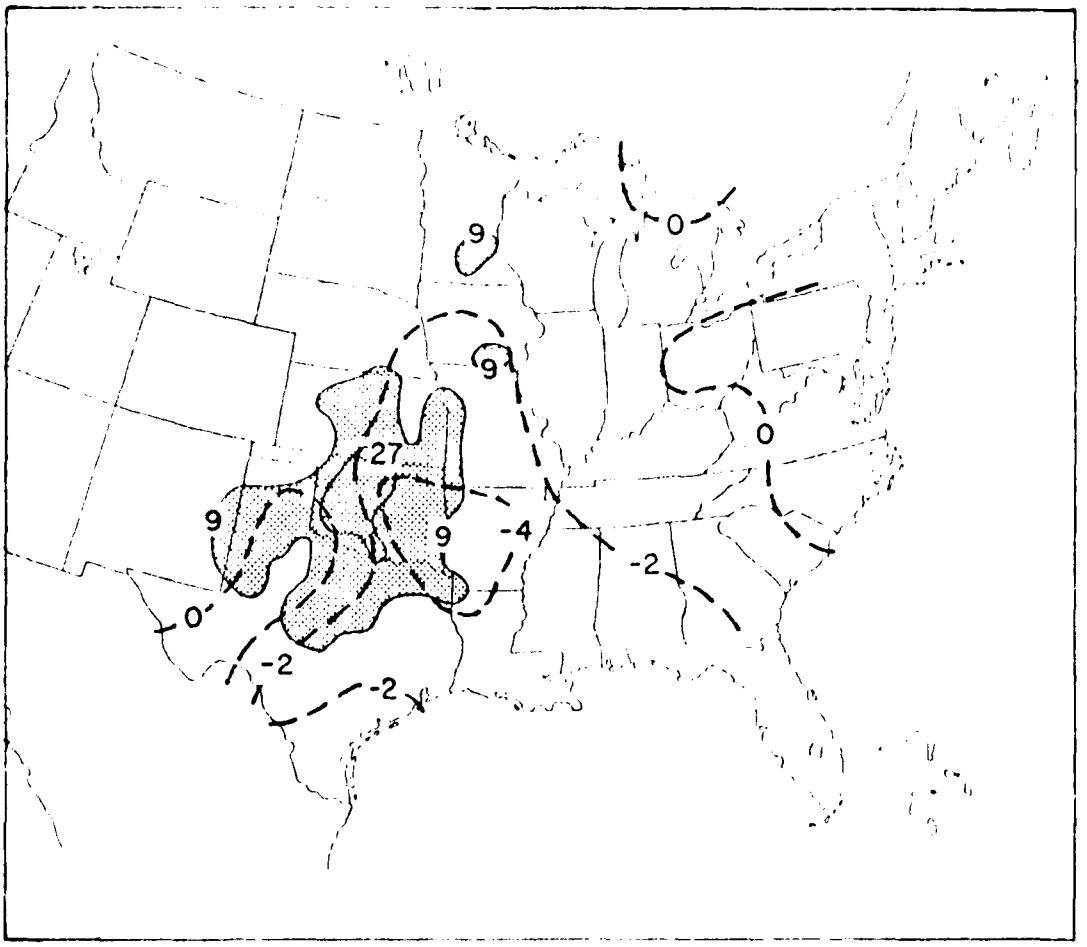

Fig. 10. Normalized and smoothed frequency (10^{-2}) of total severe storms for the D sample on day C superimposed over the 24 hour change in the lifted index from 1200 GMT, day C to 1200 GMT, day C+1.

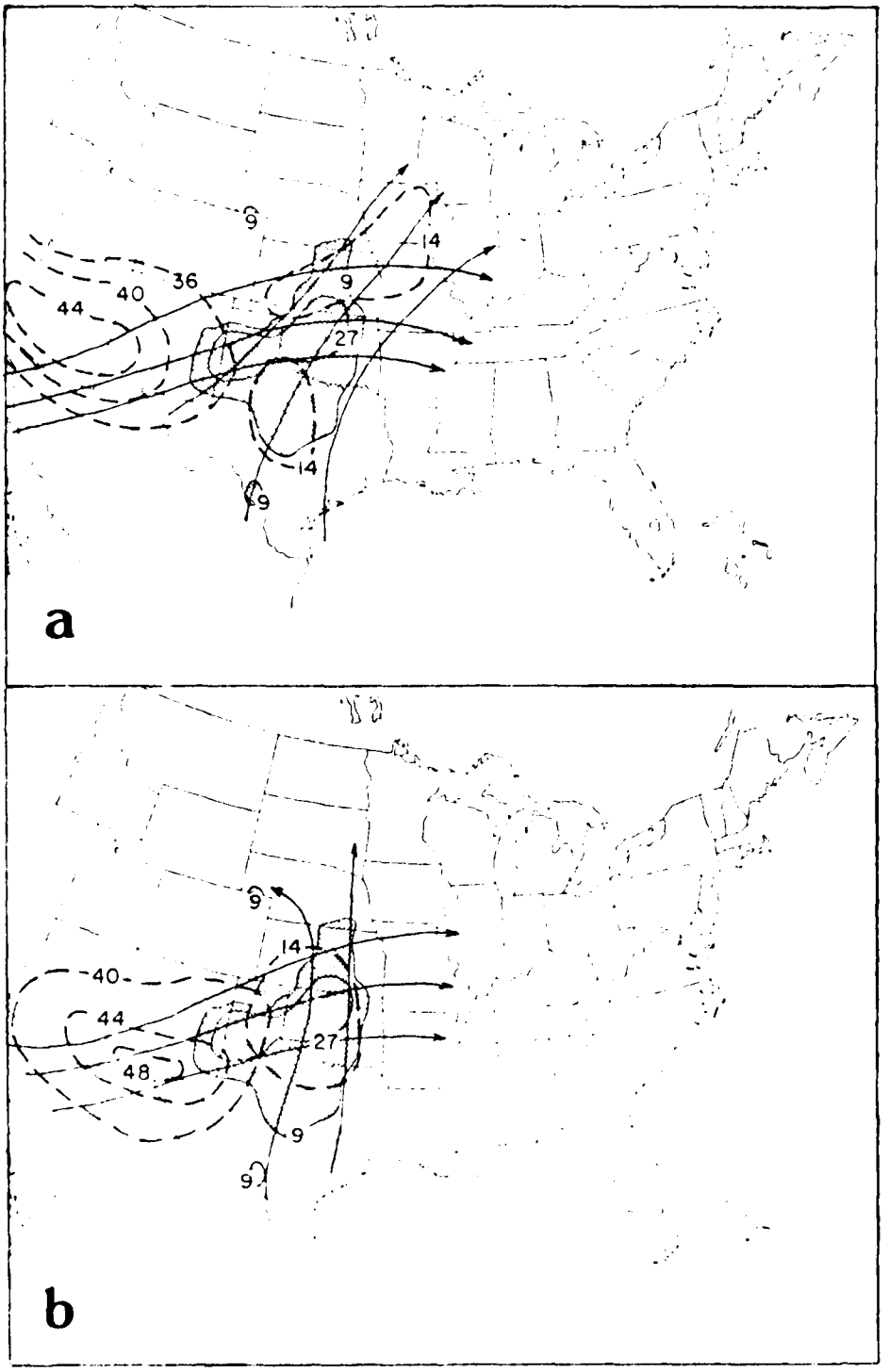

Fig. 11. Mean isotachs (m/s) and streamlines in the core areas of the 300 mb and 850 mb wind maxima on day C, superimposed over the normalized and smoothed frequency (10^{-2}) of total severe storms for the JS subsample at (a) 1200 GMT and (b) 0000 GMT.

The greatest incidence of severe weather occurs ahead of and to the right of the exit region of the propagating 300 mb wind maximum. This agrees with the concept of dynamic destabilization proposed by Johnson and Sechrist (1970) and Uccellini and Johnson (1979).

4.3 The observed severe weather frequency and distribution for day C+1

The normalized frequency of the total severe storms on day C+1 for sample D and the JS and JS' subsamples is shown in Figs. 12 a, b and c. The frequencies in the JS' subsample are noticeably weaker and more diffuse than those found in the JS sample. Compared to day C, there has been a major northeastward expansion of the area enclosed by the .09 frequency isopleth in the D and JS samples. This movement is consistent with the movement of the composite surface low from western Kansas to northwestern Iowa in the D sample. As was found on day C, the area enclosed by frequencies greater than .27 is larger in the JS subsample than in the D sample. The maximum frequency of total severe storms has increased for all three samples over the day C values. The highest frequency for both the D and JS samples is located near Kansas City, Missouri and is again greater in the JS subsample (.868) than in the D sample (.511). The maximum frequency of total severe storms for the JS' subsample is .515 and is located over western Oklahoma. The more southwesterly location of the highest incidence of total severe storms in the JS' subsample

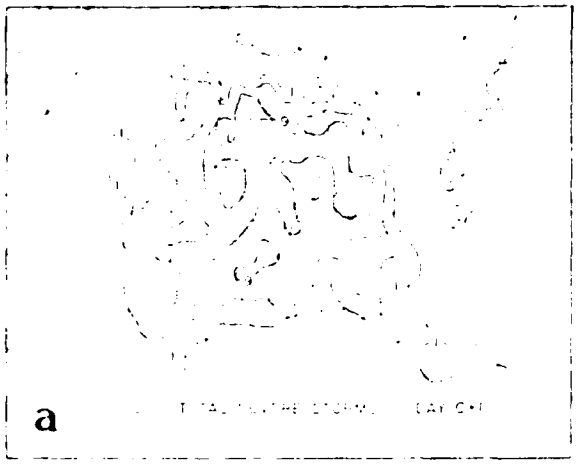

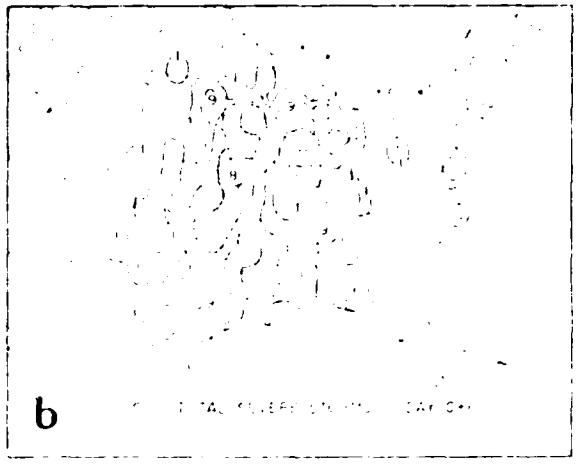

Fig. 12. Normalized and smoothed frequency (10^{-2}) of total severe storms on day C+1 for the (a) D sample, (b) JS subsample and (c) JS' subsample.

may be a result of two cases where a high incidence of severe weather occurred when there was an overlap between day C for one cyclone and and day C+1 for another cyclone within this sample. Some of the meteorological conditions at the beginning (1200 GMT) of day C+1 which helped to create a more favorable environment for the higher incidence of severe local weather compared with day C are: (1) stronger wind maxima at 300 and 850 mb, (2) a more intense mean surface low pressure center, (3) a broader and more northward extension of available low level moisture and (4) a weaker and more concentrated area of moist static stability. Maps of the frequencies of tornadoes, high winds, large hail and funnel clouds for the D sample and the JS subsample are contained in the Appendices and show a more diffuse pattern than those for day C. This is probably due to the divergence of the various storm tracks as the cyclones moved away from their sites of cyclogenesis.

Despite the various storm tracks, there is again an excellent relationship between the area of maximum incidence of severe weather and the location of the propagating 300 mb jet streak. Figs. 13 a and b show the 300 mb isotachs and streamlines at 1200 GMT and 0000 GMT superimposed over the frequency of total severe storms greater than .09 for the JS subsample. Note that the 300 mb jet streak maintains its intensity but becomes elongated by 0000 GMT. As in the previous day, the greatest incidence of severe weather occurs ahead of and to the right of the exit region of the propagating 300 mb wind maximum.

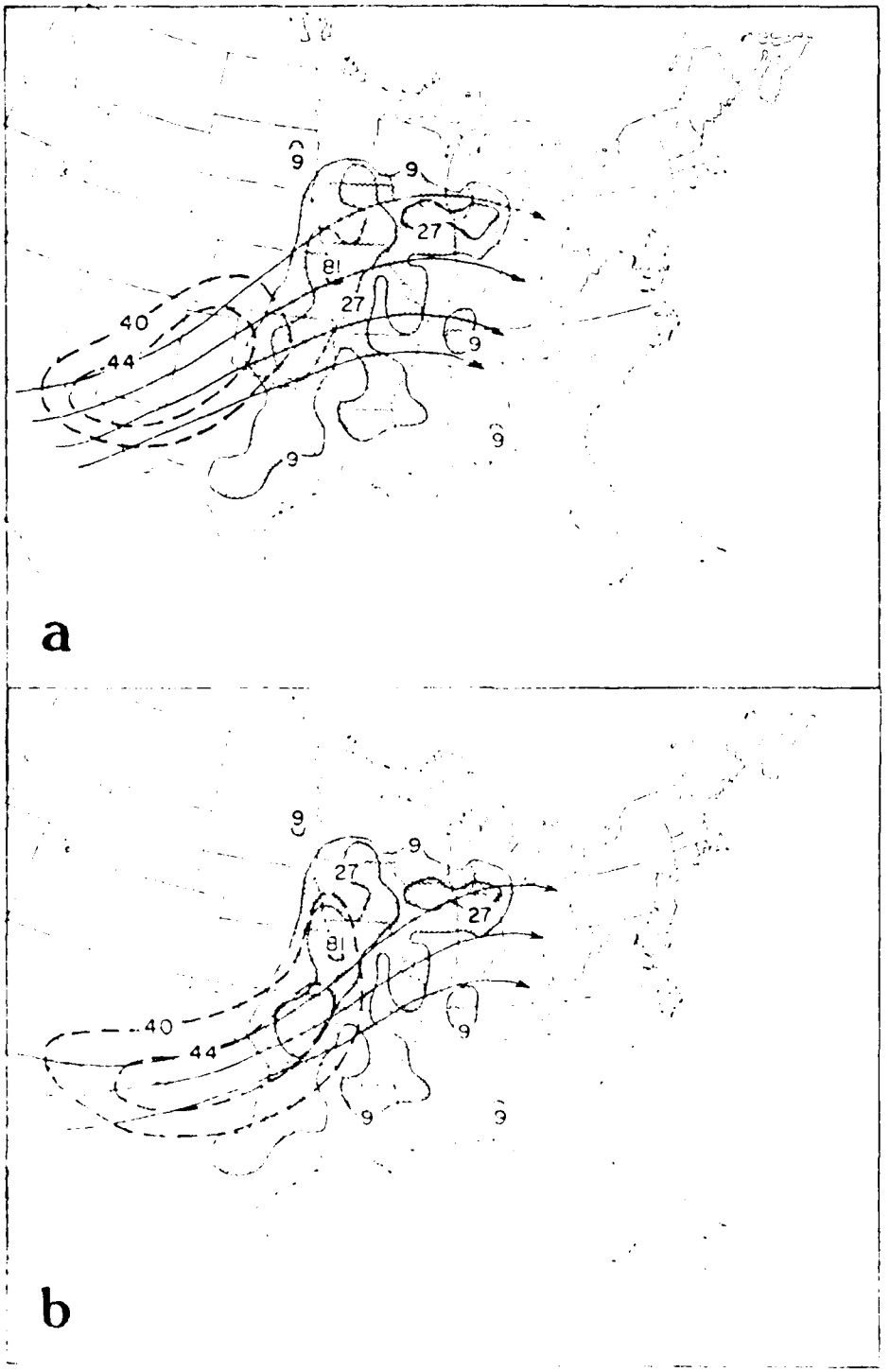

Fig. 15. Mean isotachs (m/s) and streamlines in the core area of the 300 mb wind maximum on day C+1, superimposed over the normalized and smoothed frequency (10^{-2}) of total severe storms for the JS subsample at (a) 1200 GMT and (b) 0000 GMT.

	105W							100W							095W							090W							085W							080W							075W
50N	0	0	0	0	0	0	0	0	0	0	0	0	0	0	0	0	0	0	0	0	0	0	0	0	0	0	0	0	0	0	0	0	0	0	0	0	0	0	0	0	0	0
49N	0	0	0	0	0	0	0	0	0	0	0	0	0	0	0	0	0	0	0	0	0	0	0	0	0	0	0	0	0	0	0	0	0	0	0	0	0	0	0	0	0	0
48N	0	0	0	0	0	0	0	0	0	0	0	0	0	0	0	0	0	0	0	0	0	0	0	0	0	0	0	0	0	0	0	0	0	0	0	0	0	0	0	0	0	0
47N	0	0	0	0	0	0	0	0	0	0	0	0	0	0	0	0	0	0	0	0	0	0	1	0	0	0	0	0	0	0	0	0	0	0	0	0	0	0	0	0	0	0
46N	0	0	0	0	0	0	0	0	0	0	0	0	0	0	0	0	0	0	2	1	0	0	1	0	0	0	0	0	0	0	0	0	0	0	0	0	0	0	0	0	0	0
45N	0	0	0	0	0	0	0	0	0	0	0	0	0	0	4	1	0	0	1	0	0	0	1	1	0	0	0	0	0	0	0	0	0	0	0	0	0	0	0	0	0	0
44N	0	0	0	0	0	0	0	0	0	0	0	0	4	8	2	2	0	1	0	0	0	0	1	0	0	0	0	0	0	0	0	0	0	0	0	0	0	0	0	0	0	0
43N	0	0	0	0	0	0	0	0	0	0	0	0	1	0	0	0	0	2	1	0	0	0	0	0	0	0	0	0	0	0	0	0	0	0	0	0	0	0	0	0	0	0
42N	0	0	0	0	0	0	0	1	0	1	0	0	0	0	0	0	2	0	0	0	0	0	0	0	0	0	0	0	0	0	0	0	0	0	0	0	0	0	0	0	0	0
41N	0	0	1	3	1	0	0	0	0	2	2	2	1	1	8	3	0	0	0	1	0	0	0	1	0	1	0	0	0	0	0	0	0	0	0	0	0	0	0	0	0	0
40N	0	0	1	0	3	0	0	0	1	2	2	1	1	2	3	0	2	0	0	1	0	0	1	0	0	0	0	0	0	0	0	0	0	0	0	0	0	0	0	0	0	0
39N	0	0	0	0	0	0	0	5	6	10	0	5	6	0	0	0	0	1	0	0	0	0	2	2	0	0	0	0	0	0	0	0	0	0	0	0	0	0	0	0	0	0
38N	0	0	0	0	0	3	7	3	2	3	1	7	7	4	0	0	0	0	0	0	0	2	1	0	3	0	0	0	0	0	0	0	0	0	0	0	0	0	0	0	0	0
37N	0	0	0	0	0	0	1	1	9	10	2	2	3	0	0	0	1	0	0	0	1	0	0	0	1	0	1	0	0	0	0	0	0	0	0	0	0	0	0	0	0	0
36N	0	0	0	0	1	0	0	3	15	27	9	5	11	1	0	0	1	1	2	3	2	1	0	0	1	2	0	0	0	0	0	0	0	0	0	0	0	0	0	0	0	0
35N	1	1	0	0	2	3	3	25	10	10	4	6	4	1	1	0	1	0	0	0	1	0	0	0	0	0	0	0	0	0	0	0	0	0	0	0	0	0	0	0	0	0
34N	1	0	0	10	9	12	6	5	10	15	12	12	2	1	2	0	0	0	0	1	1	1	2	1	0	0	0	0	0	0	0	0	0	0	0	0	0	0	0	0	0	0
33N	0	1	0	4	10	7	1	2	6	10	9	6	2	3	4	0	0	0	0	0	0	0	1	0	0	0	0	0	0	0	0	0	0	0	0	0	0	0	0	0	0	0
32N	0	0	1	2	3	8	3	6	6	11	1	0	7	5	0	0	0	0	0	0	0	0	0	0	0	0	0	0	0	0	0	0	0	0	0	0	0	0	0	0	0	0
31N	0	0	0	0	4	0	2	12	5	4	2	0	0	0	0	0	2	0	0	0	0	0	0	0	0	1	0	0	0	0	0	0	0	0	0	0	0	0	0	0	0	0
30N	0	0	0	0	0	0	0	2	3	0	0	0	1	1	0	0	0	0	0	0	2	0	1	0	0	0	0	0	0	0	0	0	0	0	0	0	0	0	0	0	0	0
29N	0	0	0	0	0	0	2	0	0	0	0	2	0	0	0	0	0	0	0	0	0	0	0	0	0	0	0	0	0	0	0	0	0	0	0	0	0	0	0	0	0	0
28N	0	0	0	0	0	0	5	1	0	0	0	0	0	0	0	0	0	0	0	0	0	0	0	0	0	0	0	0	0	0	0	0	0	0	0	0	0	0	0	0	0	0
27N	0	0	0	0	0	0	0	0	0	0	0	0	0	0	0	0	0	0	0	0	0	0	0	0	0	0	0	0	0	0	0	0	0	0	0	0	0	0	0	0	0	0
26N	0	0	0	0	0	0	0	0	0	0	0	0	0	0	0	0	0	0	0	0	0	0	0	0	0	0	0	0	0	0	0	1	0	0	0	0	0	0	0	0	0	0
25N	0	0	0	0	0	0	0	0	0	0	0	0	0	0	0	0	0	0	0	0	0	0	0	0	0	0	0	0	0	0	0	0	0	0	0	0	0	0	0	0	0	0

lable A7. The total number of severe storm events per 1° latitude-longitude grid box on day C for the D sample.

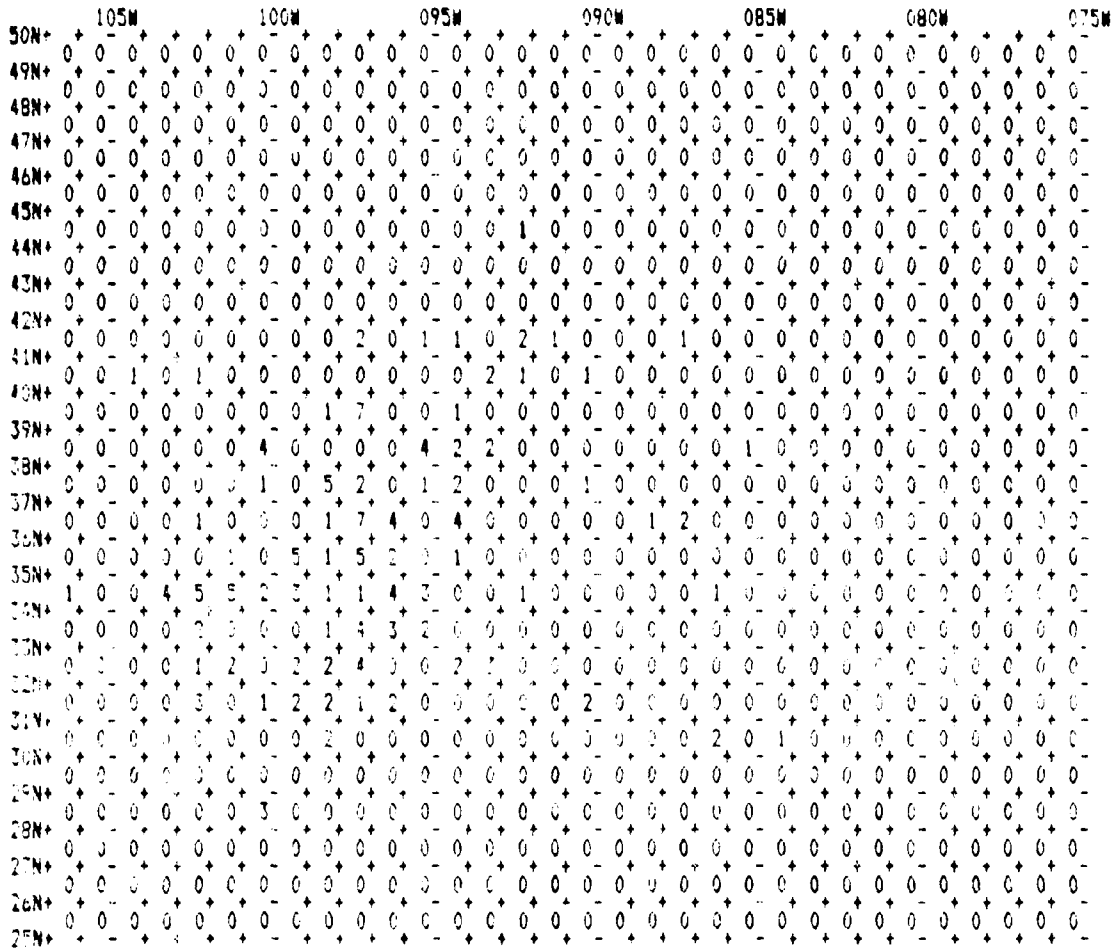

Table A6. The total number of funnel cloud genesis events per 1 latitude-longitude grid box on day C for the D sample.

	105W	100W	095W	090W	085W	080W	075W
50N	0 0 0 0 0 0 0 0 0 0 0 0 0 0 0 0 0 0 0 0 0 0 0 0 0 0 0 0 0 0 0						
49N	0 0 0 0 0 0 0 0 0 0 0 0 0 0 0 0 0 0 0 0 0 0 0 0 0 0 0 0 0 0 0						
48N	0 0 0 0 0 0 0 0 0 0 0 0 0 0 0 0 0 0 0 0 0 0 0 0 0 0 0 0 0 0 0						
47N	0 0 0 0 0 0 0 0 0 0 0 0 0 0 0 0 0 0 0 0 0 0 0 0 0 0 0 0 0 0 0						
46N	0 0 0 0 0 0 0 0 0 0 0 0 0 0 0 0 0 0 0 0 0 0 0 0 0 0 0 0 0 0 0						
45N	0 0 0 0 0 0 0 0 0 0 0 0 0 0 0 0 0 0 0 0 0 0 0 0 0 0 0 0 0 0 0						
44N	0 0 0 0 0 0 0 0 0 0 0 0 0 0 1 0 0 0 0 0 0 0 0 0 0 0 0 0 0 0 0						
43N	0 0 0 0 0 0 0 0 0 0 0 0 0 0 0 0 0 0 0 0 0 0 0 0 0 0 0 0 0 0 0						
42N	0 0 0 0 0 0 0 0 0 0 0 0 0 0 0 0 0 0 0 0 0 0 0 0 0 0 0 0 0 0 0						
41N	0 0 0 0 0 0 0 0 0 2 0 1 1 0 2 1 0 0 0 1 0 0 0 0 0 0 0 0 0 0 0						
40N	0 0 1 0 1 0 0 0 0 0 0 0 0 2 1 0 1 0 0 0 0 0 0 0 0 0 0 0 0 0 0						
39N	0 0 0 0 0 0 0 0 1 7 0 0 1 0 0 0 0 0 0 0 0 0 0 0 0 0 0 0 0 0 0						
38N	0 0 0 0 0 0 4 0 0 0 0 4 2 2 0 0 0 0 0 0 0 1 0 0 0 0 0 0 0 0 0						
37N	0 0 0 0 0 0 1 0 5 2 0 1 2 0 0 0 1 0 0 0 0 0 0 0 0 0 0 0 0 0 0						
36N	0 0 0 0 1 0 0 0 1 7 4 0 4 0 0 0 0 0 1 2 0 0 0 0 0 0 0 0 0 0 0						
35N	0 0 0 0 0 1 0 5 1 5 2 0 1 0 0 0 0 0 0 0 0 0 0 0 0 0 0 0 0 0 0						
34N	1 0 0 4 5 5 2 3 1 1 4 3 0 0 1 0 0 0 0 0 1 0 0 0 0 0 0 0 0 0 0						
33N	0 0 0 0 2 0 0 0 1 4 3 2 0 0 0 0 0 0 0 0 0 0 0 0 0 0 0 0 0 0 0						
32N	0 0 0 0 1 2 0 2 2 4 0 0 2 3 0 0 0 0 0 0 0 0 0 0 0 0 0 0 0 0 0						
31N	0 0 0 0 3 0 1 2 2 1 2 0 0 0 0 0 2 0 0 0 0 0 0 0 0 0 0 0 0 0 0						
30N	0 0 0 0 0 0 0 0 2 0 0 0 0 0 0 0 0 0 0 0 2 0 1 0 0 0 0 0 0 0 0						
29N	0 0 0 0 0 0 0 0 0 0 0 0 0 0 0 0 0 0 0 0 0 0 0 0 0 0 0 0 0 0 0						
28N	0 0 0 0 0 0 3 0 0 0 0 0 0 0 0 0 0 0 0 0 0 0 0 0 0 0 0 0 0 0 0						
27N	0 0 0 0 0 0 0 0 0 0 0 0 0 0 0 0 0 0 0 0 0 0 0 0 0 0 0 0 0 0 0						
26N	0 0 0 0 0 0 0 0 0 0 0 0 0 0 0 0 0 0 0 0 0 0 0 0 0 0 0 0 0 0 0						
25N	0 0 0 0 0 0 0 0 0 0 0 0 0 0 0 0 0 0 0 0 0 0 0 0 0 0 0 0 0 0 0						

Table A5. The total number of funnel cloud events per 1° latitude-longitude grid box on day C for the D sample.

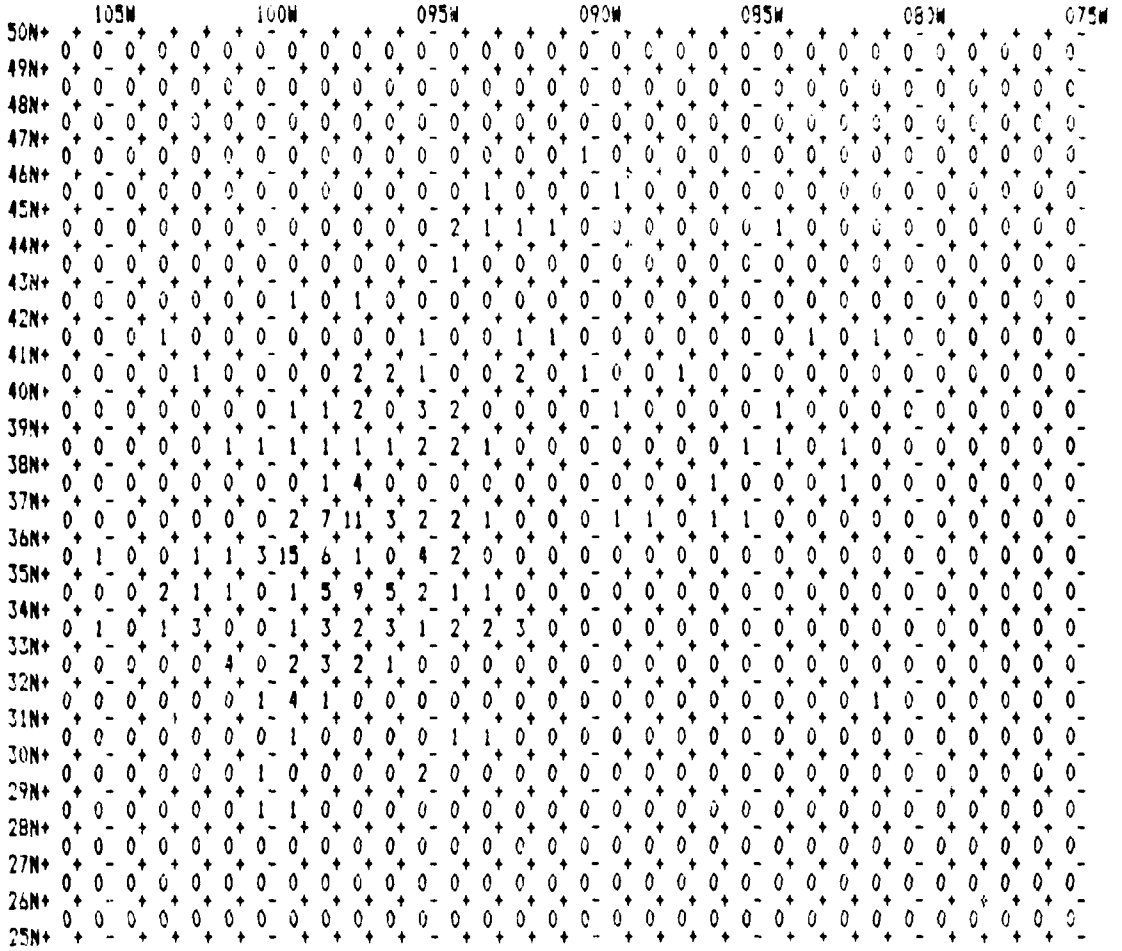

Table A4. The total number of large hail (≥ 19mm) events per 1° latitude-longitude grid box on day C for the D sample.

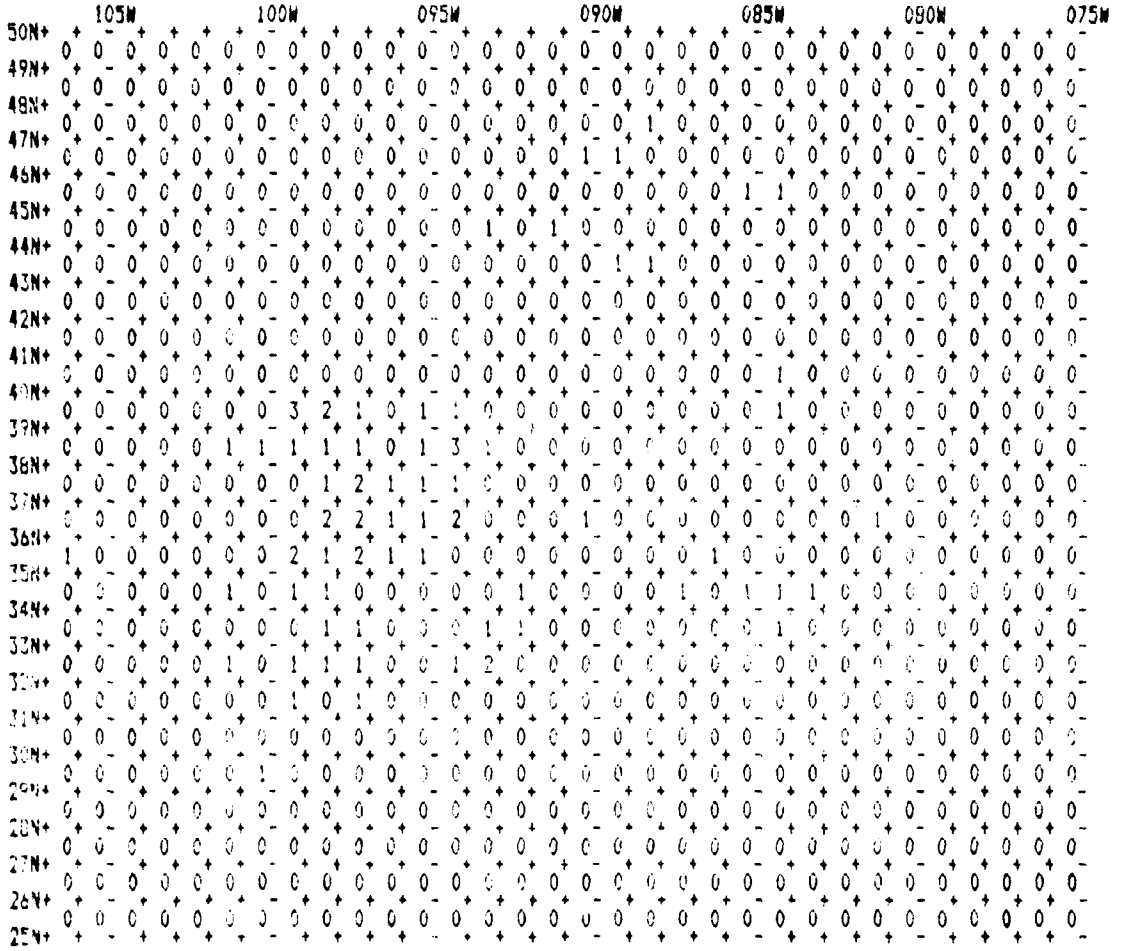

Table A3. The total number of high wind (> 20 m/s) events per 1 latitude-longitude grid box or day C for the D sample.

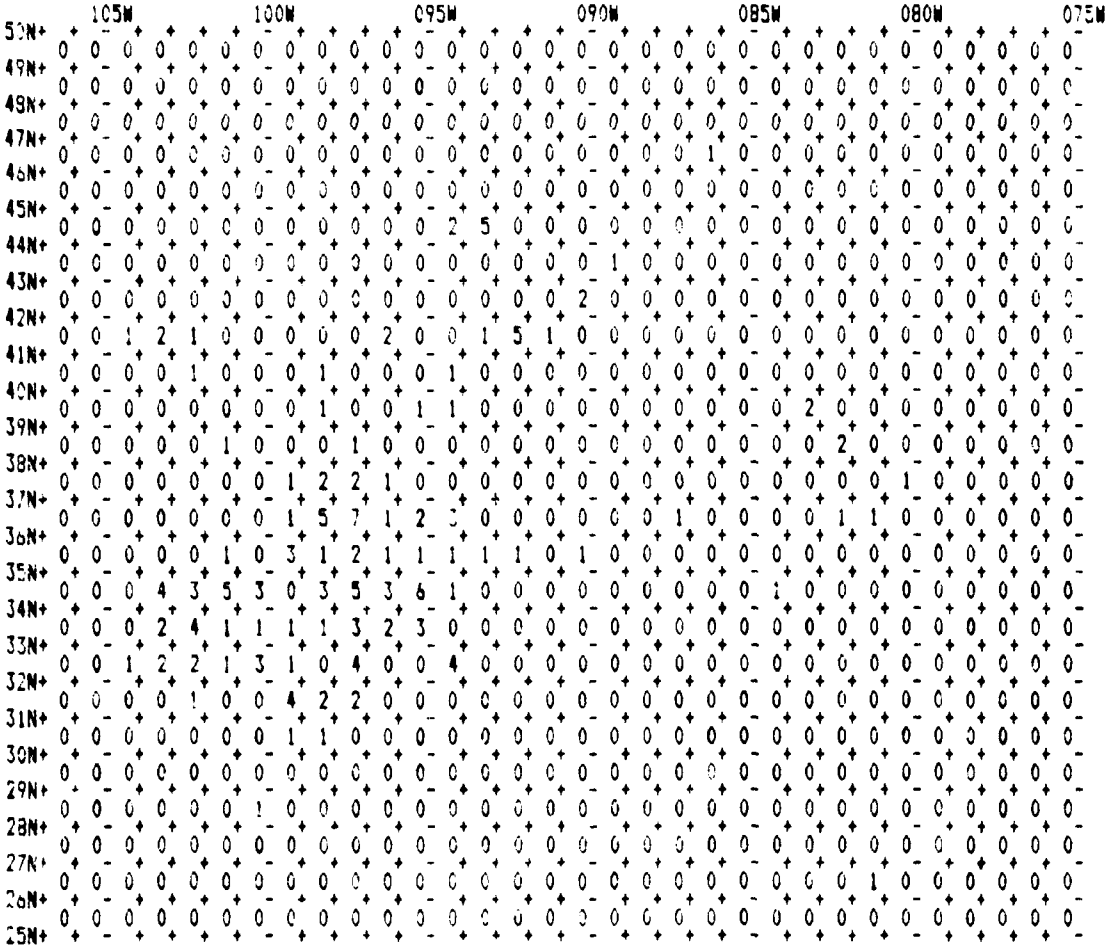

Table A2. The total number of tornado genesis events per 1 latitude-longitude grid box on day 0 for the D sample.

Appendix A. Total Severe Weather Events For Day C

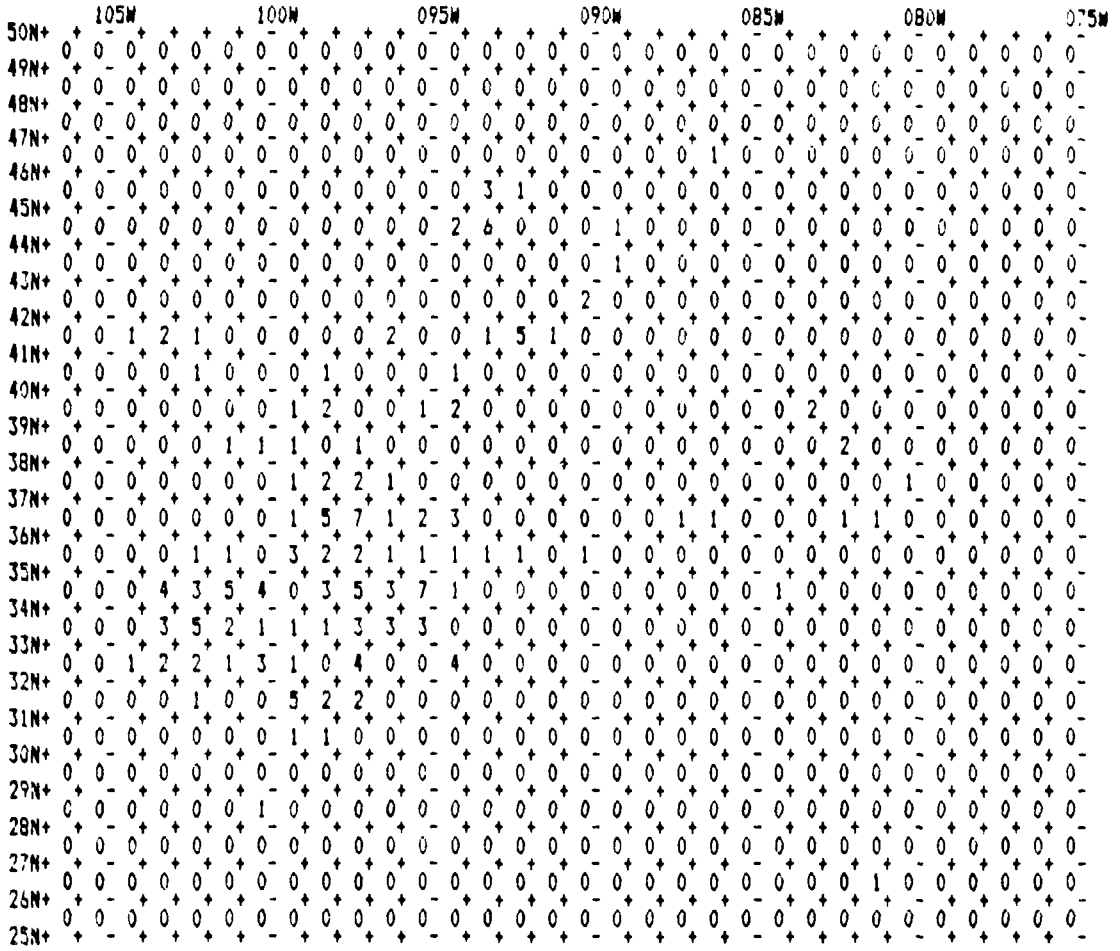

Table A1. The total number of tornado events per 1° latitude-longitude grid box on day C for the D sample.

300 and 850 mb, (2) a more intense mean mean surface low pressure center, (3) a more northward extension and a sharper horizontal gradient of available low level moisture and (4) a weaker and more concentrated area of moist static stability.

development site. On the day of cyclogenesis the severe weather events for all three samples were generally confined to a compact area extending from central Texas into Kansas. The area where severe weather occurred significantly broadened and moved northeastward on the two days following cyclogenesis. The distinct broadening of this area is probably a result of the various cyclone tracks and speed of movement of the cyclones contained in the D sample and the JS and JS' subsamples.

The relationship between the dynamic upper-tropospheric forcing mechanisms and the frequency of severe weather was examined for the JS subsample. For all three days the greatest incidence of severe weather occurred ahead of and to the right of the exit region of the propagating 300 mb wind maximum. The presence of the composite 300 mb jet streak, initially confined to a limited geographical area, in the JS subsample clearly enhanced the frequency of severe weather compared to the composites of the D sample and the JS' subsample. The JS subsample had the highest incidence of severe weather on each of the three days of the study.

The maximum frequency of total severe storms for the D sample and the JS and JS' subsamples was highest on day C+1 and lowest on day C+2. This was consistent with the results of the moisture study by Marshment and Horn and the study of upper and lower-troposheric wind fields by Achtor and Horn. Some meteorological conditions which favored the higher incidence of severe weather on day C+1 compared with the other samples are: (1) stronger composite wind maxima at

5. Conclusions

The great majority of spring season thunderstorms that produce severe weather in the central United States are associated with Colorado cyclogenesis. This study was based on 39 developing cases (those which formed and persisted for at least 72 hours) of spring season Colorado cyclone events chosen by Hovanec and Horn (1975) and later studied by Achtor and Horn (1985) and Marshment and Horn (1985). The research used a composite approach to investigate the evolution of severe weather events throughout the cyclogenetic process and the distribution of these events in relation to dynamic forcing mechanisms. The study also examined the incidence of severe weather during a subsample of 15 "jet streak" cases, selected from the 39 developing cases by Achtor and Horn, and a complement subsample of the 24 cases not contained in the jet streak subsample. To avoid diurnal variations the data set was partitioned into three 24 hour intervals with the first one beginning at 1200 GMT on the day of cyclogenesis. Composites were prepared for the normalized frequency of (1) tornadoes, (2) high winds, (3) large hail, (4) funnel clouds and (5) total severe storms (summation of items (1) to (4)) for the 39 day developing sample and the two subsamples for day C, C+1 and C+2.

The distribution of severe weather for the three days of the study was consistent with the movement of the mean synoptic features as the composite cyclone developed and moved away from its lee side

of the occurrence of severe weather in the JS' subsample is the widely divergent storm tracks contained in this period of the study. The reduced frequency of severe weather on day C+2 is consistent with the results of Achtor/Horn and Marshment/Horn. Their findings indicated a more southwesterly and weaker flow at low-levels which in the composite reduced the advection of moisture from the Gulf of Mexico. This resulted in an increase in moist static stability over the Mississippi and Ohio valleys. Of the three days of this study, Achtor and Horn found that day C+2 had the weakest 850-300 mb directional wind shear in the exit region of the composite 300 mb jet streak.

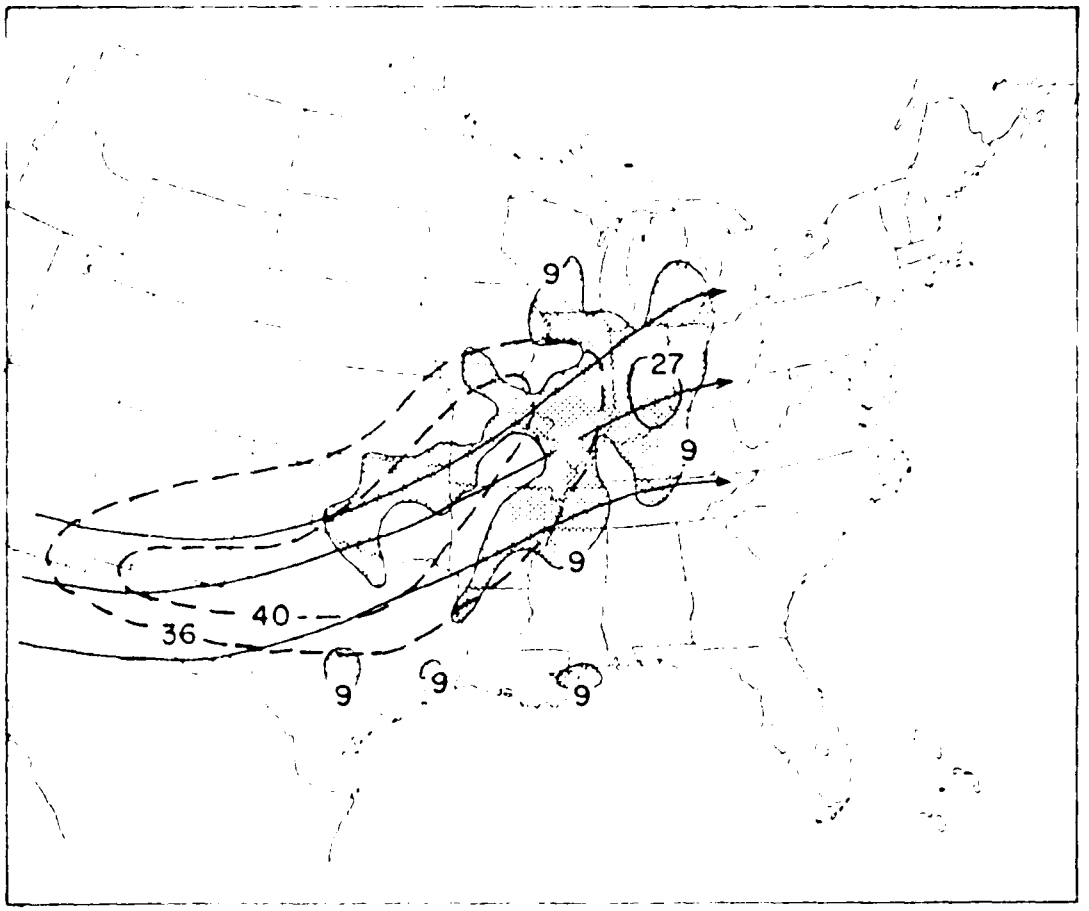

Fig. 15. Mean isotachs (m/s) and streamlines in the core of the 300 mb wind maximum on day C+2 at 1200 GMT superimposed over the normalized and smoothed frequency (10^{-4}) of total severe storms for the JS subsample.

4.4 The observed severe weather frequency and distribution for day C+2

Figs. 14 a, b and c show the incidence of total severe storms for day C+2 for sample D and the JS and JS' subsamples. Compared to day C+1, there has been a noticeable decrease in the frequency of severe local weather. For all three samples during the period of this study, day C+2 has the lowest maximum frequency of total severe storms. The JS subsample again has a higher maximum frequency of total severe storms than the D or JS samples. The relationship between the incidence of severe weather for the JS subsample and the upper-tropospheric jet streak is shown in Fig. 15. The maximum frequency for the JS sample, located over Indiana, occurs in the right front quadrant of the composite 300 mb jet streak at 1200 GMT. A comparison between Figs. 14 b and c shows that frequencies greater than .09 generally occur to the east of the Mississippi River in the JS subsample and to the west of the Mississippi River in the JS' subsample. Recall that on day C+1 (Figs. 12 b and c) there was a noticeable difference in location of the maximum frequency of total severe storms between the JS and JS' subsamples. The more westerly location of the area of severe weather in the JS' subsample on day C+2 may again be a result of overlapping. There were two cases in the JS' subsample where a high incidence of severe weather occurred when there was an overlap between day C+1 for one cyclone and day C+2 for another. Another explanation for the more westerly location

4.4 The observed severe weather frequency and distribution for day C+2

Figs. 14 a, b and c show the incidence of total severe storms for day C+2 for sample D and the JS and JS' subsamples. Compared to day C+1, there has been a noticeable decrease in the frequency of severe local weather. For all three samples during the period of this study, day C+2 has the lowest maximum frequency of total severe storms. The JS subsample again has a higher maximum frequency of total severe storms than the D or JS samples. The relationship between the incidence of severe weather for the JS subsample and the upper-tropospheric jet streak is shown in Fig. 15. The maximum frequency for the JS sample, located over Indiana, occurs in the right front quadrant of the composite 300 mb jet streak at 1200 GMT. A comparison between Figs. 14 b and c shows that frequencies greater than .09 generally occur to the east of the Mississippi River in the JS subsample and to the west of the Mississippi River in the JS' subsample. Recall that on day C+1 (Figs. 12 b and c) there was a noticeable difference in location of the maximum frequency of total severe storms between the JS and JS' subsamples. The more westerly location of the area of severe weather in the JS' subsample on day C+2 may again be a result of overlapping. There were two cases in the JS' subsample where a high incidence of severe weather occurred when there was an overlap between day C+1 for one cyclone and day C+2 for another. Another explanation for the more westerly location

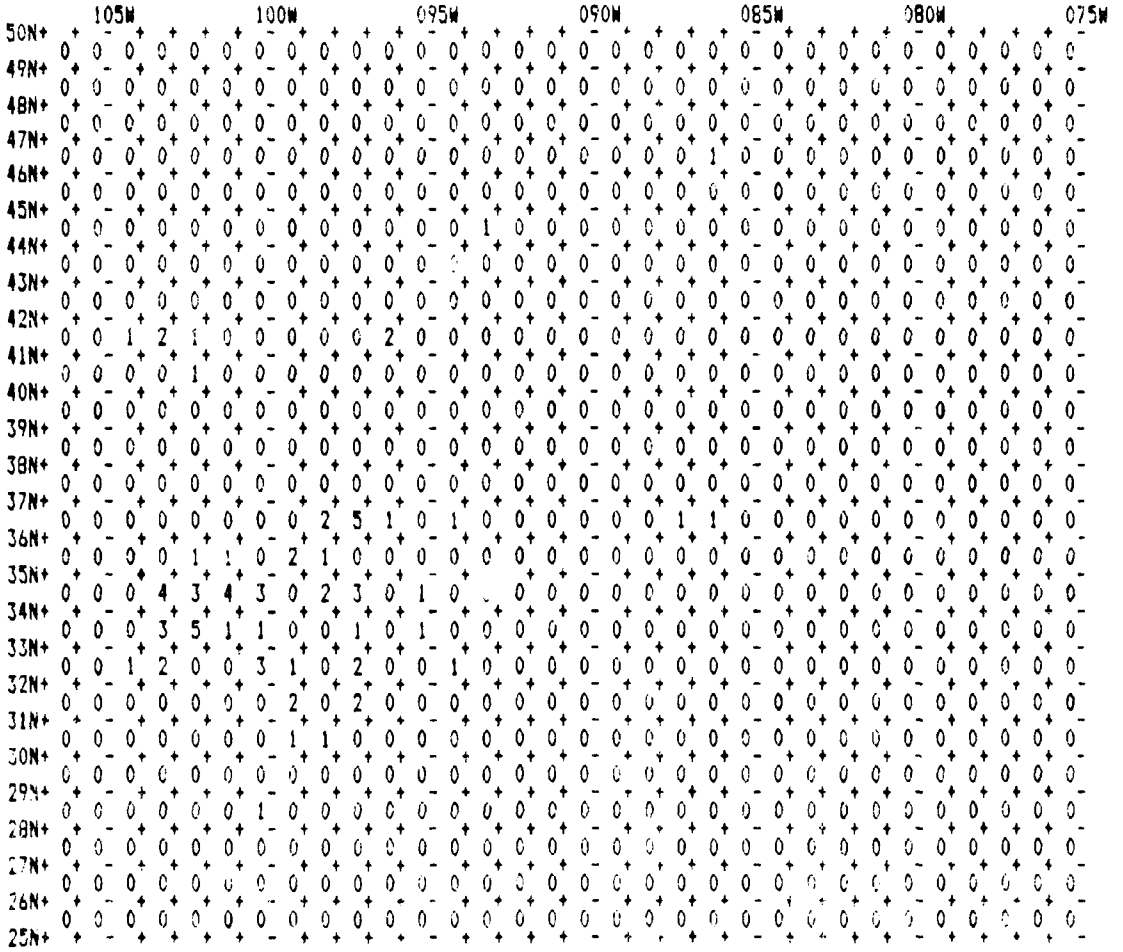

Table A8. The total number of tornado events per 1 latitude-longitude grid box on day C for the JS subsample.

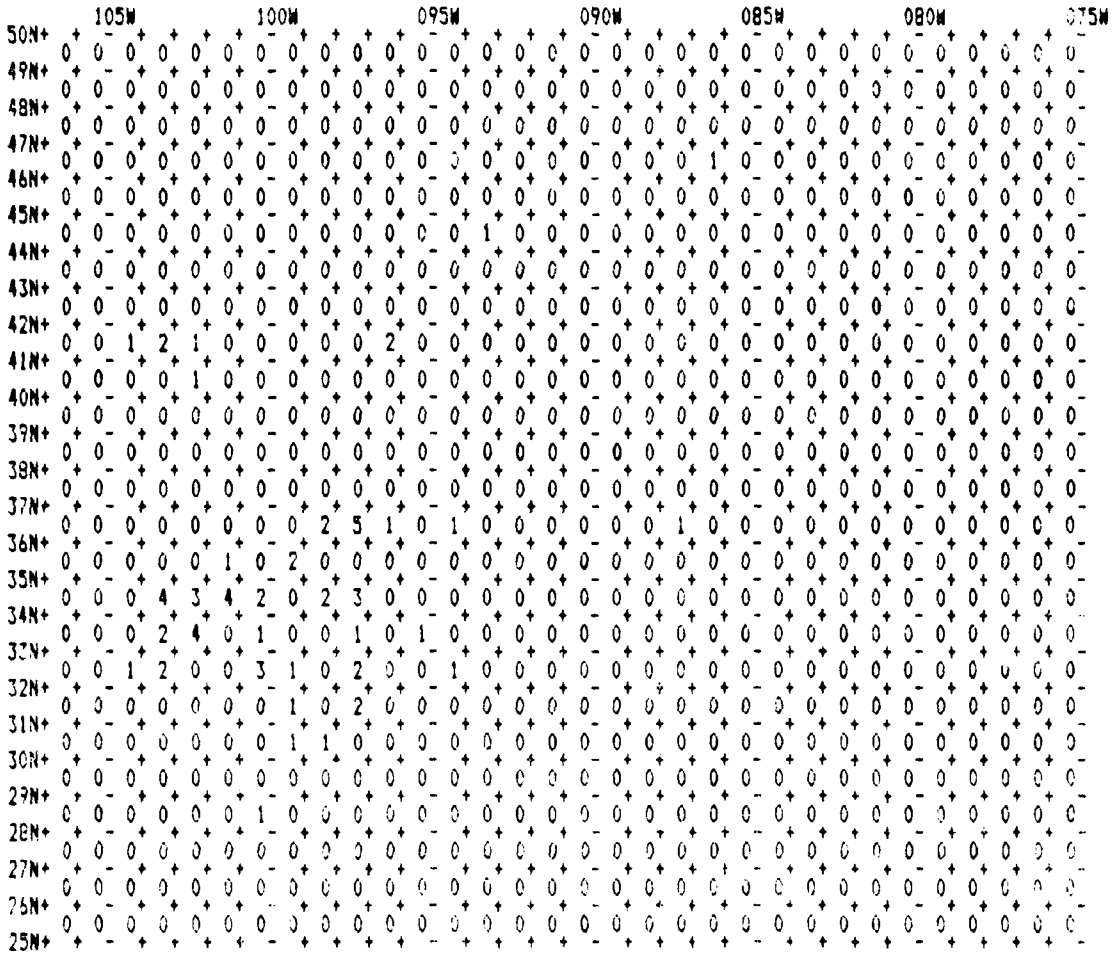

Table A9. The total number of tornado genesis events per 1° latitude-longitude grid box on day C for the JS subsample.

	105W	100W	095W	090W	085W	080W	075W
50N	0 0 0 0 0 0 0 0 0 0 0 0 0 0 0 0 0 0 0 0 0 0 0 0 0 0 0 0 0 0 0						
49N	0 0 0 0 0 0 0 0 0 0 0 0 0 0 0 0 0 0 0 0 0 0 0 0 0 0 0 0 0 0 0						
48N	0 0 0 0 0 0 0 0 0 0 0 0 0 0 0 0 0 0 0 0 0 0 0 0 0 0 0 0 0 0 0						
47N	0 0 0 0 0 0 0 0 0 0 0 0 0 0 0 0 0 0 0 0 0 0 0 0 0 0 0 0 0 0 0						
46N	0 0 0 0 0 0 0 0 0 0 0 0 0 0 0 0 0 0 0 0 0 0 0 0 0 0 0 0 0 0 0						
45N	0 0 0 0 0 0 0 0 0 0 0 0 0 0 0 0 0 0 0 0 0 0 0 0 0 0 0 0 0 0 0						
44N	0 0 0 0 0 0 0 0 0 0 0 0 0 0 0 0 0 0 0 0 0 0 0 0 0 0 0 0 0 0 0						
43N	0 0 0 0 0 0 0 0 0 0 0 0 0 0 0 0 0 0 0 0 0 0 0 0 0 0 0 0 0 0 0						
42N	0 0 0 0 0 0 0 0 0 0 0 0 0 0 0 0 0 0 0 0 0 0 0 0 0 0 0 0 0 0 0						
41N	0 0 0 0 0 0 0 0 0 0 0 0 0 0 0 0 0 0 0 0 0 0 0 0 0 0 0 0 0 0 0						
40N	0 0 0 0 0 0 0 0 0 0 0 0 0 0 0 0 0 0 0 0 0 0 0 0 0 0 0 0 0 0 0						
39N	0 0 0 0 0 0 0 1 1 0 0 0 0 0 0 0 0 0 0 0 0 0 0 0 0 0 0 0 0 0 0						
38N	0 0 0 0 0 0 0 0 1 1 0 0 1 0 0 0 0 0 0 0 0 0 0 0 0 0 0 0 0 0 0						
37N	0 0 0 0 0 0 0 0 0 0 1 1 0 0 0 0 0 0 0 0 0 0 0 0 0 0 0 0 0 0 0						
36N	0 0 0 0 0 0 0 0 0 2 2 1 0 0 0 0 0 1 0 0 0 0 0 0 0 0 0 0 0 0 0						
35N	1 0 0 0 0 0 0 0 1 1 0 0 0 0 0 0 0 0 0 0 0 0 0 0 0 0 0 0 0 0 0						
34N	0 0 0 0 0 1 0 0 0 0 0 0 0 0 0 0 0 0 0 0 0 0 0 0 0 0 0 0 0 0 0						
33N	0 0 0 0 0 0 0 0 0 1 0 0 0 0 0 0 0 0 0 0 0 0 0 0 0 0 0 0 0 0 0						
32N	0 0 0 0 0 0 0 0 1 1 0 0 1 0 0 0 0 0 0 0 0 0 0 0 0 0 0 0 0 0 0						
31N	0 0 0 0 0 0 0 0 0 0 0 0 0 0 0 0 0 0 0 0 0 0 0 0 0 0 0 0 0 0 0						
30N	0 0 0 0 0 0 0 0 0 0 0 0 0 0 0 0 0 0 0 0 0 0 0 0 0 0 0 0 0 0 0						
29N	0 0 0 0 0 0 0 0 0 0 0 0 0 0 0 0 0 0 0 0 0 0 0 0 0 0 0 0 0 0 0						
28N	0 0 0 0 0 0 0 0 0 0 0 0 0 0 0 0 0 0 0 0 0 0 0 0 0 0 0 0 0 0 0						
27N	0 0 0 0 0 0 0 0 0 0 0 0 0 0 0 0 0 0 0 0 0 0 0 0 0 0 0 0 0 0 0						
26N	0 0 0 0 0 0 0 0 0 0 0 0 0 0 0 0 0 0 0 0 0 0 0 0 0 0 0 0 0 0 0						
25N	0 0 0 0 0 0 0 0 0 0 0 0 0 0 0 0 0 0 0 0 0 0 0 0 0 0 0 0 0 0 0						

Table A10. The total number of high wind (≥ 26 m/s) events per 1° latitude-longitude grid box on day C for the JS subsample.

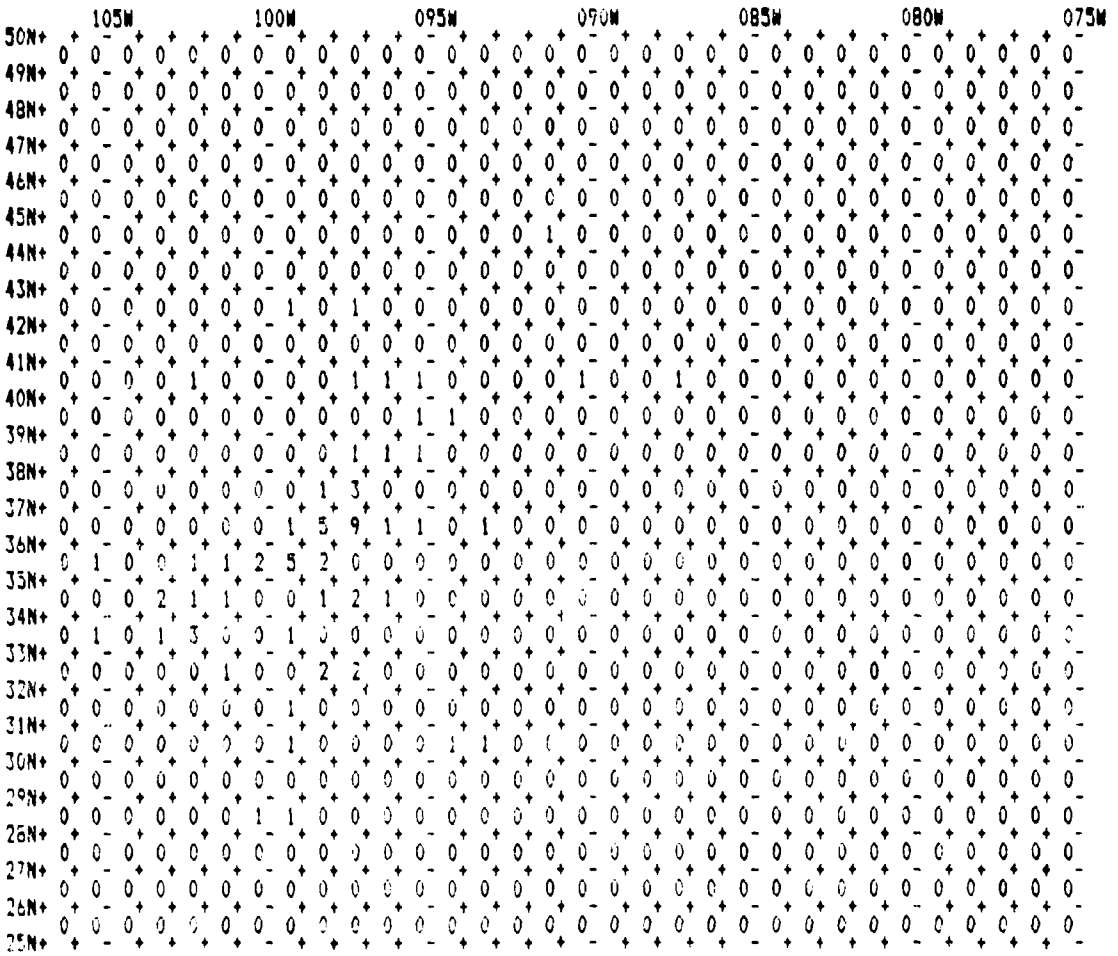

Table A11. The total number of large hail (> 19mm) events per 1 latitude-longitude grid box on day C for the JS subsample.

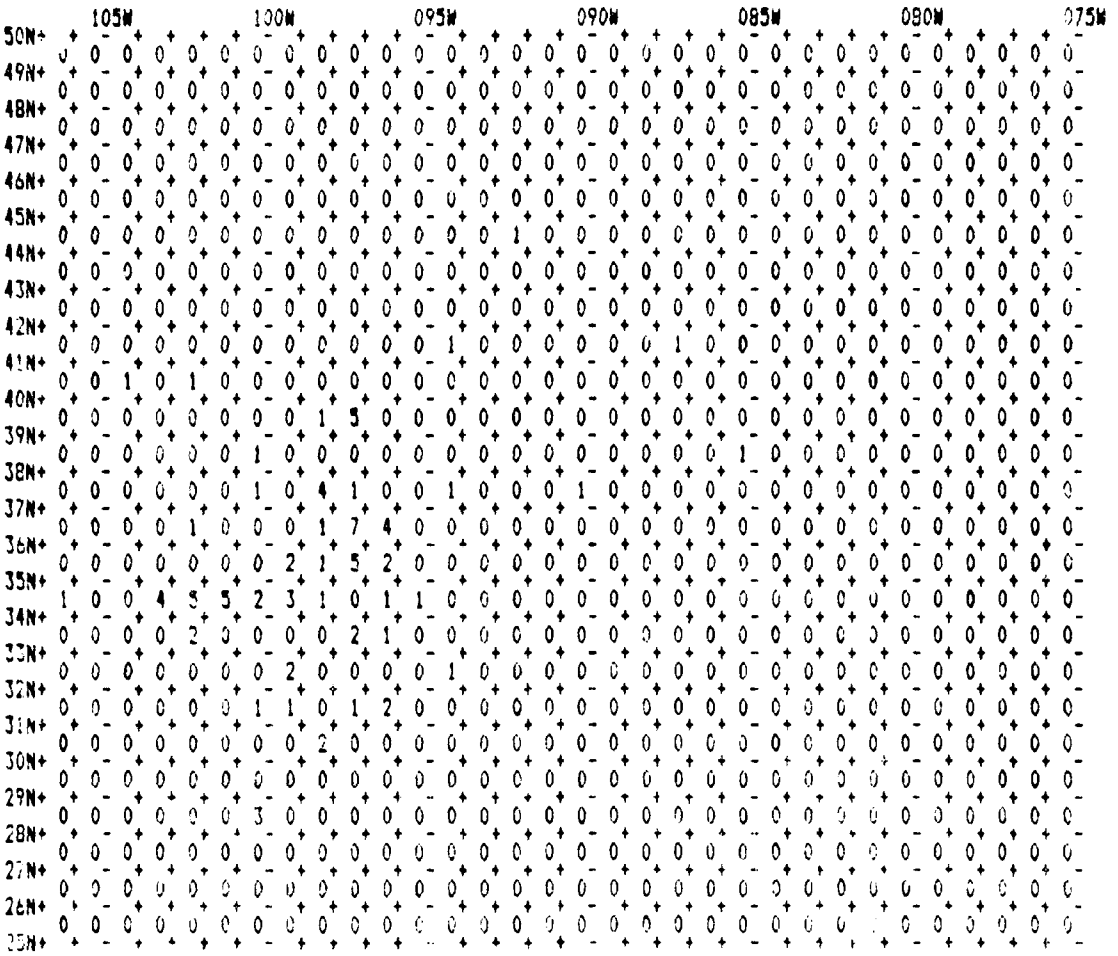

Table A12. The total number of funnel cloud events per 1° latitude-longitude grid box on day C for the JS subsample.

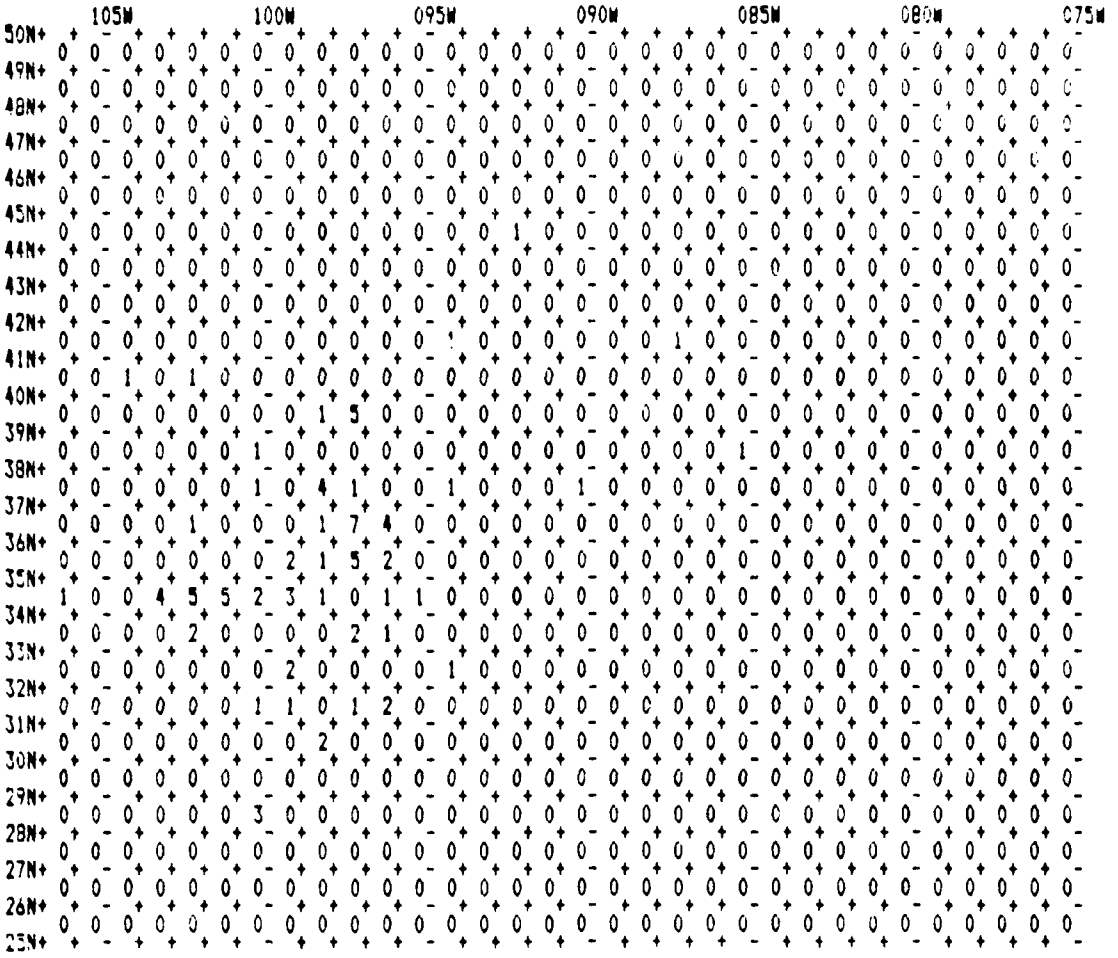

Table A13. The total number of funnel cloud genesis events per 1° latitude-longitude grid box on day C for the JS subsample.

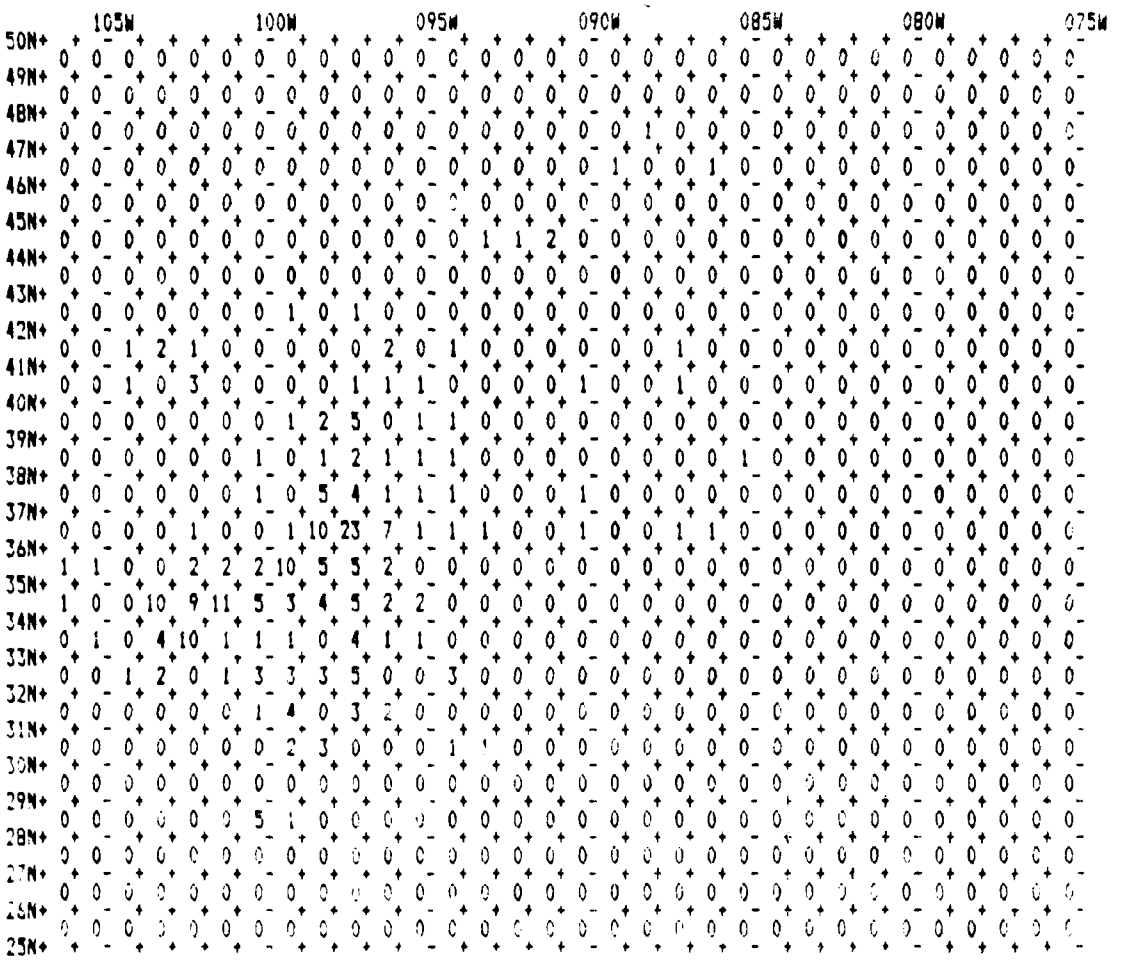

Table A14. The total number of severe storm events per 1° latitude-longitude grid box on day C for the JS subsample.

Appendix B. Total Severe Weather Events for Day C+1

	105W	100W	095W	090W	085W	080W	075W
50N	0 0 0 0 0 0 0 0 0 0 0 0 0 0 0 0 0 0 0 0 0 0 0 0 0 0 0 0 0 0 0						
49N	0 0 0 0 0 0 0 0 0 0 0 0 0 0 0 0 0 0 0 0 0 0 0 0 0 0 0 0 0 0 0						
48N	0 0 0 0 0 0 0 0 0 0 0 0 0 0 0 0 0 0 0 0 0 0 0 0 0 0 0 0 0 0 0						
47N	0 0 0 0 0 0 0 0 0 0 0 0 0 0 0 0 0 0 0 0 0 0 0 0 0 0 0 0 0 0 0						
46N	0 0 0 0 0 0 0 0 2 2 0 0 1 0 0 2 0 0 0 0 0 0 0 0 0 0 0 0 0 0 0						
45N	0 0 0 0 0 0 0 2 1 2 0 0 0 5 0 0 1 1 0 0 0 0 0 0 0 0 0 0 0 0 0						
44N	0 0 0 0 0 0 0 0 2 0 1 0 3 12 5 0 0 1 1 0 2 1 0 0 0 0 0 0 0 0 0						
43N	0 0 0 0 0 0 0 0 0 0 0 1 2 1 2 3 3 1 1 5 0 1 4 5 0 0 0 0 0 0 0						
42N	0 0 0 0 0 0 0 0 0 0 0 1 0 2 2 1 1 1 9 3 2 1 2 3 0 0 0 0 0 0 0						
41N	0 0 1 0 0 1 0 0 1 1 1 2 6 3 2 5 0 0 1 0 1 1 0 0 1 0 0 0 0 0 0						
40N	0 0 0 0 0 0 1 0 0 1 2 3 3 6 1 0 0 0 0 0 0 3 1 1 0 0 0 0 0 0 0						
39N	0 0 0 0 0 0 5 1 0 0 2 2 5 2 1 1 3 2 0 0 0 1 1 2 3 0 0 0 0 0 0						
38N	0 0 0 0 0 0 3 0 0 0 1 2 3 3 2 2 4 2 0 1 0 0 1 0 0 0 0 0 0 0 0						
37N	0 0 0 0 1 1 0 0 0 1 0 4 2 3 0 1 2 1 1 1 1 0 0 0 0 0 0 0 0 0 0						
36N	0 0 0 0 0 5 5 1 4 7 3 2 1 1 1 1 1 4 0 0 0 1 0 0 0 0 0 0 0 0 0						
35N	0 0 0 0 0 1 0 6 1 0 2 0 1 2 0 3 0 1 1 1 0 0 0 0 1 0 0 0 0 0 0						
34N	0 0 0 1 0 0 0 2 0 0 2 0 0 1 1 2 2 0 0 0 0 0 0 0 0 0 0 0 0 0 0						
33N	0 0 0 0 0 1 4 0 0 1 0 2 3 3 2 1 2 1 0 0 1 2 1 2 0 0 0 0 0 0 0						
32N	0 0 0 0 0 0 0 1 2 5 0 1 0 0 0 0 0 0 0 0 1 1 0 0 0 0 0 0 0 0 0						
31N	0 0 0 0 0 0 0 0 0 0 0 1 1 1 0 1 0 0 0 0 0 0 0 1 0 0 0 0 0 0 0						
30N	0 0 0 0 0 0 0 1 0 1 0 0 0 0 0 0 0 0 0 0 0 0 0 0 0 0 0 0 0 0 0						
29N	0 0 0 0 0 0 0 0 0 0 0 0 0 0 0 0 0 0 0 0 0 0 0 0 0 0 0 0 0 0 0						
28N	0 0 0 0 0 0 0 0 0 0 0 0 0 0 0 0 0 0 0 0 0 0 0 0 0 0 0 0 0 0 0						
27N	0 0 0 0 0 0 0 0 0 0 0 0 0 0 0 0 0 0 0 0 0 0 0 0 0 0 0 0 0 0 0						
26N	0 0 0 0 0 0 0 0 0 0 0 0 0 0 0 0 0 0 0 0 0 0 0 0 0 0 0 0 0 0 0						
25N	0 0 0 0 0 0 0 0 0 0 0 0 0 0 0 0 0 0 0 0 0 0 0 0 0 0 0 0 0 0 0						

Table B1. The total number of tornado events per 1° latitude-longitude grid box on Day C+1 for the D sample.

	105W						100W						095W						090W						085W						080W						075W
50N	0	0	0	0	0	0	0	0	0	0	0	0	0	0	0	0	0	0	0	0	0	0	0	0	0	0	0	0	0	0	0	0	0	0	0	0
49N	0	0	0	0	0	0	0	0	0	0	0	0	0	0	0	0	0	0	0	0	0	0	0	0	0	0	0	0	0	0	0	0	0	0	0	0
48N	0	0	0	0	0	0	0	0	0	0	0	0	0	0	0	0	0	0	0	0	0	0	0	0	0	0	0	0	0	0	0	0	0	0	0	0
47N	0	0	0	0	0	0	0	0	0	0	0	0	0	0	0	0	0	0	0	0	0	0	0	0	0	0	0	0	0	0	0	0	0	0	0	0
46N	0	0	0	0	0	0	0	0	0	0	0	0	0	0	0	0	0	0	0	0	0	0	0	0	0	0	0	0	0	0	0	0	0	0	0	0
45N	0	0	0	0	0	0	0	0	2	2	0	0	1	0	0	2	0	0	0	0	0	0	0	0	0	0	0	0	0	0	0	0	0	0	0	0
44N	0	0	0	0	0	0	0	2	1	2	0	0	0	2	0	0	1	1	0	0	0	0	0	0	0	0	0	0	0	0	0	0	0	0	0	0
43N	0	0	0	0	0	0	0	0	2	0	1	0	3	12	5	0	0	1	1	0	2	1	0	0	0	0	0	0	0	0	0	0	0	0	0	0
42N	0	0	0	0	0	0	0	0	0	0	1	2	1	2	3	3	1	1	5	0	1	4	4	0	0	0	0	0	0	0	0	0	0	0	0	0
41N	0	0	0	0	0	0	0	0	0	0	1	0	2	2	1	0	1	8	3	2	1	2	3	0	0	0	0	0	0	0	0	0	0	0	0	0
40N	0	0	1	0	0	1	0	0	1	1	1	2	6	2	2	4	0	0	1	0	1	1	0	0	1	0	0	0	0	0	0	0	0	0	0	0
39N	0	0	0	0	0	0	1	0	0	1	2	3	2	6	0	0	0	0	0	0	0	3	1	0	0	0	0	0	0	0	0	0	0	0	0	0
38N	0	0	0	0	0	0	2	1	0	0	2	2	5	2	1	1	3	1	0	0	0	1	1	1	3	0	0	0	0	0	0	0	0	0	0	0
37N	0	0	0	0	0	0	3	0	0	0	1	2	3	3	1	2	4	2	0	0	0	0	1	0	0	0	0	0	0	0	0	0	0	0	0	0
36N	0	0	0	0	1	1	0	0	0	0	0	4	2	3	0	1	2	1	1	0	1	0	0	0	0	0	0	0	0	0	0	0	0	0	0	0
35N	0	0	0	0	0	5	5	1	3	6	3	2	1	1	1	1	1	4	0	0	0	1	0	0	0	0	0	0	0	0	0	0	0	0	0	0
34N	0	0	0	0	0	1	0	6	0	0	2	0	1	2	0	3	0	1	1	1	0	0	0	0	1	0	0	0	0	0	0	0	0	0	0	0
33N	0	0	0	1	0	0	0	2	0	0	2	0	0	1	1	2	2	0	0	0	0	0	0	0	0	0	0	0	0	0	0	0	0	0	0	0
32N	0	0	0	0	0	1	4	0	0	1	0	2	3	3	2	1	2	1	0	0	0	0	1	2	0	0	0	0	0	0	0	0	0	0	0	0
31N	0	0	0	0	0	0	0	1	2	5	0	1	0	0	0	0	0	0	0	0	1	1	0	0	0	0	0	0	0	0	0	0	0	0	0	0
30N	0	0	0	0	0	0	0	0	0	0	1	1	1	0	1	0	0	0	0	0	0	1	0	0	0	0	0	0	0	0	0	0	0	0	0	0
29N	0	0	0	0	0	0	1	0	1	0	0	0	0	0	0	0	0	0	0	0	0	0	0	0	0	0	0	0	0	0	0	0	0	0	0	0
28N	0	0	0	0	0	0	0	0	0	0	0	0	0	0	0	0	0	0	0	0	0	0	0	0	0	0	0	0	0	0	0	0	0	0	0	0
27N	0	0	0	0	0	0	0	0	0	0	0	0	0	0	0	0	0	0	0	0	0	0	0	0	0	0	0	0	0	0	0	0	0	0	0	0
26N	0	0	0	0	0	0	0	0	0	0	0	0	0	0	0	0	0	0	0	0	0	0	0	0	0	0	0	0	0	0	0	0	0	0	0	0
25N	0	0	0	0	0	0	0	0	0	0	0	0	0	0	0	0	0	0	0	0	0	0	0	0	0	0	0	0	0	0	0	0	0	0	0	0

Table B2. The total number of tornado genesis events per 1° latitude-longitude grid box on day C+1 for the D sample.

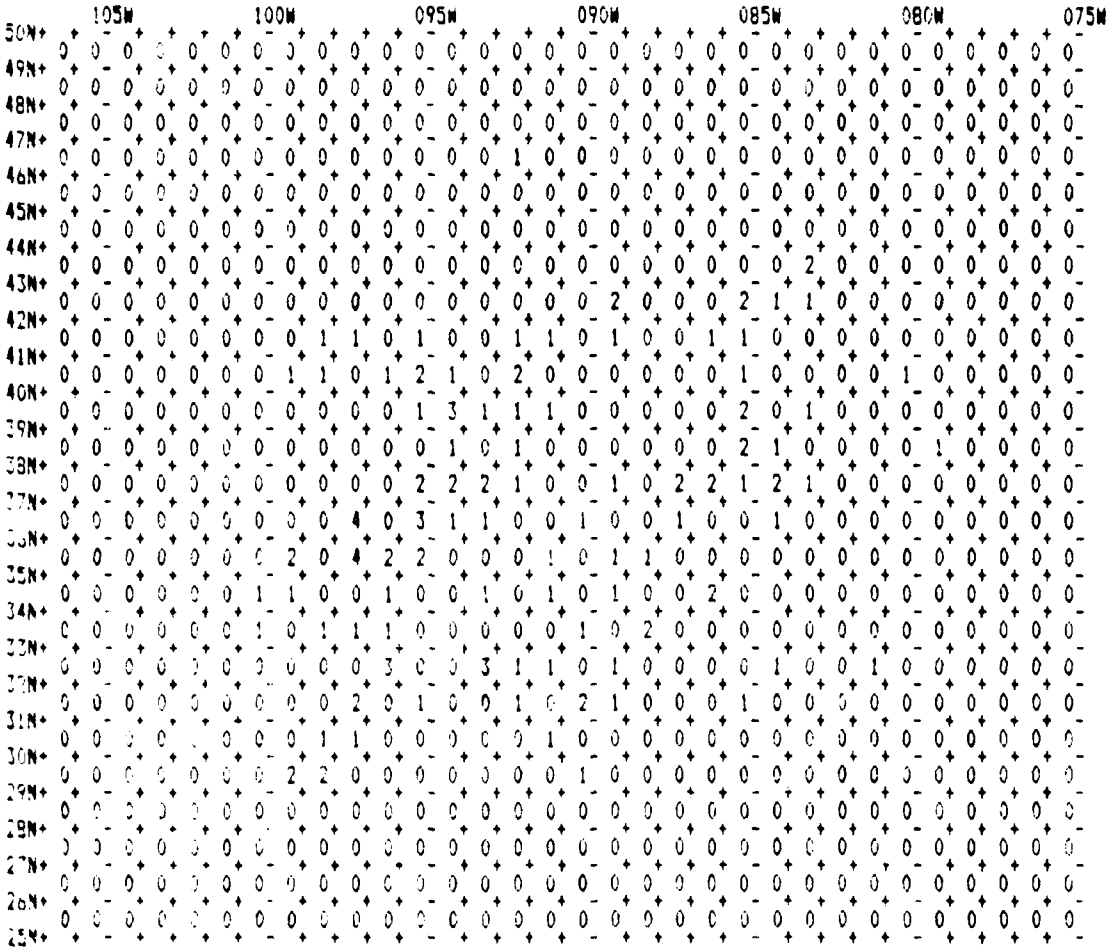

Table B7. The total number of high wind (≥ 26 m/s) events per 1° latitude-longitude grid box on day C+1 for the L sample.

	105W							100W							095W							090W							085W							080W							075W
50N	0	0	0	0	0	0	0	0	0	0	0	0	0	0	0	0	0	0	0	0	0	0	0	0	0	0	0	0	0	0	0	0	0	0	0	0	0	0	0	0	0	0
49N	0	0	0	0	0	0	0	0	0	1	0	0	0	0	0	0	0	0	0	0	0	0	0	0	0	0	0	0	0	0	0	0	0	0	0	0	0	0	0	0	0	0
48N	0	0	0	0	0	0	0	0	0	0	0	0	0	0	0	0	0	0	0	0	0	0	0	0	0	0	0	0	0	0	0	0	0	0	0	0	0	0	0	0	0	0
47N	0	0	0	0	0	0	0	0	1	0	0	0	0	0	0	0	0	0	0	0	0	0	0	0	0	0	0	0	0	0	0	0	0	0	0	0	0	0	0	0	0	0
46N	0	0	0	0	0	0	0	0	0	0	0	0	0	0	0	0	0	0	0	0	0	0	0	0	0	0	0	0	0	0	0	0	0	0	0	0	0	0	0	0	0	0
45N	0	0	0	0	0	0	0	0	0	1	0	0	1	0	0	1	1	0	0	1	0	0	0	0	0	0	0	0	0	0	0	0	0	0	0	0	0	0	0	0	0	0
44N	0	0	0	0	0	0	0	0	0	0	0	0	0	1	0	2	1	0	1	0	0	0	0	0	0	0	0	0	0	0	0	0	0	0	0	0	0	0	0	0	0	0
43N	0	0	0	0	0	0	0	0	0	0	0	0	2	1	1	1	3	0	2	0	2	0	1	0	0	0	0	0	0	0	0	0	0	0	0	0	0	0	0	0	0	0
42N	0	0	0	0	0	0	0	0	0	1	0	0	1	1	0	1	2	1	0	0	0	0	0	0	0	0	0	0	0	0	0	0	0	0	0	0	0	0	0	0	0	0
41N	0	0	0	0	0	0	2	0	0	0	3	0	1	2	1	2	2	0	0	1	0	0	0	0	0	0	0	0	0	0	0	0	0	0	0	0	0	0	0	0	0	0
40N	0	1	0	0	0	0	0	1	1	0	2	3	4	2	3	4	0	0	1	0	0	2	0	0	0	0	0	0	0	0	0	0	0	0	0	0	0	0	0	0	0	0
39N	0	1	0	0	0	0	2	2	2	1	3	7	4	0	1	4	1	3	0	0	2	2	0	0	1	0	0	0	0	1	0	0	0	0	0	0	0	0	0	0	0	0
38N	0	0	0	0	0	0	1	1	0	1	0	6	4	0	0	3	4	1	0	0	0	3	3	2	2	0	0	0	0	0	0	0	0	0	0	0	0	0	0	0	0	0
37N	0	0	0	0	0	0	3	0	0	3	0	3	5	1	0	0	0	1	0	1	0	3	1	1	0	1	0	0	0	0	0	0	0	0	0	0	0	0	0	0	0	0
36N	0	0	0	0	2	4	0	1	2	4	1	6	3	1	0	0	0	1	0	0	1	2	3	3	2	0	0	0	0	0	0	0	0	0	0	0	0	0	0	0	0	0
35N	0	0	0	0	1	1	3	9	13	4	4	2	3	1	0	0	0	2	0	1	1	2	1	1	0	0	0	0	0	0	0	0	0	0	0	0	0	0	0	0	0	0
34N	0	0	0	0	1	0	4	11	2	4	3	3	1	1	0	1	1	1	0	0	1	2	0	2	2	1	0	0	0	0	0	0	0	0	0	0	0	0	0	0	0	0
33N	0	0	0	0	0	0	1	1	2	1	1	0	0	1	1	0	1	0	1	0	0	0	2	1	1	0	1	0	0	0	0	0	0	0	0	0	0	0	0	0	0	0
32N	0	0	0	0	0	0	0	1	1	1	1	0	0	0	0	0	0	0	3	0	0	0	0	0	1	0	0	0	0	0	0	0	0	0	0	0	0	0	0	0	0	0
31N	0	0	0	0	1	0	0	1	1	2	0	0	0	0	0	0	3	0	0	0	0	0	0	0	0	0	0	0	0	0	0	0	0	0	0	0	0	0	0	0	0	0
30N	0	0	0	0	0	1	1	1	1	3	0	0	0	0	1	0	0	0	0	0	0	0	0	0	0	0	0	0	0	0	0	0	0	0	0	0	0	0	0	0	0	0
29N	0	0	0	0	0	0	0	5	4	1	0	0	0	0	0	0	0	0	0	0	0	0	0	0	0	0	0	0	0	0	0	0	0	0	0	0	0	0	0	0	0	0
28N	0	0	0	0	0	0	0	1	0	0	0	0	0	0	0	0	0	0	0	0	0	0	0	0	0	0	0	0	0	0	0	0	0	0	0	0	0	0	0	0	0	0
27N	0	0	0	0	0	0	0	0	0	0	0	0	0	0	0	0	0	0	0	0	0	0	0	0	0	0	0	0	0	0	0	0	0	0	0	0	0	0	0	0	0	0
26N	0	0	0	0	0	0	0	0	1	0	0	0	0	0	0	0	0	0	0	0	0	0	0	0	0	0	0	0	0	0	0	0	0	0	0	0	0	0	0	0	0	0
25N	0	0	0	0	0	0	0	0	0	0	0	0	0	0	0	0	0	0	0	0	0	0	0	0	0	0	0	0	0	0	0	0	0	0	0	0	0	0	0	0	0	0

Table B4. The total number of large hail (> 19mm) events per 1° latitude-longitude grid box on day C+1 for the D sample.

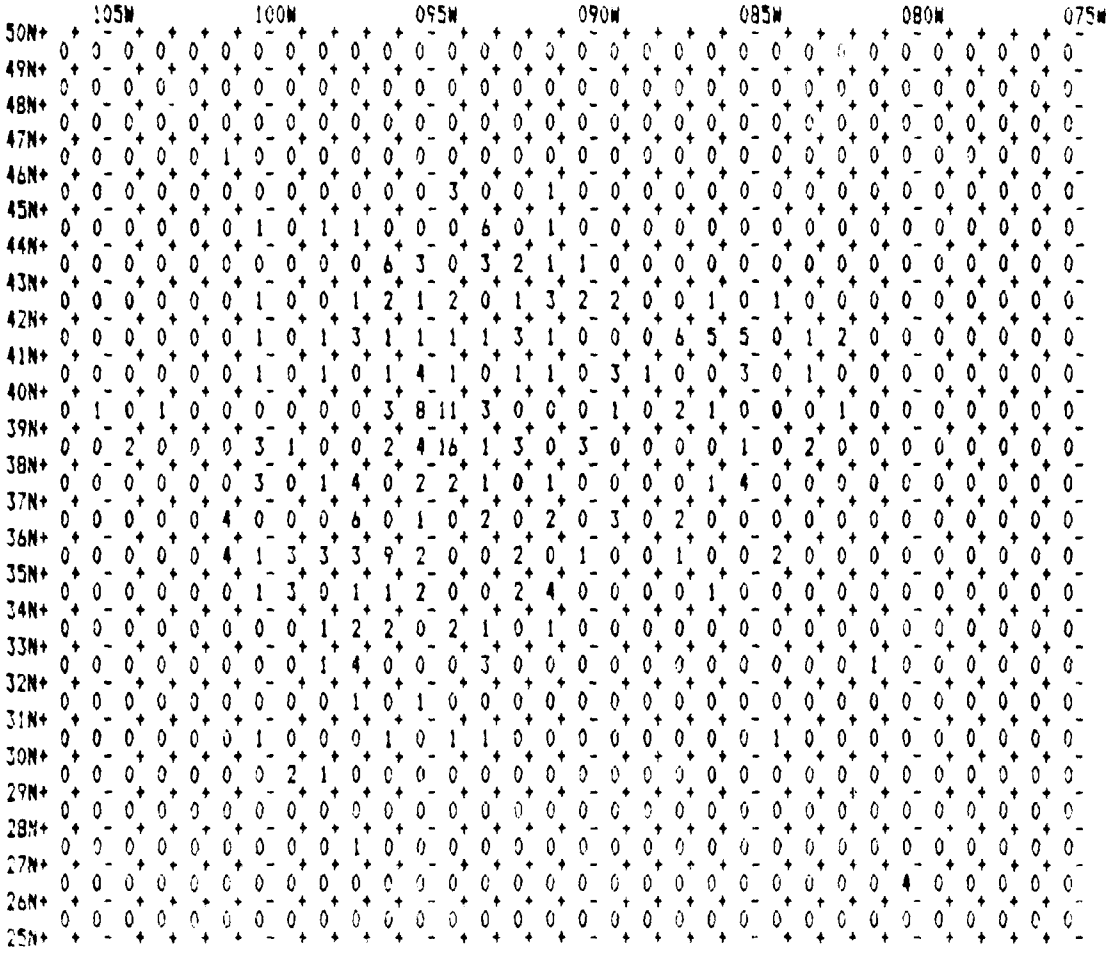

Table B5. The total number of funnel cloud events per 1° latitude-longitude grid box on day C+1 for the D sample.

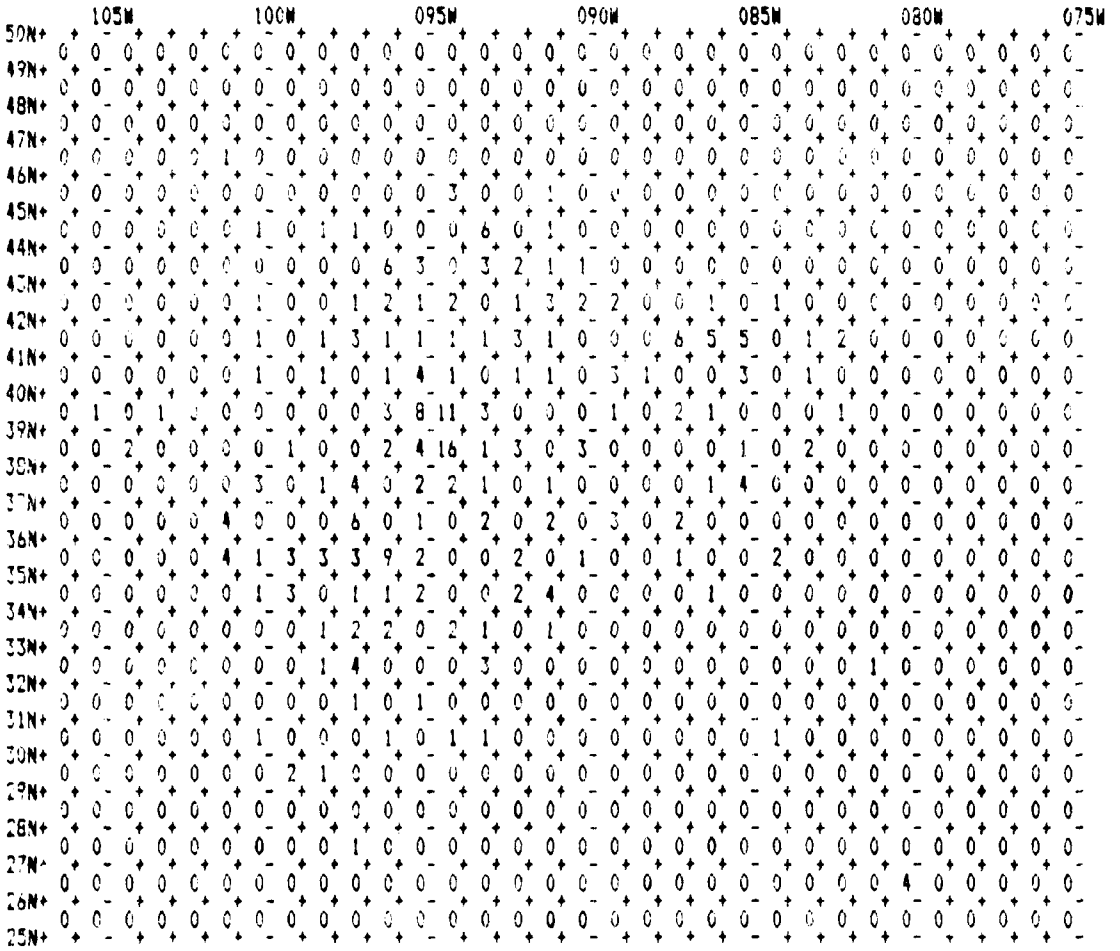

Table 26. The total number of funnel cloud genesis events per 1 latitude-longitude grid box on day (+1 for the D sample.

	105W						100W						095W						090W						085W						080W						075W
50N	0	0	0	0	0	0	0	0	0	0	0	0	0	0	0	0	0	0	0	0	0	0	0	0	0	0	0	0	0	0	0	0	0	0	0	0
49N	0	0	0	0	0	0	0	0	1	0	0	0	0	0	0	0	0	0	0	0	0	0	0	0	0	0	0	0	0	0	0	0	0	0	0	0
48N	0	0	0	0	0	0	0	0	0	0	0	0	0	0	0	0	0	0	0	0	0	0	0	0	0	0	0	0	0	0	0	0	0	0	0	0
47N	0	0	0	0	0	1	1	0	0	0	0	0	0	0	0	1	0	0	0	0	0	0	0	0	0	0	0	0	0	0	0	0	0	0	0	0
46N	0	0	0	0	0	0	0	0	3	2	0	1	4	0	1	4	0	0	1	0	0	0	0	0	0	0	0	0	0	0	0	0	0	0	0	0
45N	0	0	0	0	0	0	1	2	2	3	0	0	1	11	2	2	1	2	0	0	0	0	0	0	0	0	0	0	0	0	0	0	0	0	0	0
44N	0	0	0	0	0	0	0	0	2	0	7	3	5	16	8	2	4	1	3	0	4	1	1	2	0	0	0	0	0	0	0	0	0	0	0	0
43N	0	0	0	0	0	0	1	0	0	1	4	3	3	3	5	6	4	7	6	0	2	6	7	1	0	0	0	0	0	0	0	0	0	0	0	0
42N	0	0	0	0	0	0	3	0	2	4	5	2	4	5	6	5	3	10	3	9	7	8	3	1	2	0	0	0	0	0	0	0	0	0	0	0
41N	0	1	1	0	0	1	1	2	4	1	5	11	12	5	8	10	0	3	3	0	1	7	0	1	1	0	1	0	0	0	0	0	0	0	0	0
40N	0	2	0	1	0	0	3	2	2	2	8	19	21	10	3	5	1	4	0	2	3	7	1	2	2	0	0	0	0	1	0	0	0	0	0	0
39N	0	0	2	0	0	0	9	3	0	1	4	12	26	3	5	4	10	3	0	0	0	7	5	6	5	0	0	1	0	0	0	0	0	0	0	0
38N	0	0	0	0	0	0	9	0	1	7	1	9	12	7	3	3	4	4	0	4	3	8	4	2	0	1	0	0	0	0	0	0	0	0	0	0
37N	0	0	0	0	3	9	0	1	2	15	1	14	6	7	0	3	3	5	1	4	2	2	4	3	2	0	0	0	0	0	0	0	0	0	0	0
36N	0	0	0	0	1	10	9	15	20	18	18	8	4	2	3	2	2	7	1	2	1	3	3	1	0	0	0	0	0	0	0	0	0	0	0	0
35N	0	0	0	0	1	1	6	21	3	5	7	5	2	4	2	9	1	3	1	1	4	2	0	2	3	1	0	0	0	0	0	0	0	0	0	0
34N	0	0	0	1	0	0	2	3	4	4	6	0	2	3	2	3	4	0	3	0	0	0	2	1	1	0	1	0	0	0	0	0	0	0	0	0
33N	0	0	0	0	0	1	4	1	2	6	4	2	3	9	3	2	2	2	3	0	1	2	2	2	0	3	0	0	0	0	0	0	0	0	0	0
32N	0	0	0	0	1	0	0	2	3	10	0	3	0	0	1	0	5	1	0	0	1	2	0	0	0	0	0	0	0	0	0	0	0	0	0	0
31N	0	0	0	0	0	1	2	1	2	4	2	1	2	1	2	1	0	0	0	0	0	0	2	0	0	0	0	0	0	0	0	0	0	0	0	0
30N	0	0	0	0	0	0	1	9	8	1	0	0	0	0	0	1	0	0	0	0	0	0	0	0	0	0	0	0	0	0	0	0	0	0	0	0
29N	0	0	0	0	0	0	0	1	0	0	0	0	0	0	0	0	0	0	0	0	0	0	0	0	0	0	0	0	0	0	0	0	0	0	0	0
28N	0	0	0	0	0	0	0	0	0	1	0	0	0	0	0	0	0	0	0	0	0	0	0	0	0	0	0	0	0	0	0	0	0	0	0	0
27N	0	0	0	0	0	0	0	0	1	0	0	0	0	0	0	0	0	0	0	0	0	0	0	0	0	0	4	0	0	0	0	0	0	0	0	0
26N	0	0	0	0	0	0	0	0	0	0	0	0	0	0	0	0	0	0	0	0	0	0	0	0	0	0	0	0	0	0	0	0	0	0	0	0
25N																																				

Table B7. The total number of severe storm events per 1° latitude-longitude grid box on day C+1 for the D sample.

	105W							100W							095W							090W							085W							080W							075W
50N	0	0	0	0	0	0	0	0	0	0	0	0	0	0	0	0	0	0	0	0	0	0	0	0	0	0	0	0	0	0	0	0	0	0	0	0	0	0	0	0	0
49N	0	0	0	0	0	0	0	0	0	0	0	0	0	0	0	0	0	0	0	0	0	0	0	0	0	0	0	0	0	0	0	0	0	0	0	0	0	0	0	0	0
48N	0	0	0	0	0	0	0	0	0	1	0	3	0	0	0	0	0	0	0	0	0	0	0	0	0	0	0	0	0	0	0	0	0	0	0	0	0	0	0	0	0
47N	0	0	0	0	0	1	0	0	0	1	1	1	0	0	0	0	0	0	0	0	0	0	0	0	0	0	0	0	0	0	0	0	0	0	0	0	0	0	0	0	0
46N	0	0	0	0	0	4	0	0	0	1	1	2	1	2	3	0	0	0	1	0	0	0	1	0	0	0	0	0	0	0	0	0	0	0	0	0	0	0	0	0	0
45N	0	0	0	0	0	3	0	0	2	3	0	0	7	3	5	0	2	2	0	0	1	0	0	0	0	0	0	0	0	0	0	0	0	0	0	0	0	0	0	0	0
44N	0	0	0	0	0	0	0	5	0	2	4	2	0	9	14	9	1	2	6	1	3	0	2	5	1	0	0	0	0	0	0	0	0	0	0	0	0	0	0	0	0
43N	0	0	0	0	0	3	2	5	3	7	3	4	4	4	4	5	4	2	1	0	1	6	2	1	0	0	0	0	0	0	1	0	0	0	0	0	0	0	0	0	0
42N	0	0	0	0	0	3	6	5	5	0	0	6	1	3	4	4	3	1	9	0	4	1	6	1	2	0	0	0	0	0	0	0	0	0	0	0	0	0	0	0	0
41N	0	0	0	0	0	1	1	1	4	4	3	8	10	6	4	2	4	4	6	6	7	12	2	3	2	9	0	0	1	0	0	0	0	0	0	0	0	0	0	0	0
40N	0	0	0	1	0	0	0	0	1	3	3	6	7	7	6	4	2	6	2	3	13	9	6	5	1	1	0	0	0	0	0	0	0	0	0	0	0	0	0	0	0
39N	0	0	0	0	0	0	0	1	1	4	4	5	16	5	5	1	9	1	0	3	2	7	4	3	3	2	1	1	1	0	0	0	0	0	0	0	0	0	0	0	0
38N	0	0	0	0	0	0	0	1	5	4	1	7	14	2	1	2	2	5	2	2	2	7	3	0	2	1	1	0	0	0	0	0	0	0	0	0	0	0	0	0	0
37N	0	0	0	0	0	0	0	0	0	8	2	8	7	2	2	4	5	6	6	1	9	7	3	0	1	2	1	1	1	0	1	0	0	0	0	0	0	0	0	0	0
36N	0	0	0	0	0	0	0	4	3	4	1	5	3	1	4	5	5	16	5	3	1	0	2	2	0	1	2	2	1	0	1	0	0	0	0	0	0	0	0	0	0
35N	0	0	0	0	0	0	4	4	8	8	1	1	1	1	8	2	8	7	4	2	3	0	1	1	1	4	5	1	2	1	0	0	0	0	0	0	0	0	0	0	0
34N	0	0	0	0	0	0	1	2	1	5	0	0	2	3	4	0	2	1	0	2	3	1	1	0	0	1	0	0	0	0	0	0	0	0	0	0	0	0	0	0	0
33N	0	0	0	0	0	1	4	2	1	7	4	3	1	7	1	0	4	1	1	1	2	0	1	0	0	1	0	0	0	0	0	0	0	0	0	0	0	0	0	0	0
32N	0	0	0	2	2	0	1	6	3	0	0	0	5	3	2	0	3	1	1	0	0	1	1	1	1	3	0	0	0	0	0	0	0	0	0	0	0	0	0	0	0
31N	0	0	0	0	1	0	0	1	4	5	0	3	1	3	1	2	0	6	5	1	0	0	3	1	0	0	0	0	0	0	0	0	0	0	0	0	0	0	0	0	0
30N	0	0	0	0	0	0	1	0	5	3	0	2	1	1	1	1	2	1	0	0	0	0	0	0	0	0	0	0	0	0	0	0	0	0	0	0	0	0	0	0	0
29N	0	0	0	0	0	0	0	2	0	0	0	0	0	0	0	0	0	0	0	0	0	0	0	0	0	0	0	0	0	0	0	0	0	0	0	0	0	0	0	0	0
28N	0	0	0	0	0	0	0	1	2	4	0	0	0	0	0	0	0	0	0	0	0	0	0	0	0	0	0	0	0	0	0	0	0	0	0	0	0	0	0	0	0
27N	0	0	0	0	0	0	0	0	2	0	0	0	0	0	0	0	0	0	0	0	0	0	0	0	0	0	0	0	0	0	0	0	0	0	0	0	0	0	0	0	0
26N	0	0	0	0	0	0	0	0	0	0	0	0	0	0	0	0	0	0	0	0	0	0	0	0	0	0	0	0	0	0	0	0	0	0	0	0	0	0	0	0	0
25N	0	0	0	0	0	0	0	0	0	0	0	0	0	0	0	0	0	0	0	0	0	0	0	0	0	0	0	0	0	0	0	0	0	0	0	0	0	0	0	0	0

Table C7. The total number of severe storm events per 1° latitude-longitude grid box on day C+2 for the D sample.

	105W						100W						095W						090W						085W						080W						075W
50N																																				
49N	0	0	0	0	0	0	0	0	0	0	0	0	0	0	0	0	0	0	0	0	0	0	0	0	0	0	0	0	0	0	0	0	0	0	0	0
48N	0	0	0	0	0	0	0	0	0	0	0	0	0	0	0	0	0	0	0	0	0	0	0	0	0	0	0	0	0	0	0	0	0	0	0	0
47N	0	0	0	0	0	0	0	0	0	0	1	0	0	0	0	0	0	0	0	0	0	0	0	0	0	0	0	0	0	0	0	0	0	0	0	0
46N	0	0	0	0	0	1	0	0	0	0	1	0	0	0	0	0	0	0	0	0	0	0	0	0	0	0	0	0	0	0	0	0	0	0	0	0
45N	0	0	0	0	0	0	1	0	0	0	1	0	0	0	0	0	1	0	0	0	0	0	0	0	0	0	0	0	0	0	0	0	0	0	0	0
44N	0	0	0	0	0	0	0	0	0	0	1	0	0	0	1	2	0	0	0	0	0	0	0	0	0	0	0	0	0	0	0	0	0	0	0	0
43N	0	0	0	0	0	0	0	0	0	0	3	0	0	3	5	2	0	0	3	1	2	0	0	1	0	0	0	0	0	0	0	0	0	0	0	0
42N	0	0	0	0	0	0	0	0	0	0	2	1	0	1	1	1	0	0	1	1	0	0	2	0	0	0	0	0	0	0	0	0	0	0	0	0
41N	0	0	0	0	0	0	0	2	0	0	0	0	3	1	1	1	2	0	0	3	0	3	1	4	0	0	0	0	0	0	0	0	0	0	0	0
40N	0	0	0	0	0	1	1	0	1	0	0	4	3	1	1	0	1	0	1	4	0	4	1	0	0	1	0	0	0	0	0	0	0	0	0	0
39N	0	0	0	1	0	0	0	0	1	1	2	0	1	0	1	0	0	1	1	2	5	0	1	1	0	0	0	0	0	0	0	0	0	0	0	0
38N	0	0	0	0	0	0	0	0	0	3	2	2	7	2	4	1	3	0	0	0	1	1	0	0	0	0	0	0	0	0	0	0	0	0	0	0
37N	0	0	0	0	0	0	0	0	2	0	0	0	7	0	0	0	0	3	0	0	0	1	0	0	0	0	0	0	0	0	0	0	0	0	0	0
36N	0	0	0	0	0	0	0	0	0	4	0	4	1	0	0	0	0	1	0	0	1	1	0	0	0	0	0	0	0	0	1	0	0	0	0	0
35N	0	0	0	0	0	0	0	2	0	0	0	0	0	1	0	0	4	1	0	0	0	0	0	0	0	0	0	0	0	0	0	0	0	0	0	0
34N	0	0	0	0	0	1	0	5	4	1	0	0	0	2	1	3	1	0	0	0	0	0	0	0	2	0	0	0	0	0	0	0	0	0	0	0
33N	0	0	0	0	0	0	0	1	1	1	0	0	0	0	0	0	1	0	0	0	0	0	1	0	0	1	0	0	0	0	0	0	0	0	0	0
32N	0	0	0	0	0	0	0	1	5	1	0	0	1	0	0	2	0	0	0	0	0	0	0	0	0	0	0	0	0	0	0	0	0	0	0	0
31N	0	0	0	0	1	0	0	3	2	0	0	0	0	1	0	0	1	0	1	0	0	0	0	0	0	0	0	0	0	0	0	0	0	0	0	0
30N	0	0	0	0	0	0	0	0	0	1	0	1	0	1	0	0	0	2	1	0	0	0	0	0	0	0	0	0	0	0	0	0	0	0	0	0
29N	0	0	0	0	0	0	0	0	1	0	0	2	0	0	0	1	0	1	0	0	0	0	0	0	0	0	0	0	0	0	0	0	0	0	0	0
28N	0	0	0	0	0	0	0	1	0	0	0	0	0	0	0	0	0	0	0	0	0	0	0	0	0	0	0	0	0	0	0	0	0	0	0	0
27N	0	0	0	0	0	0	0	0	1	2	0	0	0	0	0	0	0	0	0	0	0	0	0	0	0	0	0	0	0	0	0	0	0	0	0	0
26N	0	0	0	0	0	0	0	0	0	0	0	0	0	0	0	0	0	0	0	0	0	0	0	0	0	0	0	0	0	0	0	0	0	0	0	0
25N	0	0	0	0	0	0	0	0	0	0	0	0	0	0	0	0	0	0	0	0	0	0	0	0	0	0	0	0	0	0	0	0	0	0	0	0

Table C6. The total number of funnel cloud genesis events per 1° latitude-longitude grid box on day C+2 for the D sample.

	105W							100W							095W							090W							085W							080W							075W
50N	0	0	0	0	0	0	0	0	0	0	0	0	0	0	0	0	0	0	0	0	0	0	0	0	0	0	0	0	0	0	0	0	0	0	0	0	0	0	0	0	0	0
49N	0	0	0	0	0	0	0	0	0	0	0	0	0	0	0	0	0	0	0	0	0	0	0	0	0	0	0	0	0	0	0	0	0	0	0	0	0	0	0	0	0	0
48N	0	0	0	0	0	0	0	0	0	0	0	1	0	0	0	0	0	0	0	0	0	0	0	0	0	0	0	0	0	0	0	0	0	0	0	0	0	0	0	0	0	0
47N	0	0	0	0	0	1	0	0	0	0	1	0	0	0	0	0	0	0	0	0	0	0	0	0	0	0	0	0	0	0	0	0	0	0	0	0	0	0	0	0	0	0
46N	0	0	0	0	0	0	1	0	0	0	1	0	0	0	0	0	1	0	0	0	0	0	0	0	0	0	0	0	0	0	0	0	0	0	0	0	0	0	0	0	0	0
45N	0	0	0	0	0	0	0	0	0	0	1	0	0	0	1	2	0	0	0	0	0	0	0	0	0	0	0	0	0	0	0	0	0	0	0	0	0	0	0	0	0	0
44N	0	0	0	0	0	0	0	0	0	0	3	0	0	3	5	3	0	0	3	1	2	0	0	1	0	0	0	0	0	0	0	0	0	0	0	0	0	0	0	0	0	0
43N	0	0	0	0	0	0	0	0	0	2	1	0	1	1	1	1	0	0	1	1	0	0	2	0	0	0	0	0	0	0	0	0	0	0	0	0	0	0	0	0	0	0
42N	0	0	0	0	0	0	0	2	0	0	0	0	3	1	1	1	2	0	0	3	0	3	1	4	0	0	0	0	0	0	0	0	0	0	0	0	0	0	0	0	0	0
41N	0	0	0	0	0	1	1	0	1	0	0	4	3	1	1	0	1	0	1	4	0	4	1	0	0	1	0	0	0	0	0	0	0	0	0	0	0	0	0	0	0	0
40N	0	0	0	1	0	0	0	0	1	1	2	0	1	0	1	0	0	1	1	2	5	0	1	1	0	0	0	0	0	0	0	0	0	0	0	0	0	0	0	0	0	0
39N	0	0	0	0	0	0	0	0	3	2	2	7	2	4	1	3	0	0	0	1	1	0	0	0	0	0	0	0	0	0	0	0	0	0	0	0	0	0	0	0	0	0
38N	0	0	0	0	0	0	0	0	2	0	0	0	7	0	0	0	0	3	0	0	0	1	0	0	0	0	0	0	0	0	0	0	0	0	0	0	0	0	0	0	0	0
37N	0	0	0	0	0	0	0	0	0	4	0	4	1	0	0	0	0	1	0	0	1	2	0	0	0	0	0	0	0	0	0	0	0	0	0	0	0	1	0	0	0	0
36N	0	0	0	0	0	0	0	2	0	0	0	0	0	1	0	0	4	1	0	0	0	0	0	0	0	0	0	0	0	0	0	0	0	0	0	0	0	0	0	0	0	0
35N	0	0	0	0	0	0	1	0	5	4	1	0	0	0	2	1	3	1	0	0	0	0	0	0	0	0	2	0	0	0	0	0	0	0	0	0	0	0	0	0	0	0
34N	0	0	0	0	0	0	1	1	1	0	0	0	0	0	0	1	0	0	0	0	0	1	0	0	1	0	0	0	0	0	0	0	0	0	0	0	0	0	0	0	0	0
33N	0	0	0	0	0	0	0	1	5	1	0	0	1	0	0	2	0	0	0	0	0	0	0	0	0	0	0	0	0	0	0	0	0	0	0	0	0	0	0	0	0	0
32N	0	0	0	0	1	0	0	3	2	0	0	0	0	1	0	0	1	0	1	0	0	0	0	0	0	0	0	0	0	0	0	0	0	0	0	0	0	0	0	0	0	0
31N	0	0	0	0	0	0	0	0	1	0	1	0	1	0	0	0	2	1	0	0	0	0	0	0	0	0	0	0	0	0	0	0	0	0	0	0	0	0	0	0	0	0
30N	0	0	0	0	0	0	0	1	0	0	2	0	0	0	1	0	1	0	0	0	0	0	0	0	0	0	0	0	0	0	0	0	0	0	0	0	0	0	0	0	0	0
29N	0	0	0	0	0	0	0	1	0	0	0	0	0	0	0	0	0	0	0	0	0	0	0	0	0	0	0	0	0	0	0	0	0	0	0	0	0	0	0	0	0	0
28N	0	0	0	0	0	0	0	0	1	2	0	0	0	0	0	0	0	0	0	0	0	0	0	0	0	0	0	0	0	0	0	0	0	0	0	0	0	0	0	0	0	0
27N	0	0	0	0	0	0	0	0	0	0	0	0	0	0	0	0	0	0	0	0	0	0	0	0	0	0	0	0	0	0	0	0	0	0	0	0	0	0	0	0	0	0
26N	0	0	0	0	0	0	0	0	0	0	0	0	0	0	0	0	0	0	0	0	0	0	0	0	0	0	0	0	0	0	0	0	0	0	0	0	0	0	0	0	0	0
25N	0	0	0	0	0	0	0	0	0	0	0	0	0	0	0	0	0	0	0	0	0	0	0	0	0	0	0	0	0	0	0	0	0	0	0	0	0	0	0	0	0	0

Table C5. The total number of funnel cloud events per 1 latitude-longitude grid box on day C+2 for the D sample.

	105W						100W						095W						090W						085W						080W						075W
50N	0	0	0	0	0	0	0	0	0	0	0	0	0	0	0	0	0	0	0	0	0	0	0	0	0	0	0	0	0	0	0	0	0	0	0	0
49N	0	0	0	0	0	0	0	0	0	0	0	0	0	0	0	0	0	0	0	0	0	0	0	0	0	0	0	0	0	0	0	0	0	0	0	0
48N	0	0	0	0	0	0	0	0	0	0	1	0	0	0	0	0	0	0	0	0	0	0	0	0	0	0	0	0	0	0	0	0	0	0	0	0
47N	0	0	0	0	0	0	0	0	0	0	0	0	0	0	0	0	0	0	0	0	0	0	0	0	0	0	0	0	0	0	0	0	0	0	0	0
46N	0	0	0	0	0	0	0	0	0	0	0	0	0	1	0	1	0	0	0	1	0	0	0	0	0	0	0	0	0	0	0	0	0	0	0	0
45N	0	0	0	0	0	0	0	0	0	2	0	0	0	3	1	2	0	1	0	0	0	0	0	0	0	0	0	0	0	0	0	0	0	0	0	0
44N	0	0	0	0	0	0	0	1	0	0	0	0	0	3	3	2	0	0	1	0	0	0	0	0	0	0	0	0	0	0	0	0	0	0	0	0
43N	0	0	0	0	0	0	1	0	0	0	0	0	1	1	2	0	0	0	0	0	0	0	0	0	0	0	0	0	0	0	0	0	0	1	0	0
42N	0	0	0	0	0	0	1	1	1	1	0	0	1	0	0	3	1	0	0	3	0	1	0	0	0	1	0	0	0	0	0	0	0	0	0	0
41N	0	0	0	0	0	0	0	0	1	1	1	2	2	3	2	1	0	1	1	1	0	2	0	0	0	2	0	0	0	0	0	0	0	0	0	0
40N	0	0	0	0	0	0	0	0	0	1	0	0	3	2	1	2	2	2	0	1	3	2	1	0	0	0	0	0	0	0	0	0	0	0	0	0
39N	0	0	0	0	0	0	0	0	0	1	0	0	1	0	0	0	4	0	0	0	0	1	1	1	1	1	0	0	1	0	0	0	0	0	0	0
38N	0	0	0	0	0	0	0	1	1	3	0	2	3	1	0	0	0	0	1	1	1	0	1	0	1	0	0	0	0	0	0	0	0	0	0	0
37N	0	0	0	0	0	0	0	0	0	0	2	1	1	2	2	0	0	2	2	2	0	3	2	2	0	0	0	1	0	0	0	0	0	0	0	0
36N	0	0	0	0	0	0	0	0	2	2	2	0	1	1	0	1	0	2	4	1	1	0	0	1	1	0	0	1	0	0	0	0	0	0	0	0
35N	0	0	0	0	0	0	3	2	1	2	0	1	0	1	3	0	1	1	0	0	1	0	0	1	1	1	0	0	0	0	0	0	0	0	0	0
34N	0	0	0	0	0	0	0	1	0	1	0	0	1	2	3	0	0	1	0	2	0	0	0	0	0	0	0	0	0	0	0	0	0	0	0	0
33N	0	0	0	0	0	1	1	1	0	0	1	1	0	1	0	0	0	0	1	1	0	0	0	0	1	0	0	0	0	0	0	0	0	0	0	0
32N	0	0	0	1	0	0	0	1	1	0	0	0	1	0	0	0	0	0	0	0	0	1	0	0	0	2	0	0	0	0	0	0	0	0	0	0
31N	0	0	0	0	0	0	0	1	2	2	0	0	0	1	0	0	0	0	0	0	0	1	0	0	0	0	0	0	0	0	0	0	0	0	0	0
30N	0	0	0	0	0	0	0	0	4	2	0	0	0	0	0	0	0	0	0	0	0	0	0	0	0	0	0	0	0	0	0	0	0	0	0	0
29N	0	0	0	0	0	0	0	1	0	0	0	0	0	0	0	0	0	0	0	0	0	0	0	0	0	0	0	0	0	0	0	0	0	0	0	0
28N	0	0	0	0	0	0	0	1	1	0	0	0	0	0	0	0	0	0	0	0	0	0	0	0	0	0	0	0	0	0	0	0	0	0	0	0
27N	0	0	0	0	0	0	0	0	1	0	0	0	0	0	0	0	0	0	0	0	0	0	0	0	0	0	0	0	0	0	0	0	0	0	0	0
26N	0	0	0	0	0	0	0	0	0	0	0	0	0	0	0	0	0	0	0	0	0	0	0	0	0	0	0	0	0	0	0	0	0	0	0	0
25N																																				

Table C4. The total number of large hail (> 19mm) events per 1° latitude-longitude grid box on day C+2 for the D sample.

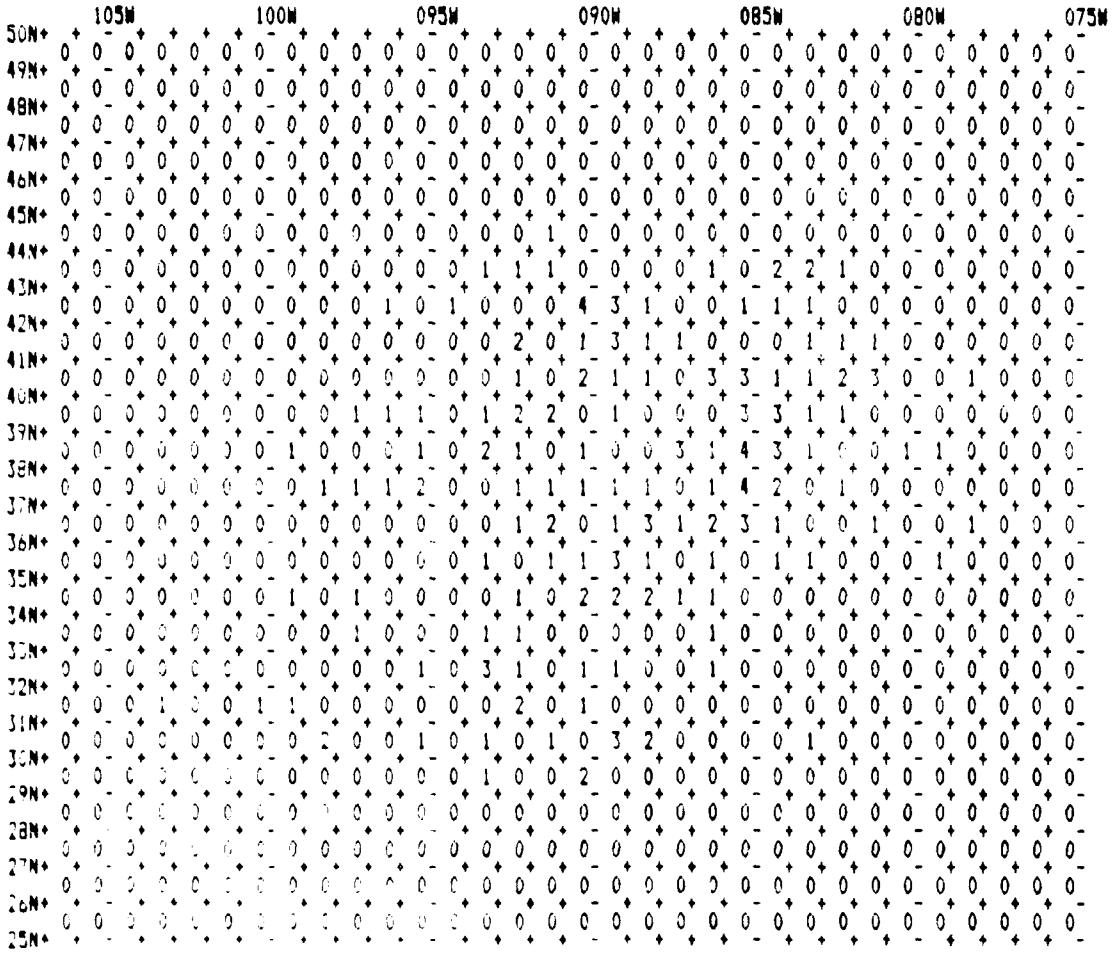

Table C. The total number of high wind (≥ 26 m/s) events per 1° latitude-longitude grid box on day C+2 for the D sample.

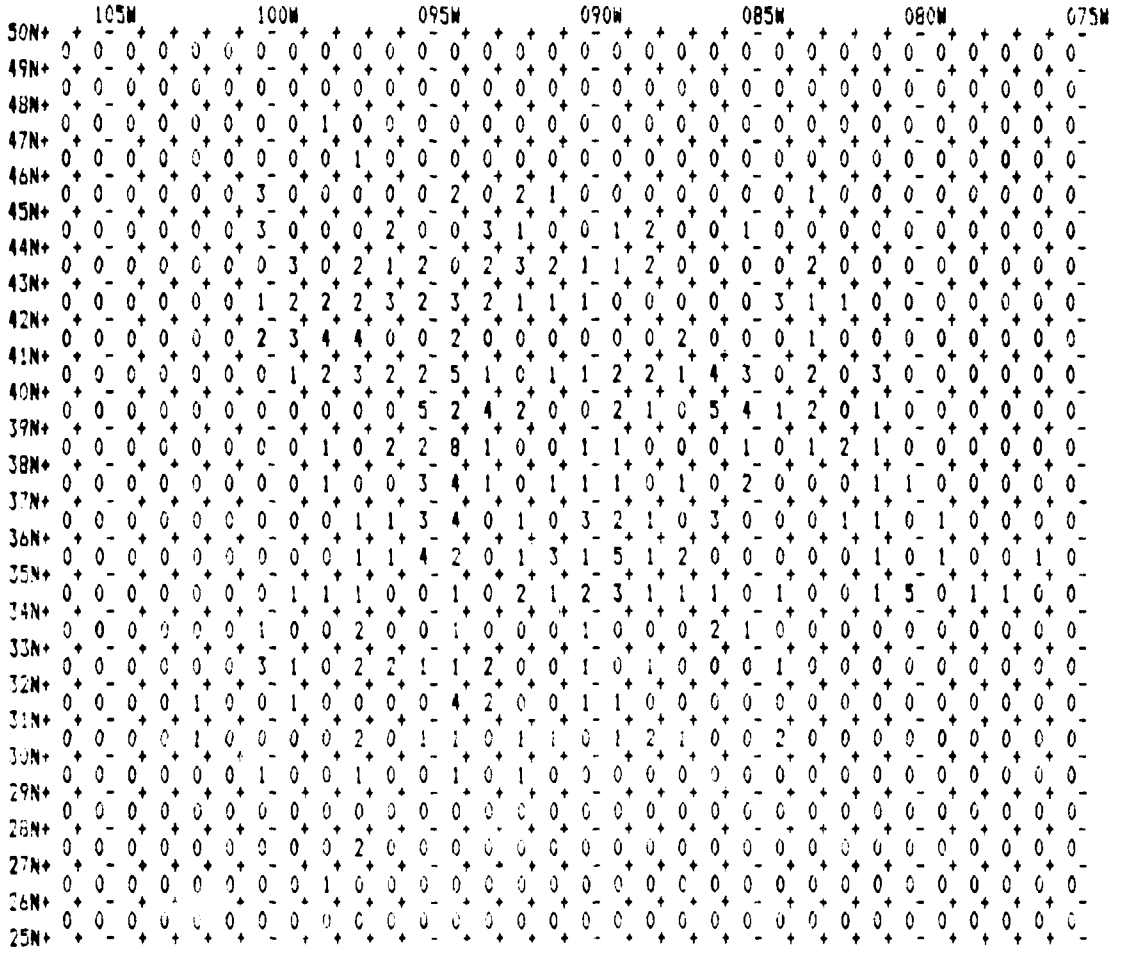

Table C2. The total number of tornado genesis events per 1° latitude-longitude grid box on July 0+2 for the D sample.

Appendix C. Total Severe Weather Events For Day C+2

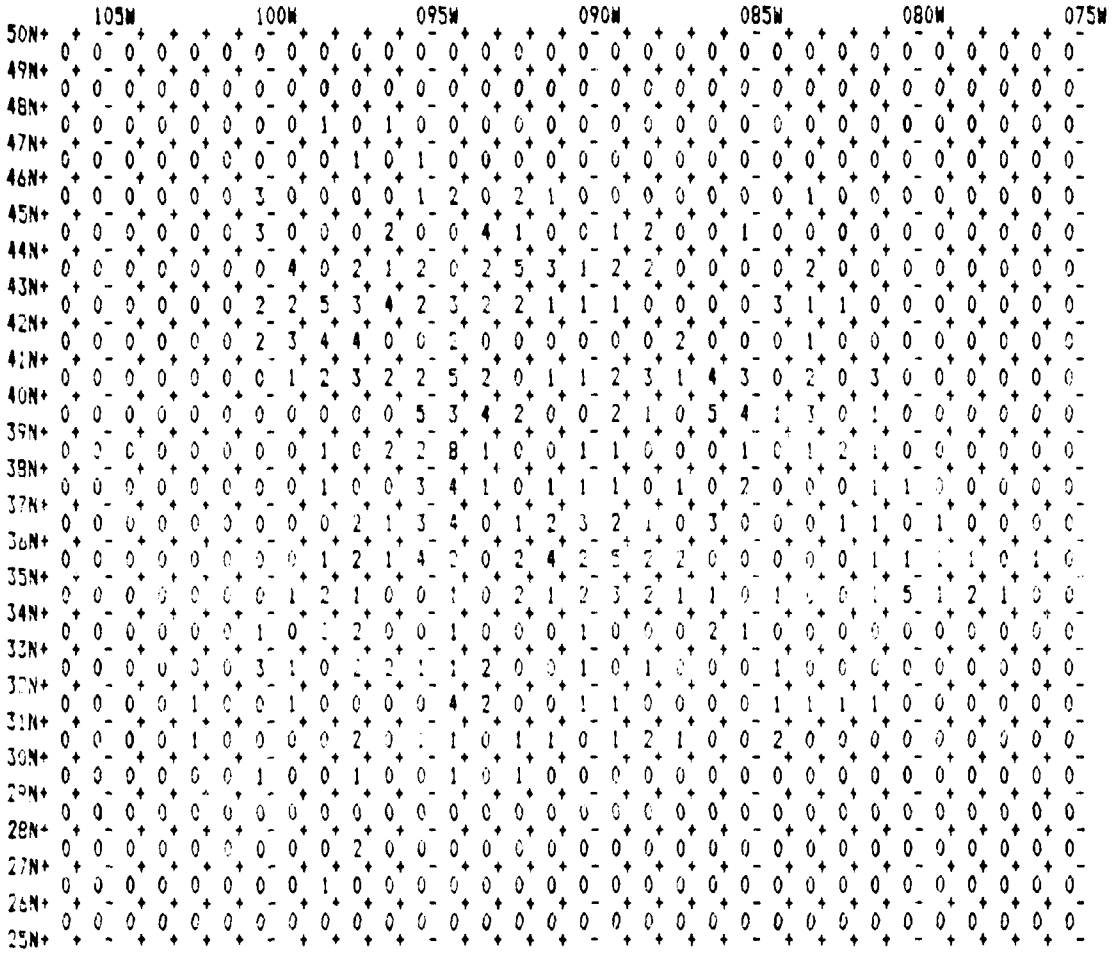

Table C1. The total number of tornado events per 1° latitude-longitude grid box on day C+2 for the D sample.

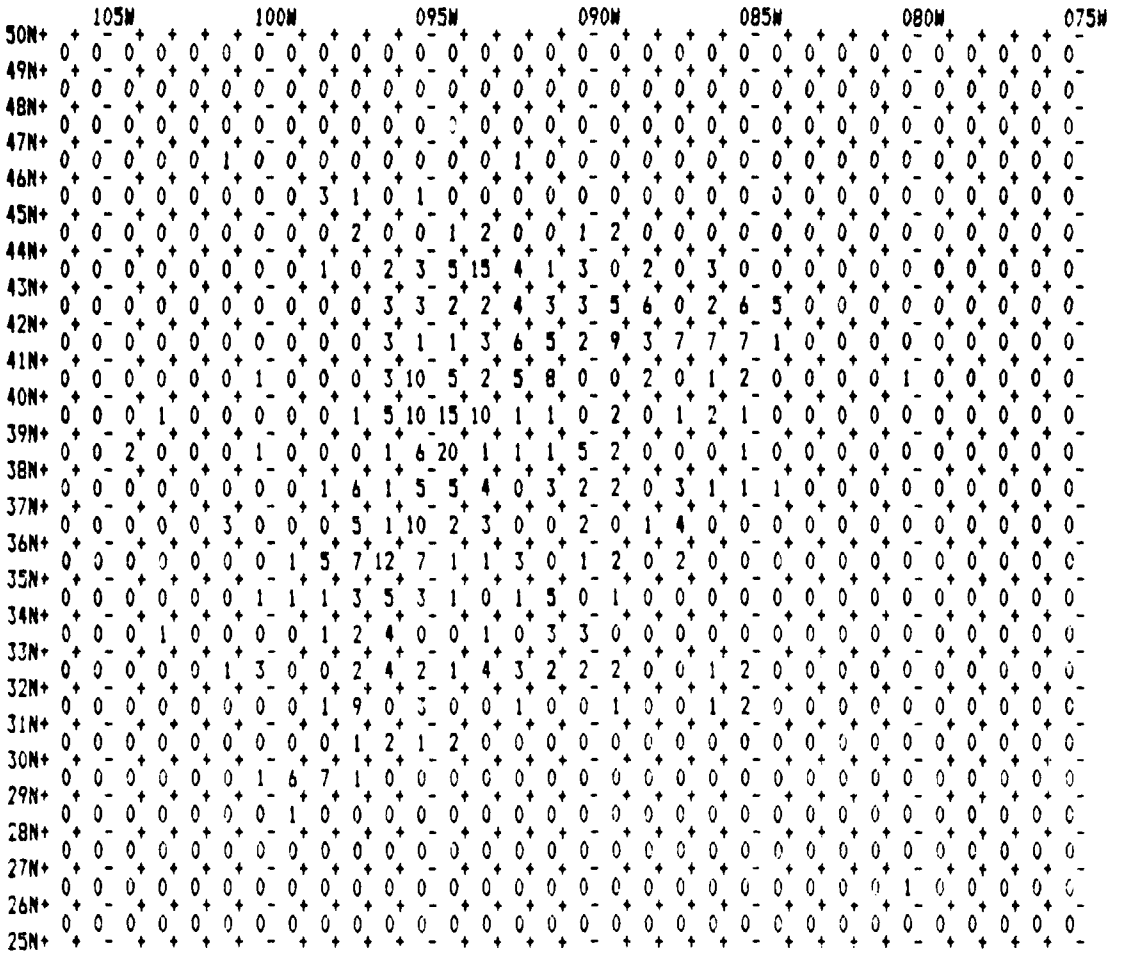

Table B14. The total number of severe storm events per 1° latitude-longitude grid box on day C+1 for the JS subsample.

	105W						100W						095W						090W						085W						080W						075W
50N	0	0	0	0	0	0	0	0	0	0	0	0	0	0	0	0	0	0	0	0	0	0	0	0	0	0	0	0	0	0	0	0	0	0	0	0
49N	0	0	0	0	0	0	0	0	0	0	0	0	0	0	0	0	0	0	0	0	0	0	0	0	0	0	0	0	0	0	0	0	0	0	0	0
48N	0	0	0	0	0	0	0	0	0	0	0	0	0	0	0	0	0	0	0	0	0	0	0	0	0	0	0	0	0	0	0	0	0	0	0	0
47N	0	0	0	0	0	0	0	0	0	0	0	0	0	0	0	0	0	0	0	0	0	0	0	0	0	0	0	0	0	0	0	0	0	0	0	0
46N	0	0	0	0	0	1	0	0	0	0	0	0	0	0	0	0	0	0	0	0	0	0	0	0	0	0	0	0	0	0	0	0	0	0	0	0
45N	0	0	0	0	0	0	0	0	0	0	0	0	0	0	0	0	0	0	0	0	0	0	0	0	0	0	0	0	0	0	0	0	0	0	0	0
44N	0	0	0	0	0	0	0	0	0	0	0	0	0	0	0	0	0	0	0	0	0	0	0	0	0	0	0	0	0	0	0	0	0	0	0	0
43N	0	0	0	0	0	0	0	0	0	0	1	3	0	3	1	0	0	0	0	0	0	0	0	0	0	0	0	0	0	0	0	0	0	0	0	0
42N	0	0	0	0	0	0	0	0	0	1	1	1	0	1	1	1	1	0	0	1	0	0	0	0	0	0	0	0	0	0	0	0	0	0	0	0
41N	0	0	0	0	0	0	0	0	0	0	1	0	0	3	1	0	0	0	5	5	5	0	0	0	0	0	0	0	0	0	0	0	0	0	0	0
40N	0	0	0	0	0	0	1	0	0	0	0	4	1	0	0	1	0	0	1	0	0	1	0	0	0	0	0	0	0	0	0	0	0	0	0	0
39N	0	0	0	1	0	0	0	0	0	0	1	6	8	3	0	0	0	1	0	1	1	0	0	0	0	0	0	0	0	0	0	0	0	0	0	0
38N	0	0	2	0	0	0	0	0	0	0	0	3	14	1	0	0	2	0	0	0	0	0	0	0	0	0	0	0	0	0	0	0	0	0	0	0
37N	0	0	0	0	0	0	0	0	1	4	0	0	0	1	0	1	0	0	0	0	0	1	0	0	0	0	0	0	0	0	0	0	0	0	0	0
36N	0	0	0	0	0	2	0	0	0	2	0	1	0	0	0	0	0	0	0	2	0	0	0	0	0	0	0	0	0	0	0	0	0	0	0	0
35N	0	0	0	0	0	0	0	0	2	2	7	2	0	0	2	0	0	0	0	1	0	0	0	0	0	0	0	0	0	0	0	0	0	0	0	0
34N	0	0	0	0	0	0	0	0	0	0	0	2	0	0	1	0	0	0	0	0	0	0	0	0	0	0	0	0	0	0	0	0	0	0	0	0
33N	0	0	0	0	0	0	0	0	0	1	1	0	0	0	0	1	0	0	0	0	0	0	0	0	0	0	0	0	0	0	0	0	0	0	0	0
32N	0	0	0	0	0	0	0	0	0	0	0	0	0	0	0	0	0	0	0	0	0	0	0	0	0	0	0	0	0	0	0	0	0	0	0	0
31N	0	0	0	0	0	0	0	0	0	1	0	1	0	0	0	0	0	0	0	0	0	0	0	0	0	0	0	0	0	0	0	0	0	0	0	0
30N	0	0	0	0	0	0	0	0	0	0	1	0	1	0	0	0	0	0	0	0	0	0	0	0	0	0	0	0	0	0	0	0	0	0	0	0
29N	0	0	0	0	0	0	0	0	0	1	0	0	0	0	0	0	0	0	0	0	0	0	0	0	0	0	0	0	0	0	0	0	0	0	0	0
28N	0	0	0	0	0	0	0	0	0	0	0	0	0	0	0	0	0	0	0	0	0	0	0	0	0	0	0	0	0	0	0	0	0	0	0	0
27N	0	0	0	0	0	0	0	0	0	0	0	0	0	0	0	0	0	0	0	0	0	0	0	0	0	0	0	0	0	0	0	0	0	0	0	0
26N	0	0	0	0	0	0	0	0	0	0	0	0	0	0	0	0	0	0	0	0	0	0	0	0	0	0	0	0	1	0	0	0	0	0	0	0
25N	0	0	0	0	0	0	0	0	0	0	0	0	0	0	0	0	0	0	0	0	0	0	0	0	0	0	0	0	0	0	0	0	0	0	0	0

Table B13. The total number of funnel cloud genesis events per 1° latitude-longitude grid box on day C+1 for the JS subsample.

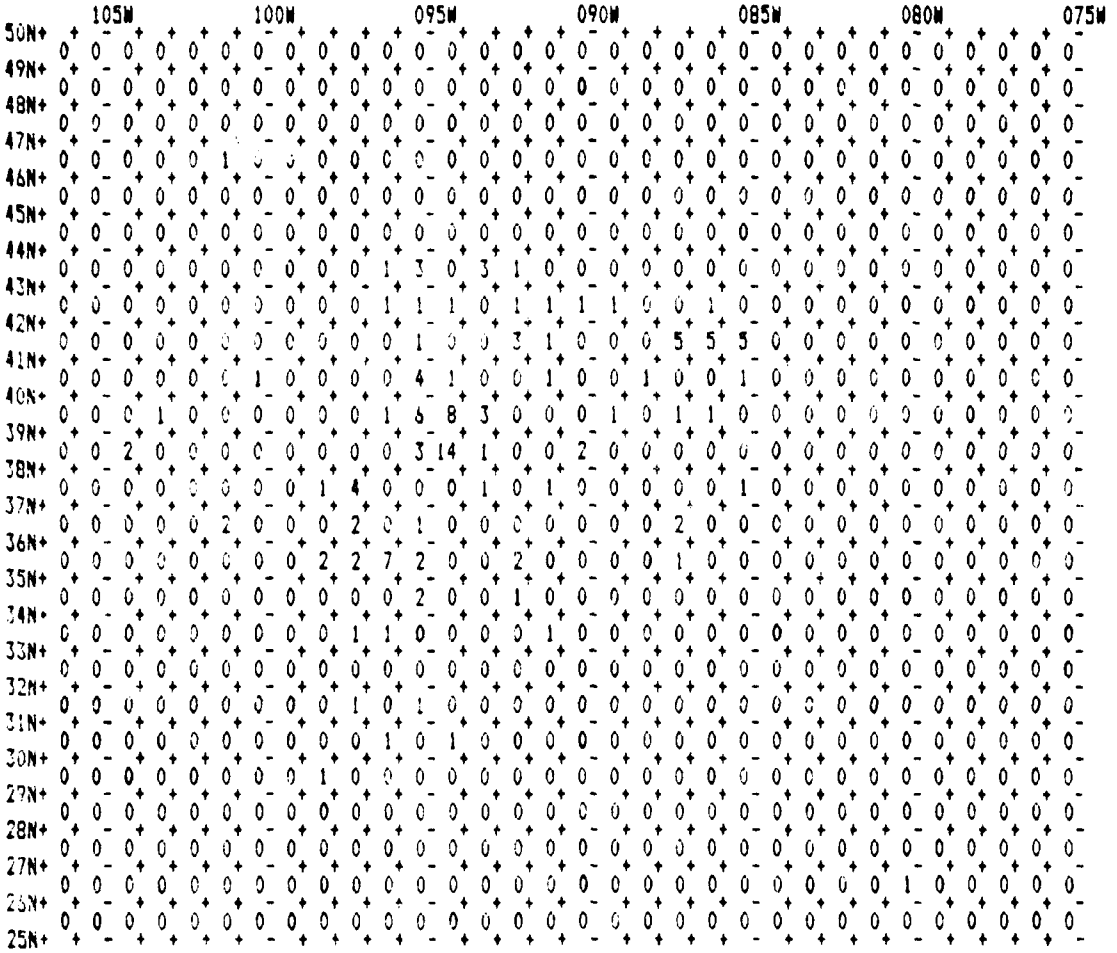

Table 12. The total number of funnel cloud events per 1° latitude-longitude grid box on day C+1 for the JS subsample.

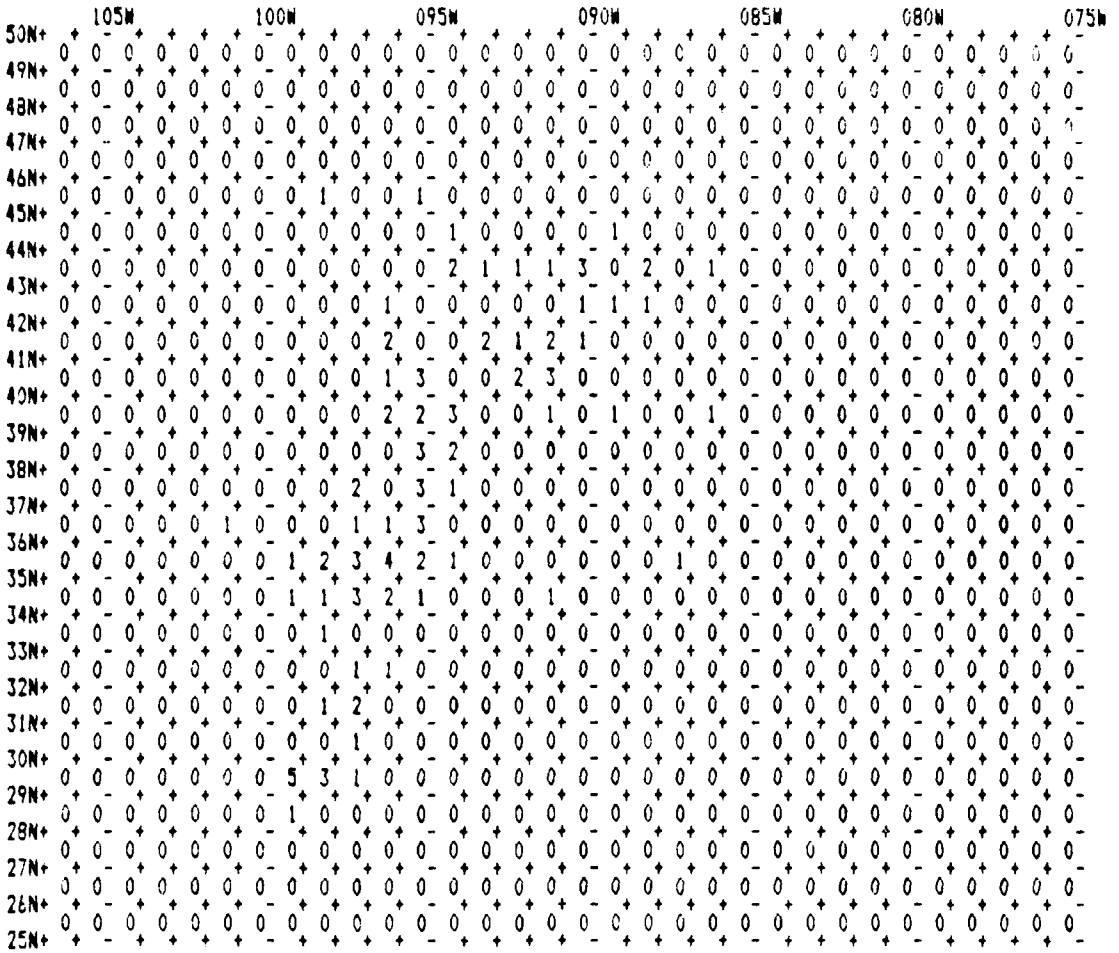

Table B11. The total number of large hail (> 19mm) events per 1° latitude-longitude grid box on day C+1 for the JS subsample.

	105W	100W	095W	090W	085W	080W	075W
50N	0 0 0 0 0 0 0 0 0 0 0 0 0 0 0 0 0 0 0 0 0 0 0 0 0 0 0 0 0 0 0						
49N	0 0 0 0 0 0 0 0 0 0 0 0 0 0 0 0 0 0 0 0 0 0 0 0 0 0 0 0 0 0 0						
48N	0 0 0 0 0 0 0 0 0 0 0 0 0 0 0 0 0 0 0 0 0 0 0 0 0 0 0 0 0 0 0						
47N	0 0 0 0 0 0 0 0 0 0 0 0 0 0 0 0 0 0 0 0 0 0 0 0 0 0 0 0 0 0 0						
46N	0 0 0 0 0 0 0 0 0 0 0 0 0 0 0 0 0 0 0 0 0 0 0 0 0 0 0 0 0 0 0						
45N	0 0 0 0 0 0 0 0 0 0 0 0 0 0 0 0 0 0 0 0 0 0 0 0 0 0 0 0 0 0 0						
44N	0 0 0 0 0 0 0 0 0 0 0 0 0 0 0 0 0 0 0 0 0 0 0 0 0 0 0 0 0 0 0						
43N	0 0 0 0 0 0 0 0 0 0 0 0 0 0 0 0 0 0 0 0 0 0 0 0 0 0 0 0 0 0 0						
42N	0 0 0 0 0 0 0 0 0 0 0 0 0 0 0 0 0 0 0 0 0 0 0 0 0 0 0 0 0 0 0						
41N	0 0 0 0 0 0 0 0 0 0 0 0 0 0 0 0 0 0 0 0 0 0 0 0 0 0 0 0 0 0 0						
40N	0 0 0 0 0 0 0 0 0 0 1 2 1 0 1 0 0 0 0 0 0 0 0 0 0 1 0 0 0 0 0						
39N	0 0 0 0 0 0 0 0 0 0 0 0 3 1 0 0 0 0 0 0 0 0 0 0 0 0 0 0 0 0 0						
38N	0 0 0 0 0 0 0 0 0 0 0 0 1 0 0 0 0 0 0 0 0 0 0 0 0 0 0 0 0 0 0						
37N	0 0 0 0 0 0 0 0 0 0 0 1 2 2 0 0 0 0 0 2 1 0 1 0 0 0 0 0 0 0 0						
36N	0 0 0 0 0 0 0 0 0 2 0 2 1 0 0 0 0 0 0 1 0 0 0 0 0 0 0 0 0 0 0						
35N	0 0 0 0 0 0 0 0 0 1 0 2 0 0 0 0 0 0 0 0 0 0 0 0 0 0 0 0 0 0 0						
34N	0 0 0 0 0 0 1 0 0 0 1 0 0 0 0 1 0 0 0 0 0 0 0 0 0 0 0 0 0 0 0						
33N	0 0 0 0 0 0 0 0 0 1 1 0 0 0 0 0 1 0 0 0 0 0 0 0 0 0 0 0 0 0 0						
32N	0 0 0 0 0 0 0 0 0 0 3 0 0 1 1 1 0 1 0 0 0 0 0 0 0 0 0 0 0 0 0						
31N	0 0 0 0 0 0 0 0 0 1 0 1 0 0 1 0 0 1 0 0 0 1 0 0 0 0 0 0 0 0 0						
30N	0 0 0 0 0 0 0 0 0 0 0 0 0 0 0 0 0 0 0 0 0 0 0 0 0 0 0 0 0 0 0						
29N	0 0 0 0 0 0 0 1 2 0 0 0 0 0 0 0 0 0 0 0 0 0 0 0 0 0 0 0 0 0 0						
28N	0 0 0 0 0 0 0 0 0 0 0 0 0 0 0 0 0 0 0 0 0 0 0 0 0 0 0 0 0 0 0						
27N	0 0 0 0 0 0 0 0 0 0 0 0 0 0 0 0 0 0 0 0 0 0 0 0 0 0 0 0 0 0 0						
26N	0 0 0 0 0 0 0 0 0 0 0 0 0 0 0 0 0 0 0 0 0 0 0 0 0 0 0 0 0 0 0						
25N	0 0 0 0 0 0 0 0 0 0 0 0 0 0 0 0 0 0 0 0 0 0 0 0 0 0 0 0 0 0 0						

Table B10. The total number of high wind (≥ 26 m/s) events per 1 latitude-longitude grid box on day 0+1 for the JS subsample.

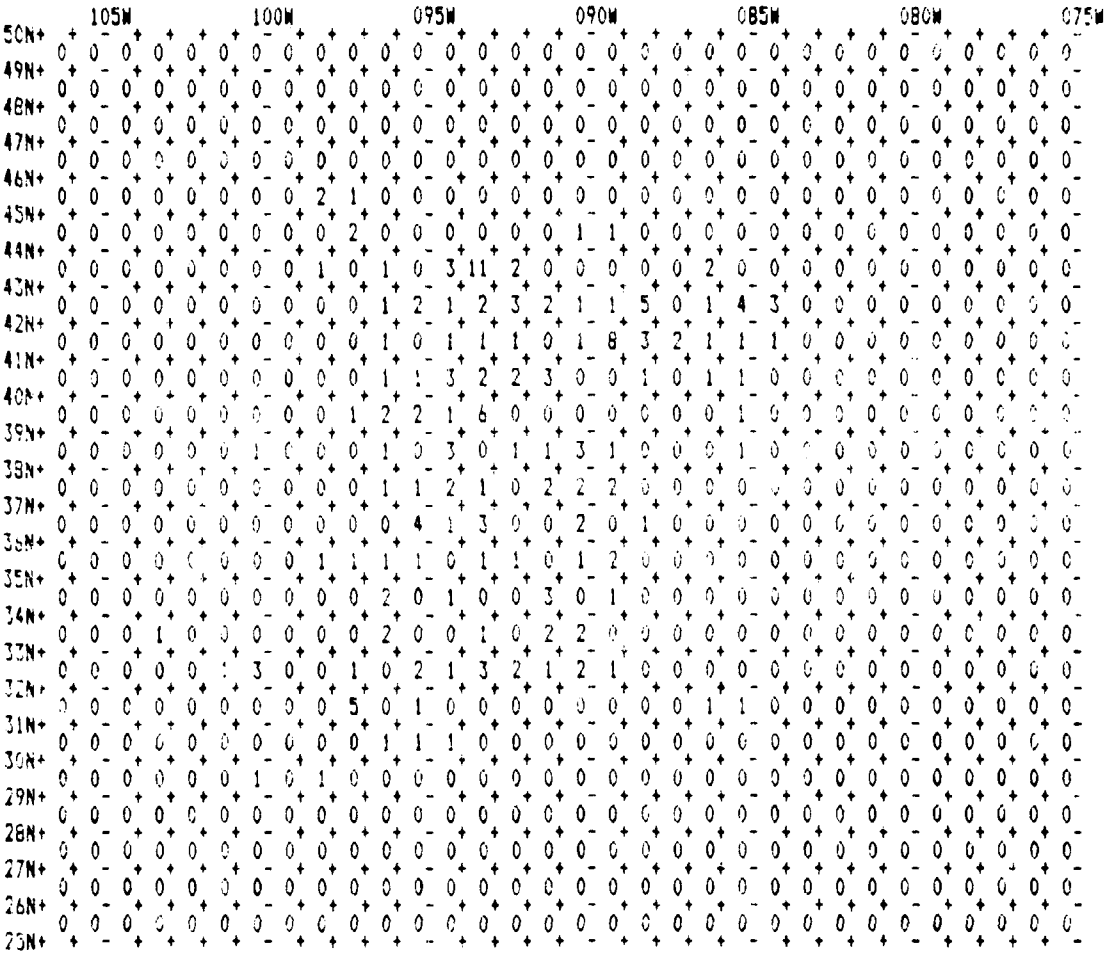

Table B9. The total number of tornado genesis events per 1° latitude-longitude grid box on day C+1 for the JS subsample.

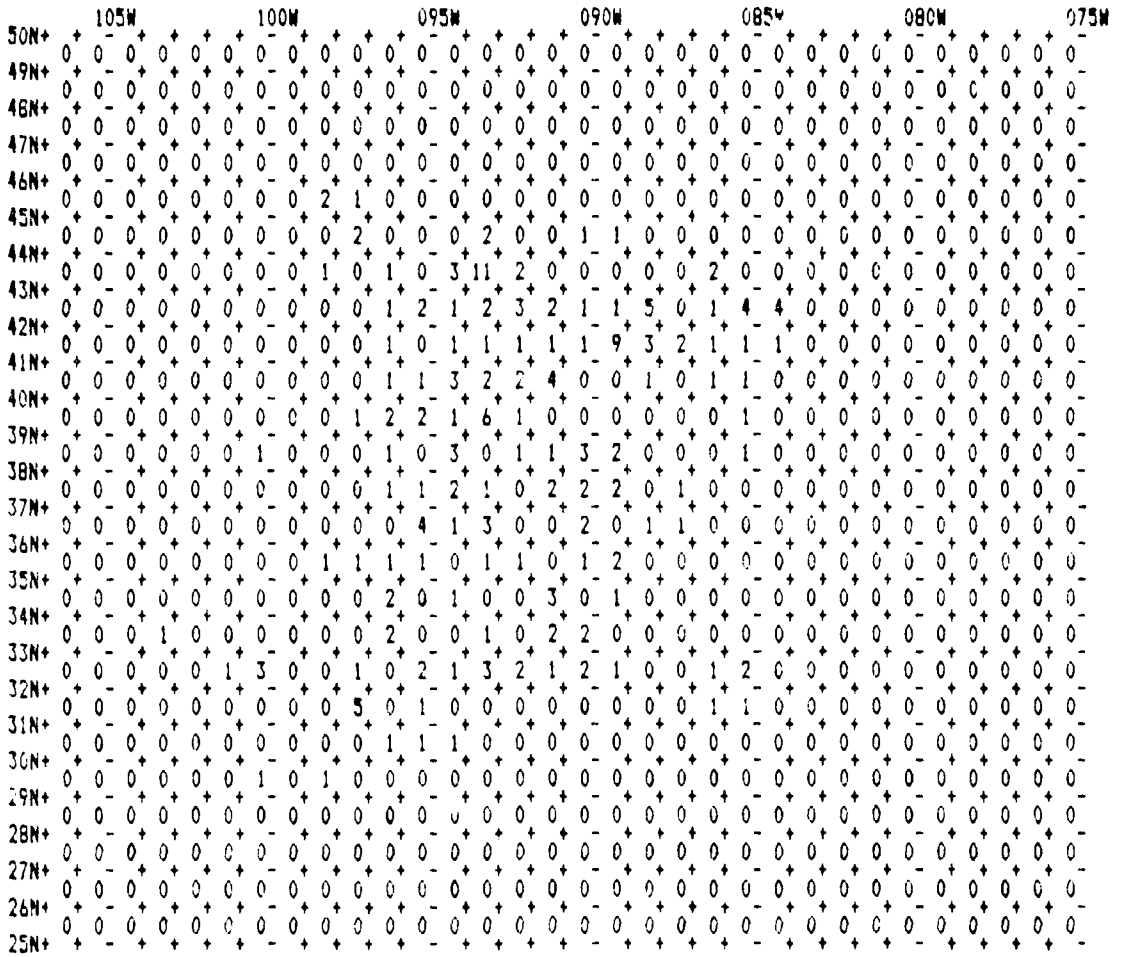

Table B8. The total number of tornado events per 1° latitude-longitude grid box on day C+1 for the JS subsample.

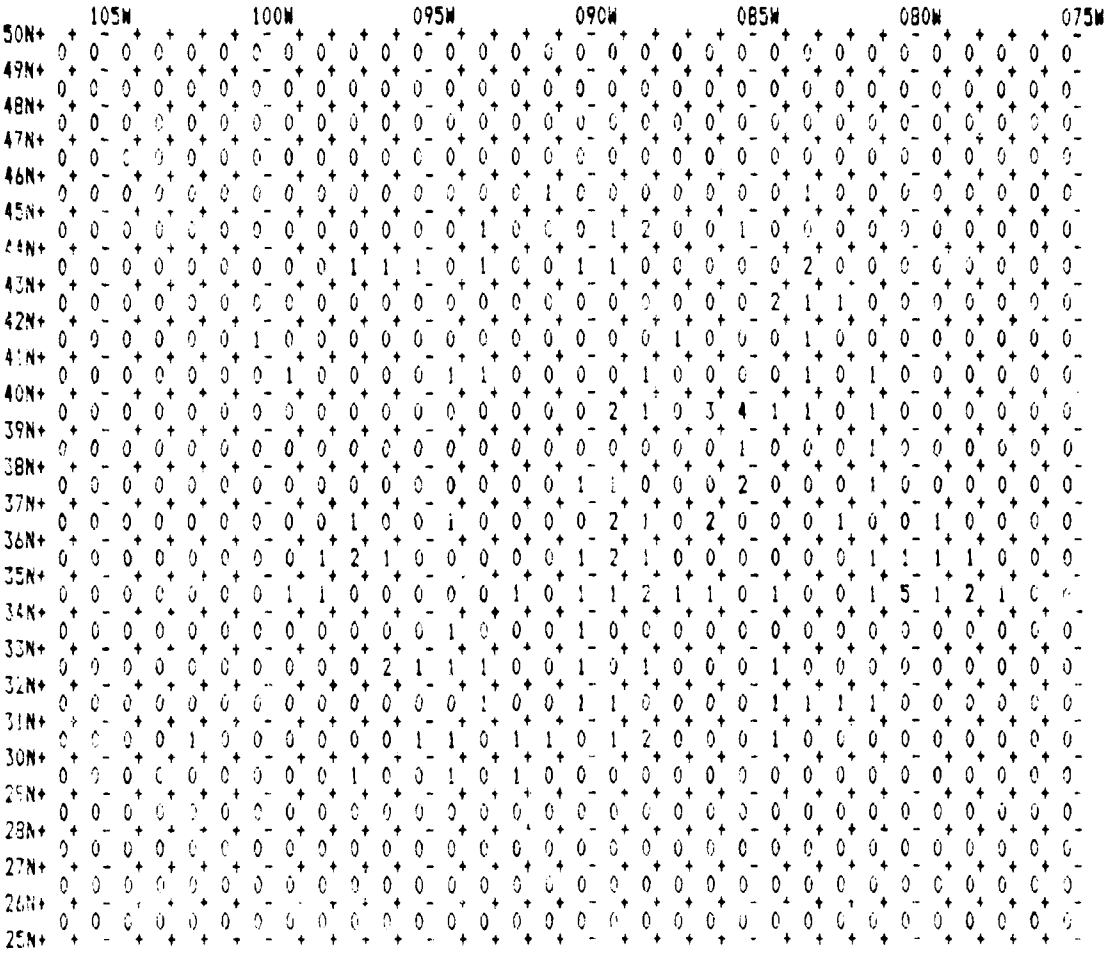

Table C8. The total number of tornado events per 1° latitude-longitude grid box on day C+2 for the 70 subsample.

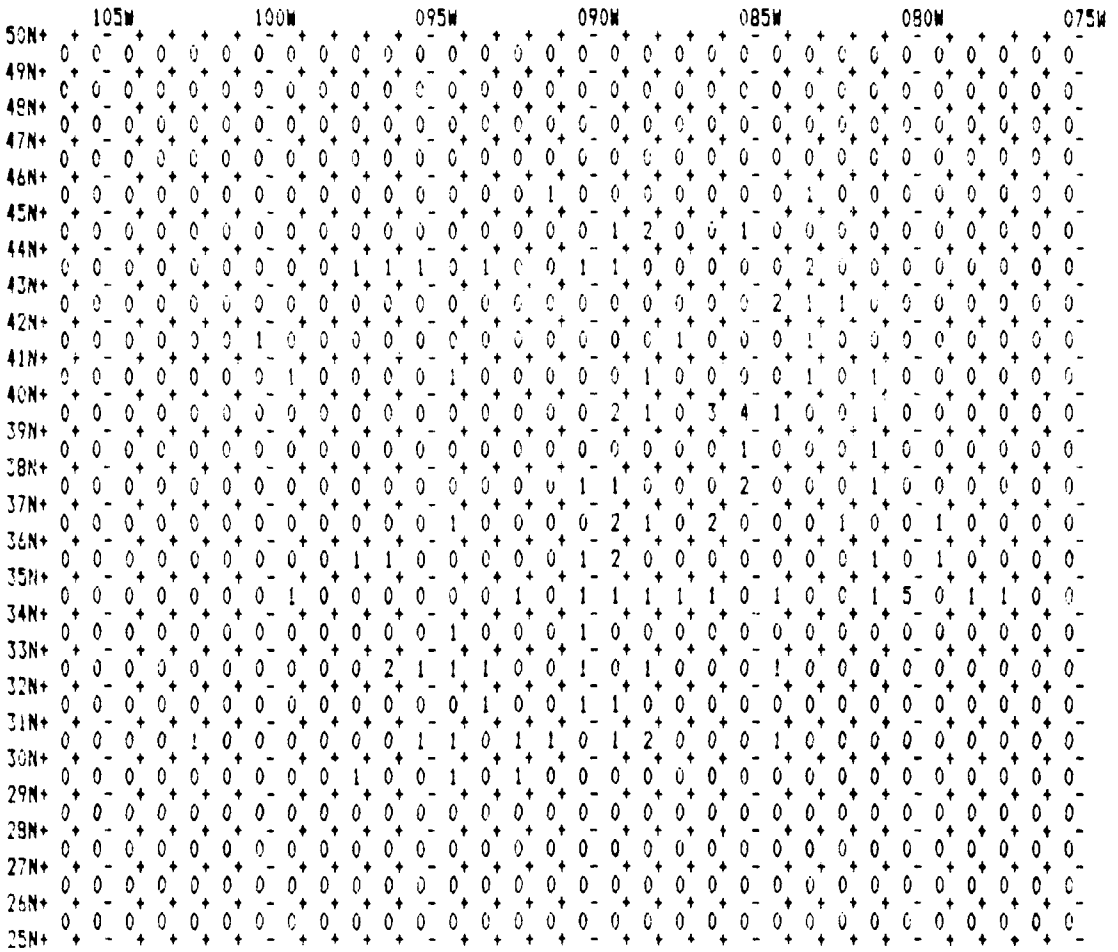

Table C9. The total number of tornado genesis events per 1° latitude-longitude grid box on day C+2 for the JS subsample.

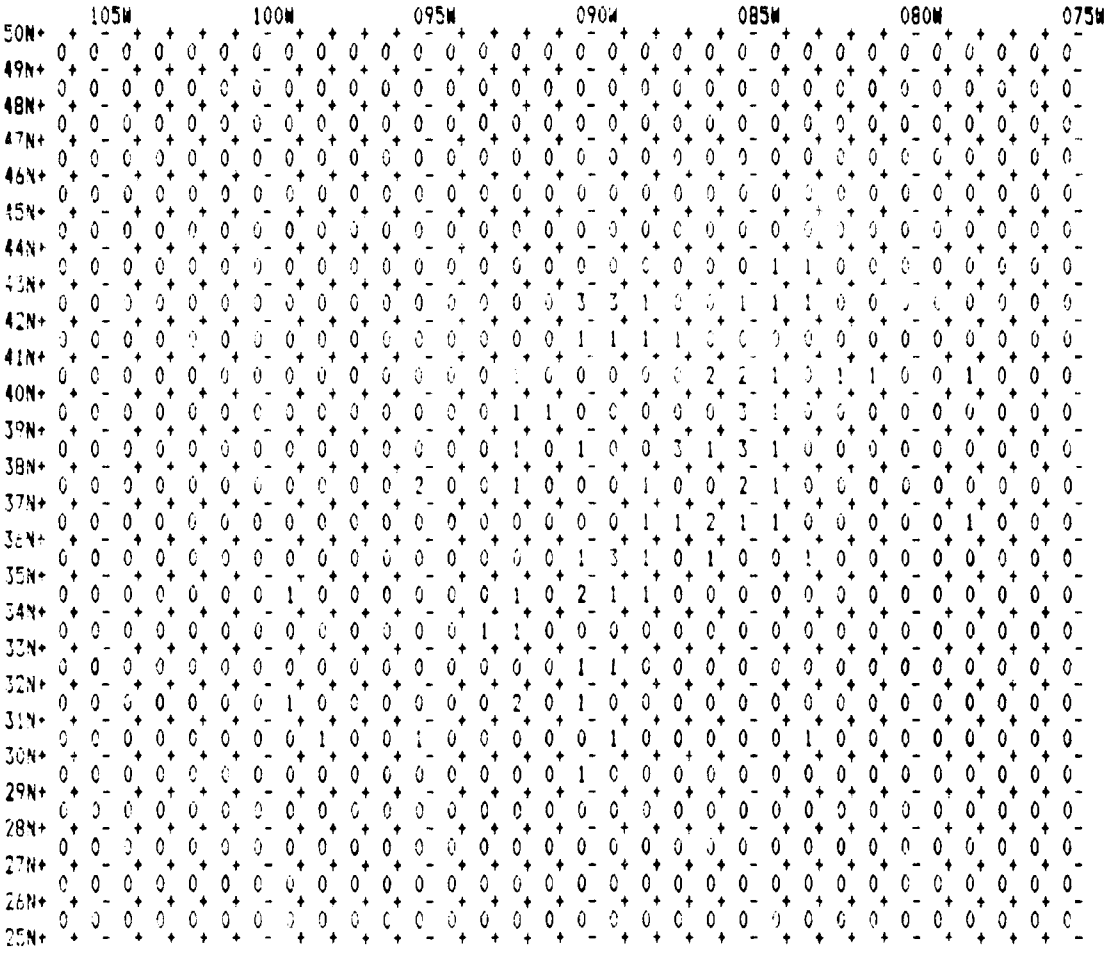

Table C10. The total number of high wind (≥ 26 m/s) events per 1° latitude-longitude grid box on day C+2 for the JS subsample.

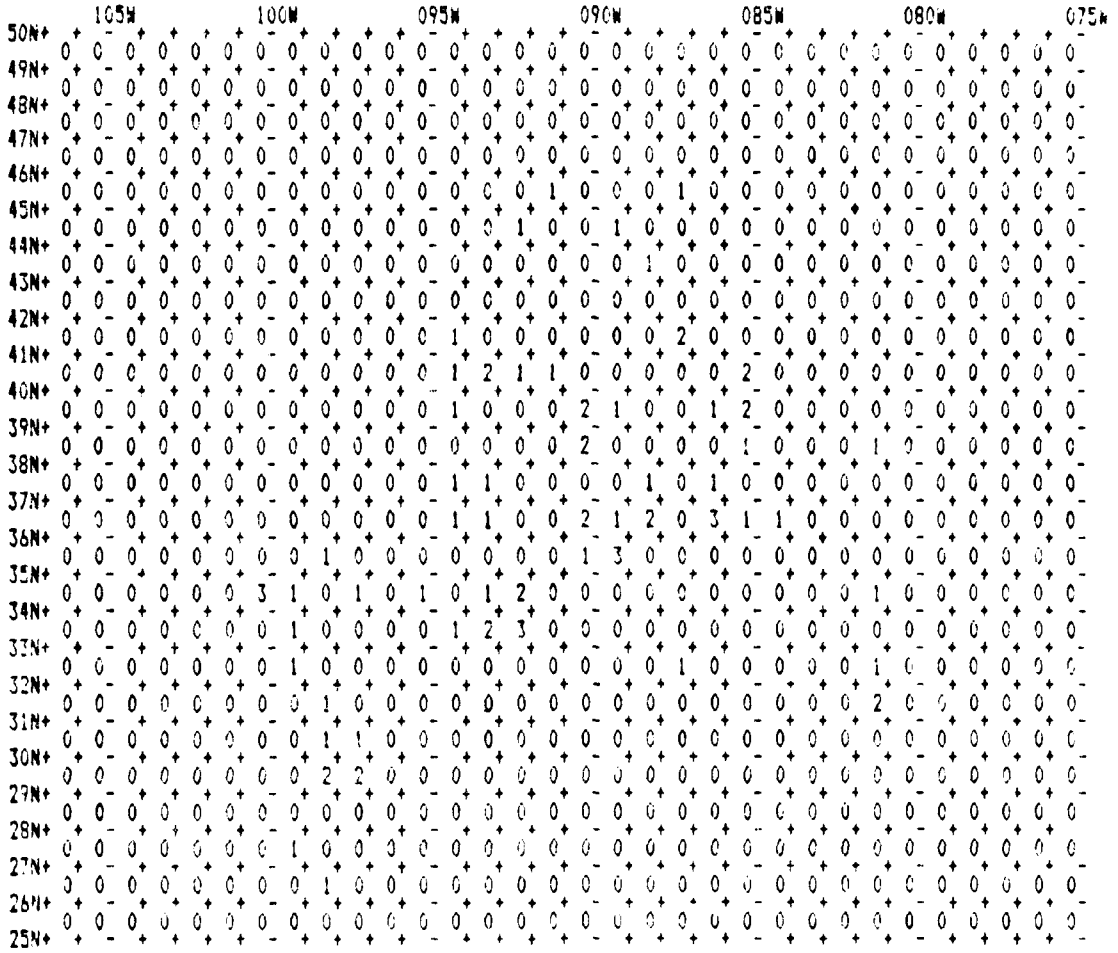

Table C11. The total number of large hail (> 19mm) events per 1 latitude-longitude grid box on day C+2 for the JS subsample.

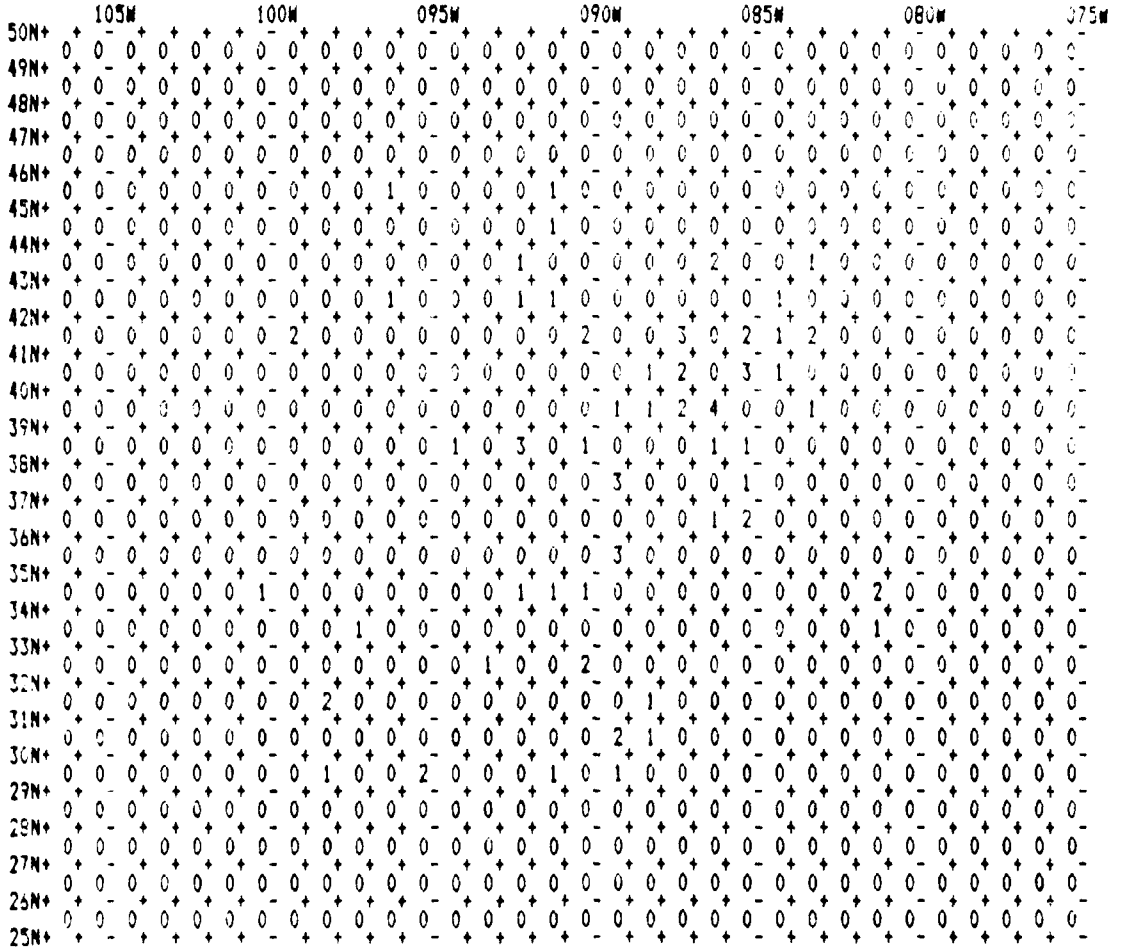

Table C12. The total number of funnel cloud events per 1° latitude-longitude grid box on day C+2 for the JS subsample.

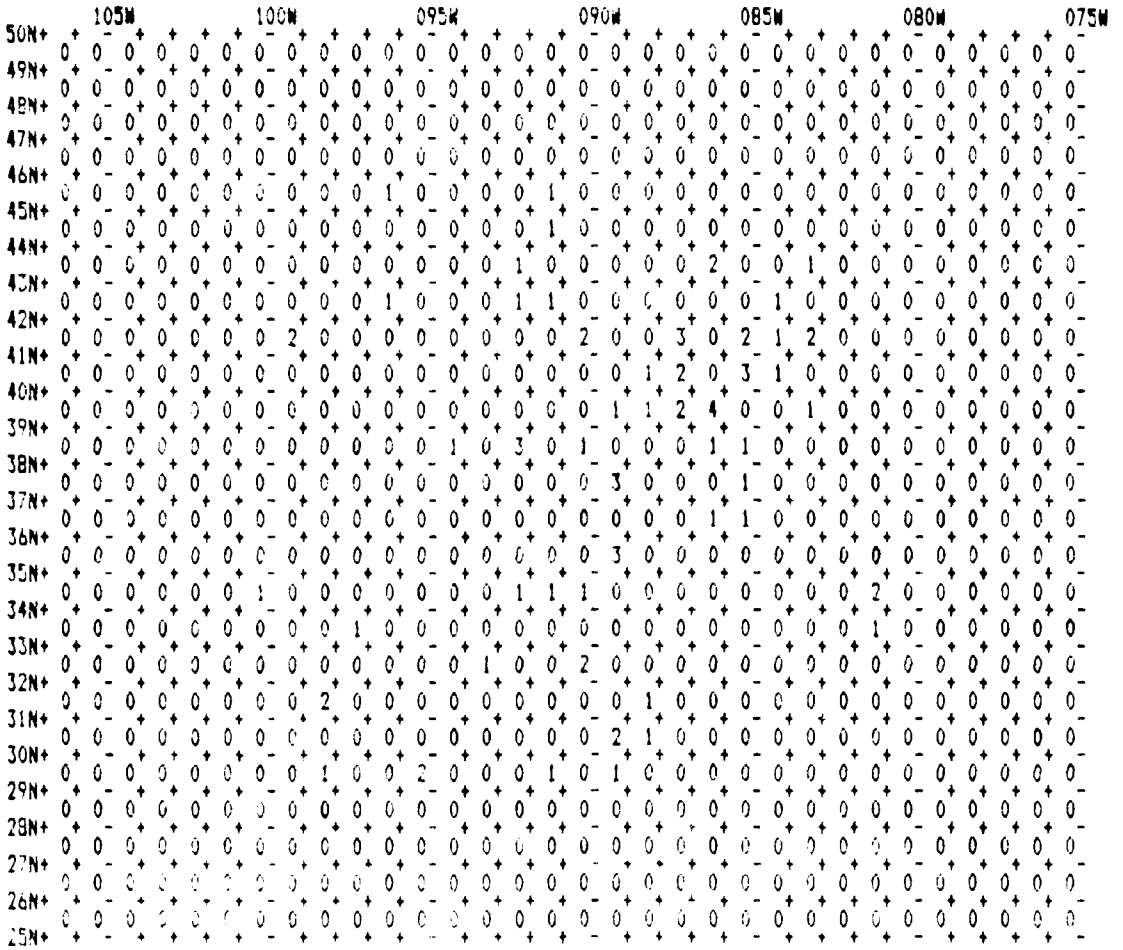

Table C14. The total number of funnel cloud genesis events per 1° latitude-longitude grid box on day C+2 for the JS subsample.

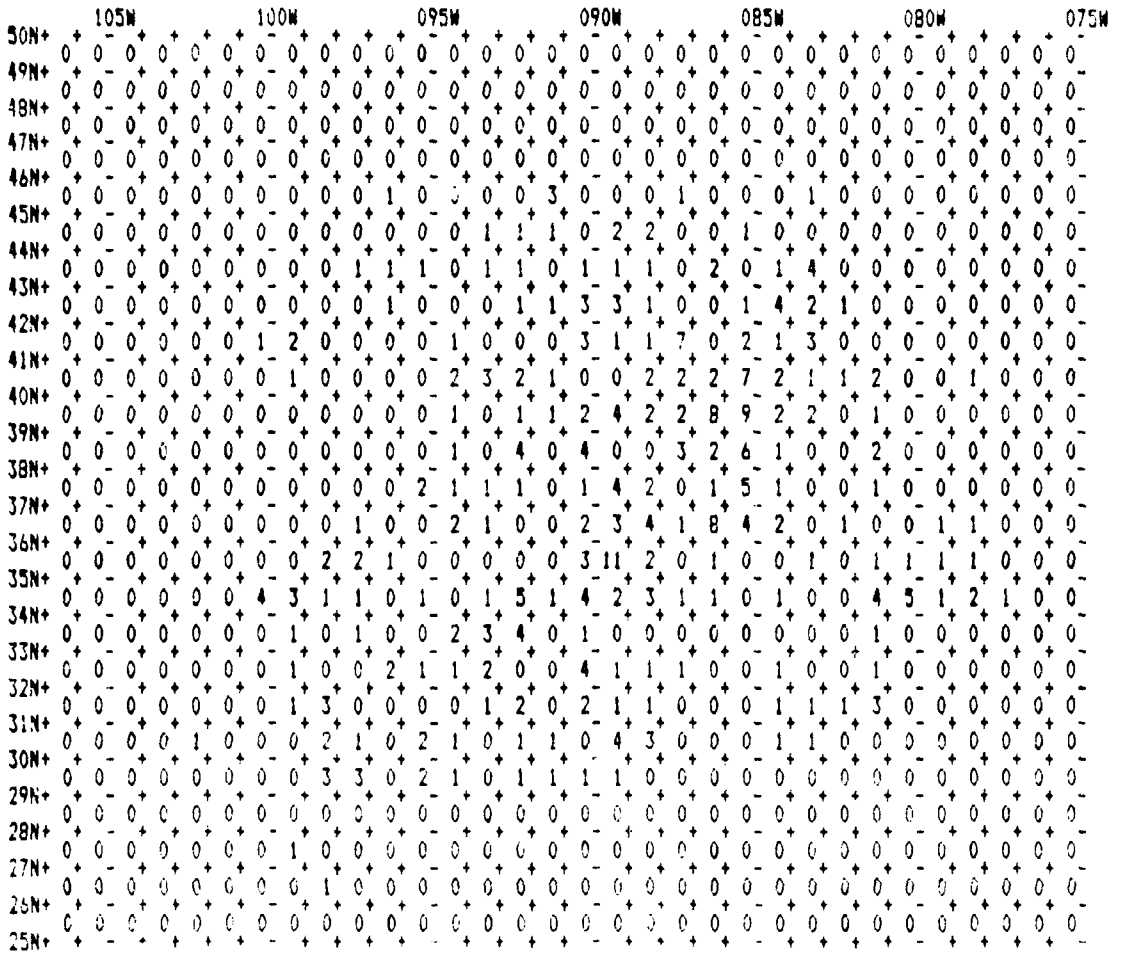

Table C14. The total number of severe storm events per 1° latitude-longitude grid box on day C+2 for the JS subsample.

Appendix D. Normalized JS' Total Severe Storm Events For Day C

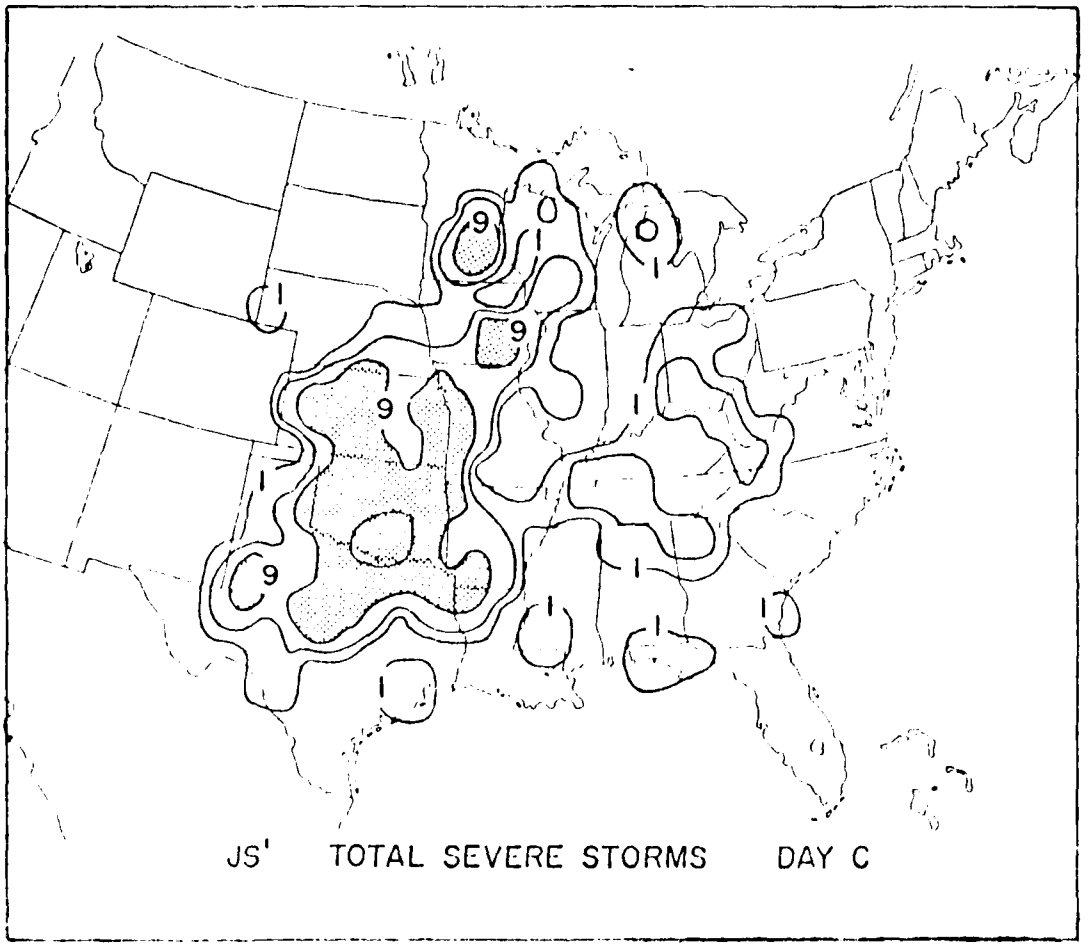

Fig. D1. Normalized and smoothed frequency (10^{-2}) of total severe storms for the JS' subsample on day C.

Appendix E. Normalized Severe Storm Events For Day C+1

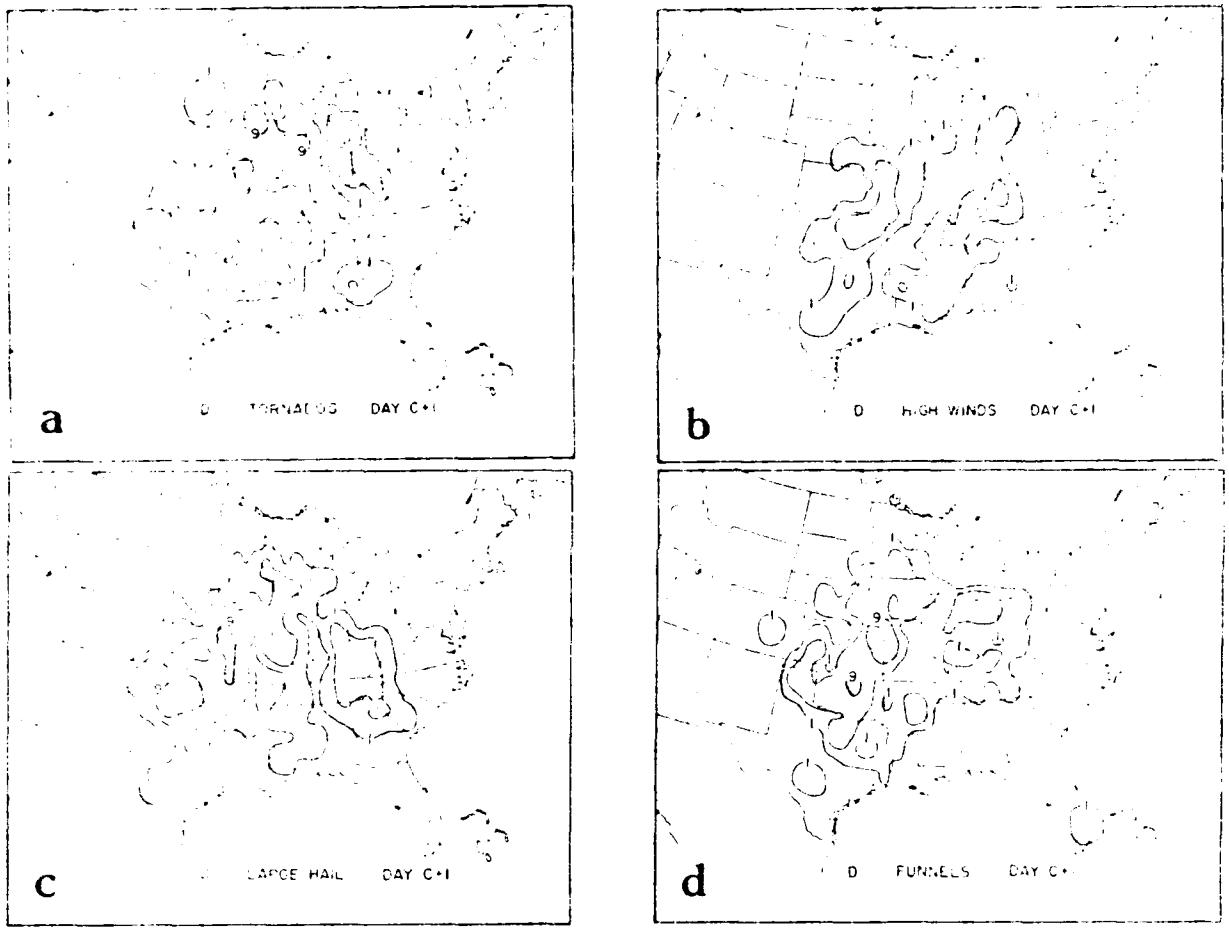

Fig. E1. Normalized and smoothed frequency (10^{-2}) of (a) tornados, (b) high winds (≥ 26 m/s), (c) large hail (> 19mm) and (d) funnel clouds for the D sample on day C+1.

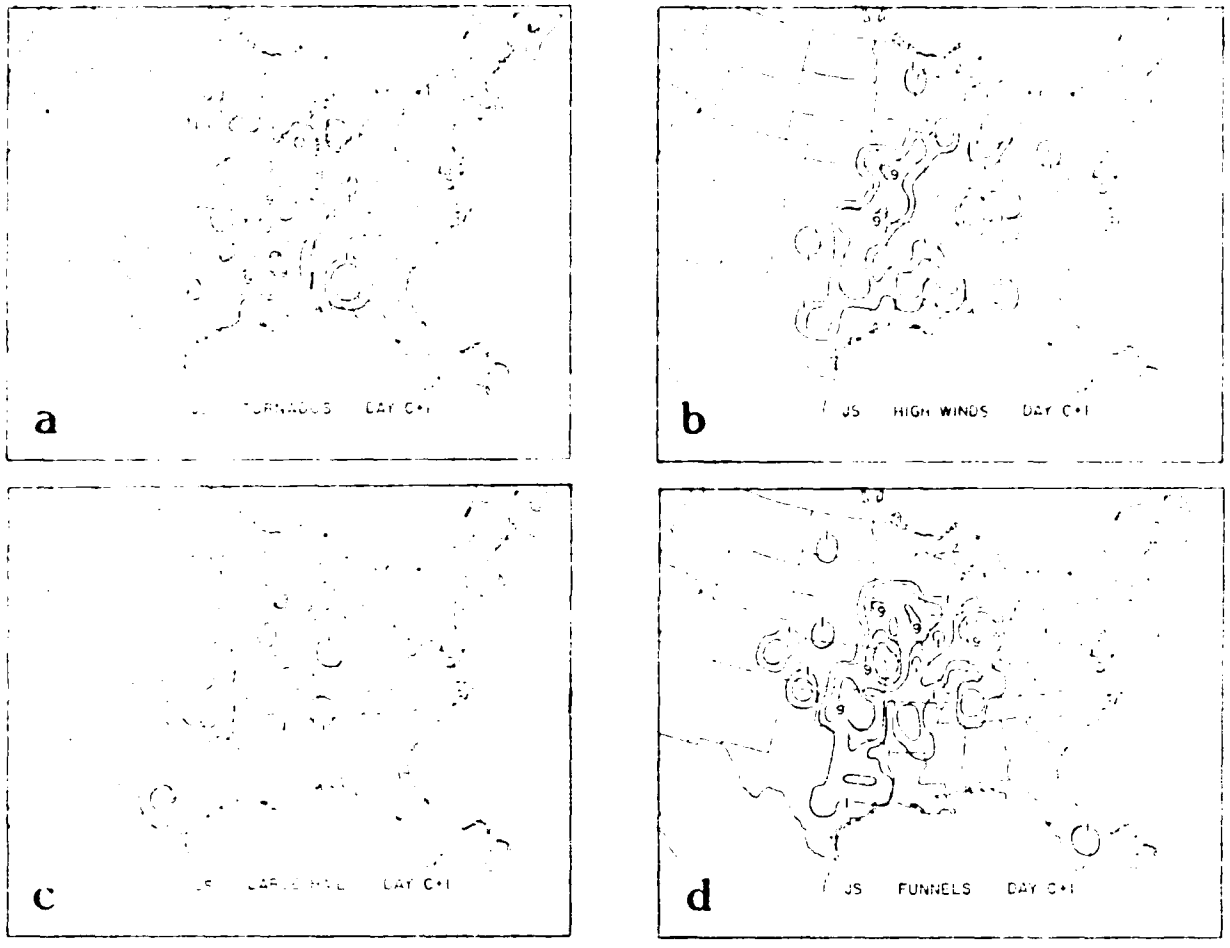

Fig. E2. Normalized and smoothed frequency (10^{-2}) of (a) tornados, (b) high winds ($\geq$ 26 m/s), (c) large hail (> 19mm) and (d) funnel clouds for the JS subsample on day C+1.

Appendix F. Normalized Severe Storm Events For Day C+2

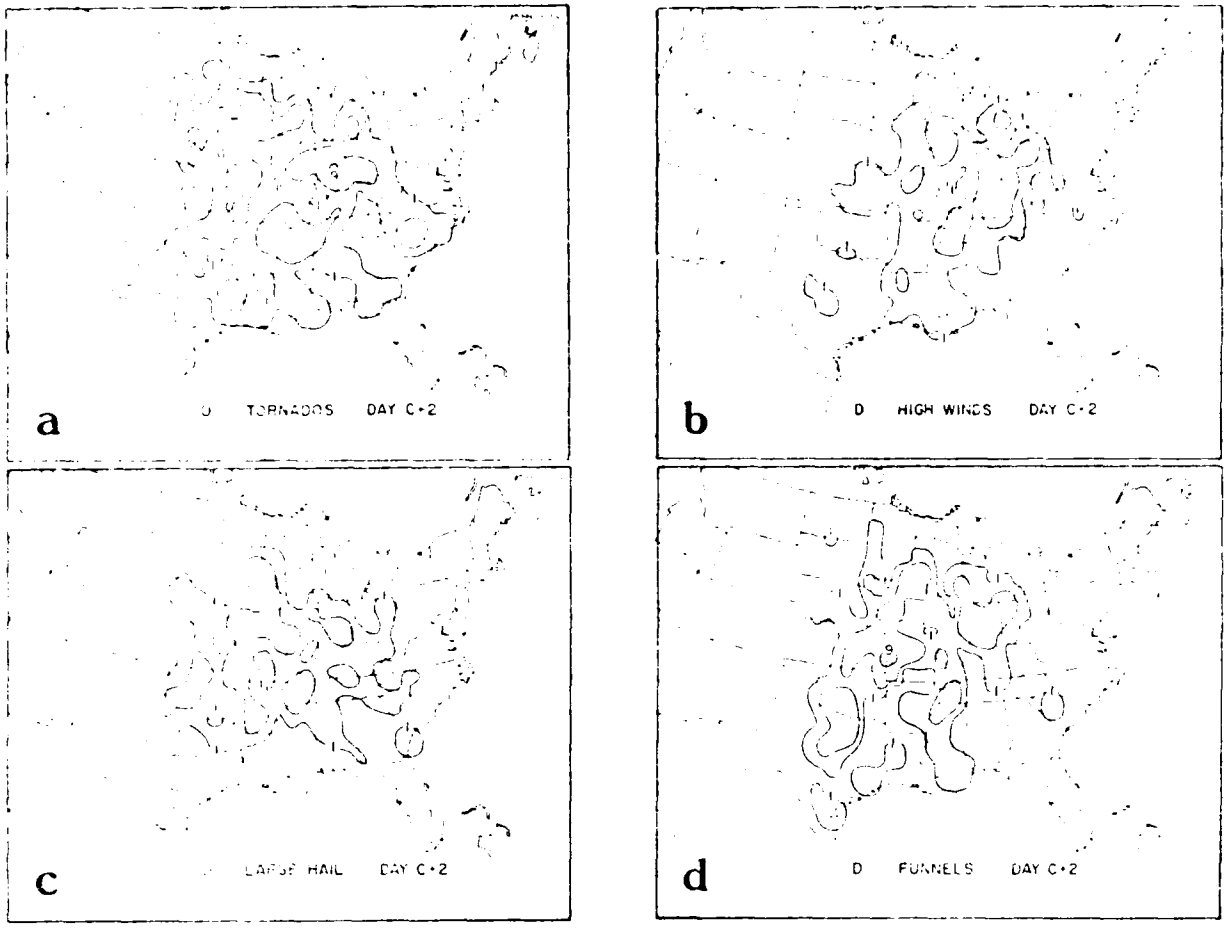

Fig. F1. Normalized and smoothed frequency (10^{-2}) of (a) tornados, (b) high winds (≥ 26 m/s), (c) large hail (> 19mm) and (d) funnel clouds for the D sample on day C+2.

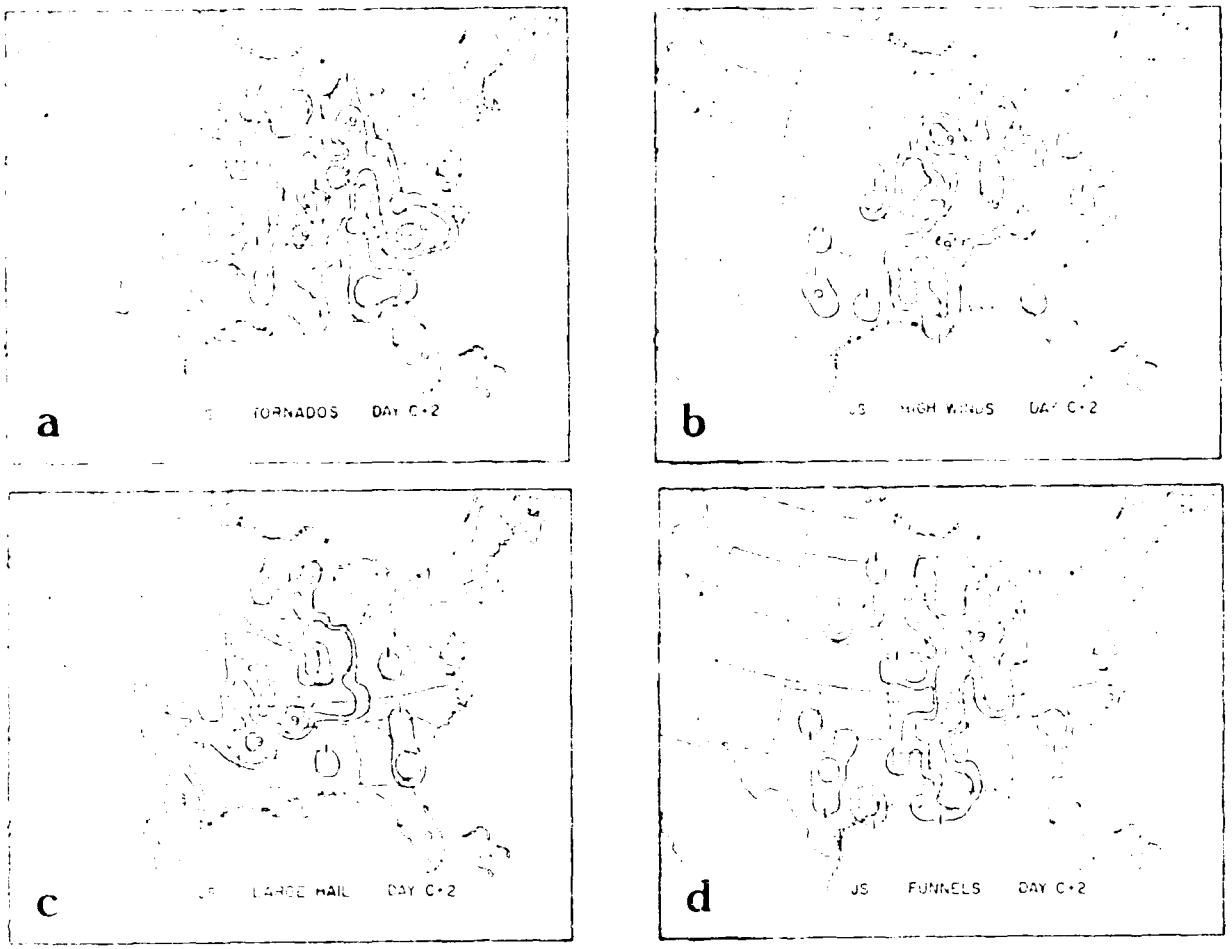

Fig. F2. Normalized and smoothed frequency (10^{-2}) of (a) tornados, (b) high winds ($\geq$ 26 m/s), (c) large hail (> 19mm) and (d) funnel clouds for the JS subsample on day C+2.

REFERENCES

Achtor, T.H., and L.H. Horn, 1985: Spring season Colorado cyclones. Part I. Use of composites to relate upper and lower tropospheric wind fields. submitted to J. Clim. Appl. Meteor.

Carlson, T.N. and F. Ludlum, 1963: Conditions for the occurrence of severe local storms. Tellus, 20, 203-226.

Court, A., 1974: The climate of the conterminous United States. In Climates of North America, World Survey of Climatology, 11, Elsevier, New York, 193-343.

Fawbush, E.J., and R.C. Miller, 1953: The tornado situation of 17 March 1951. Bull. Amer. Meteor. Soc., 34, 139-145.

____, and ____, 1954: The types of air masses in which North American tornadoes form. Bull. Amer. Meteor. Soc., 35, 154-165.

Hovanec, R.D., and L.H. Horn, 1975: Static stability and the 300 mb isotach field in the Colorado cyclogenetic area. Mon. Wea. Rev., 103, 628-638.

Johnson, D.R. and F. Sechrist, 1979: On the isentropic representation of storms, dynamic destabilization and squall line formation. Paper presented at 51st Annual Meeting of American Geophysical Union, Washington, D.C., Abstract, EOS Transaction. Amer. Geophys. Union, 51, 4, 294.

Kelly, D.L., J.T. Schaefer, R.P. McNulty and C.A. Doswell III, 1978: An augmented tornado climatology. Mon. Wea. Rev., 106, 1172-1183.

Marchment, A.A., and L.H. Horn, 1985: Spring season Colorado cyclones. Part II. Composites of atmospheric moisture and moist convective activity. Submitted to J. Clim. Appl. Meteor.

Uccellini, L.W., 1980: On the role of upper tropospheric jet streaks and leading baroclinic zones in the development of low-level jets in the Great Plains. Mon. Wea. Rev., 108, 1689-1696.

____, and D.R. Johnson, 1979: The coupling of upper and lower tropospheric jet streaks and implications for the development of severe convective storms. Mon. Wea. Rev., 107, 682-703.

U.S. Air Force, 1969: Air Force Meteorological Watch Program. Air Weather Service Regulation 105-9, 15 May 1969, 11, pp 17.

U.S. Department of Commerce, 1984: Storm Data, 26, 12, 33-46.

END

FILMED

8-85

DTIC